TROPICAL PROPAGATION RESEARCH

John J. Hicks, et al

Atlantic Research Corporation

Prepared for:

Army Electronics Command
Advanced Research Projects Agency

December 1972

TROPICAL PROPAGATION RESEARCH (U)

FINAL REPORT , VOLUME IV

Prepared by

John J. Hicks
Richard G. Robertson
Charles B. Sykes
Per A. Anti

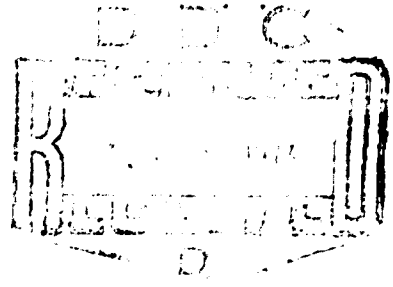

Submitted to

U.S. ARMY ELECTRONICS COMMAND
Fort Monmouth, New Jersey

Contract No.
DA 36-039 SC-90889

Sponsored by
ADVANCED RESEARCH PROJECTS AGENCY
Department of Defense
ARPA Order 371
and
U.S. ARMY ELECTRONICS COMMAND

ATLANTIC RESEARCH

A DIVISION OF THE SUSQUEHANNA CORPORATION

UNCLASSIFIED

Security Classification

DOCUMENT CONTROL DATA - R & D

(Security classification of title, body of abstract and indexing annotation must be entered when the overall report is classified)

1. ORIGINATING ACTIVITY (Corporate author)
Atlantic Research Corporation
A Division of the Susquehanna Corporation
J&B Engineering Department
Shirley Hwy at Edsall Rd, Alexandria, Va 22314

2a. REPORT SECURITY CLASSIFICATION
UNCLASSIFIED

2b GROUP

3. REPORT TITLE

Tropical Propagation Research (U)

4. DESCRIPTIVE NOTES (Type of report and inclusive dates)
Final Report, Volume IV

5. AUTHOR(S) (First name, middle initial, last name)

John J. Hicks
Richard G. Robertson
Charles B. Sykes
Per A. Anti

6. REPORT DATE	7a. TOTAL NO. OF PAGES	7b. NO. OF REFS
December 1972	129	20

8a. CONTRACT OR GRANT NO.	9a. ORIGINATOR'S REPORT NUMBER(S)
DA 36-039 SC-90889	
b. PROJECT NO.	TR-PL-10126-00-0
c.	9b. OTHER REPORT NO(S) (Any other numbers that may be assigned this report)
d.	

10. DISTRIBUTION STATEMENT
This document has been approved for public release and sale; its distribution is unlimited.

11. SUPPLEMENTARY NOTES	12. SPONSORING MILITARY ACTIVITY
	Advanced Research Projects Agency Washington, D. C. and US Army Electronics Command Fort Monmouth, New Jersey 07703

13. ABSTRACT

This report concludes a series of sixteen reports on an extensive experimental and analytical research program on the propagation of radio waves in a tropical jungle environment. The experimental data were obtained from a special test area in Thailand, selected on a systematic basis of its physical environmental parameters. The data discussed in this report were obtained from a test area classed as a tropical rain forest environment.

This report presents results from a special series of measurements designed to characterize the influence of a jungle environment on the transmission of digital signals. Measurements were conducted by transmitting a swept frequency signal, 4 MHz wide about the center frequencies of 50, 100 and 150 MHz, and photographically recording the received envelope and phase, compared to a fixed reference antenna at the receiving terminal. The test antenna was incrementally moved along both a radial and transverse direction with respect to the line of transmission from the transmitter.

The photographically recorded data has been machine reduced and computer analyzed to yield frequency correlation curves, and other statistical data, useful in studying the transmission of digital signals in tropical jungle environments. Data were obtained and analyzed for a variety of antenna heights, and for both horizontally and vertically transmitted polarizations.

DD FORM 1 NOV 68 1473 REPLACES DD FORM 1473, 1 JAN 64, WHICH IS OBSOLETE FOR ARMY USE.

UNCLASSIFIED

Security Classification

14. KEY WORDS	LINK A		LINK B		LINK C	
	ROLE	WT	ROLE	WT	ROLE	WT
Propagation						
Techniques						
Tropical Environment						
SEA - Southeast Asis						
Thailand						
SEACORE						

TROPICAL PROPAGATION RESEARCH (U)

FINAL REPORT, VOLUME IV

Prepared by

John J. Hicks
Richard G. Robertson
Charles B. Sykes
Per A. Anti

Submitted to

U. S. ARMY ELECTRONICS COMMAND
Fort Monmouth, New Jersey

Contract No.
DA 36-039 SC-90889

Sponsored by

ADVANCED RESEARCH PROJECTS AGENCY
Department of Defense
ARPA Order 371
and
U. S. ARMY ELECTRONICS COMMAND

ATLANTIC RESEARCH CORPORATION
Shirley Highway at Edsall Road
Alexandria, Virginia 22314

CONTENTS

CONTENTS (continued)

LIST OF ILLUSTRATIONS

LIST OF ILLUSTRATIONS (continued)

LIST OF ILLUSTRATIONS (continued)

LIST OF TABLES

1. INTRODUCTION

This Final Report, Volume IV, concludes the series of reports on the Tropical Propagation Research Program sponsored by the Advanced Research Projects Agency, and contractually and technically directed by the U.S. Army Electronics Command, Fort Monmouth, New Jersey. It is preceded by fifteen Semiannual and Final reports, which are listed in the REFERENCES for convenience, with Defense Documentation Center reference numbers.

The experimental data for this program were obtained from jungle test areas in Thailand, selected on the basis of their quantitative environmental characteristics. The geographic locations of these test areas, and a description of the associated environmental characteristics have been presented in preceding Final Reports. A repetition of this data in this report would be too redundant and impractical, and the reader is referred to these preceding reports for this information.

This Final Report contains the results of two principal tasks. The first section presents the results of attempts to obtain a set of frequency dependent constituentive parameters applicable to the uniform, homogeneous slab model of radio wave propagation in forested environments. The first part of this report presents these results.

The second task was to analyze the results from a special series of swept frequency measurements leading to a better understanding of the influence of the jungle environment upon the transmission of digital signals. Here, the principal phenomena of concern are the multipath, frequency-selective fading caused by scattering from the trees. The bulk of the

data from these measurements was in the form of photographs, which were machine translated to punched cards for computer processing and analysis. Frequency correlation curves, and various other curves which are presented in this report add to the basic knowledge of propagation in forest environments, as well as being useful in the problems related to the transmission of digital signals in such environments.

Finally, an initial mathematical development of a vertically nonhomogeneous slab model is presented in Appendix A, for horizontally polarized transmission. This represents a further step in refining the understanding of the slab model concept of propagation in forested environments, but much work yet remains to be done before this model can be considered sufficiently complete for useful application.

2. SLAB MODEL CONCEPTS

A homogeneous slab model for explaining propagation in a forest environment has been proposed by Sachs and Wyatt [1966, 1968], Sachs [1966] and Tamir [1967]. They obtained agreement, to within a few dB, between theoretical and experimental transmission loss with the differences averaged over the frequency range of 6 - 100 MHz, with a set of frequency independent slab parameters. However, when theoretical and experimental results are compared at discrete frequencies within this range it is found that the agreement is not uniform over the range and may, in fact, be considerably worse at some frequencies than anticipated on the basis of the over-all, or average-over-frequency, agreement [Hicks, et al., 1970]. It was also found that the results at some frequencies were quite sensitive to changes in the model parameters while those at other frequencies were not. This has led to the suggestion that a frequency dependent set of slab parameters might provide better agreement between theory and experiment and extend the frequency range of validity of the model [Hicks, et al., 1969].

The initial effort here was thus an attempt to obtain a set of frequency dependent parameters for the homogeneous slab model. In so doing, however, it was found that there is no unique set of homogeneous slab parameters. Stated differently, equal agreement between homogeneous slab model theory and experiment can be obtained with any of several combinations of slab parameters. Results from this investigation prompted the development of a nonhomogeneous model, but first it will be helpful to examine some of the results employing frequency dependent parameters in the homogeneous slab model.

In this regard the homogeneous slab model needs to be briefly discussed. A sketch of the model is given in Figure 2.1.

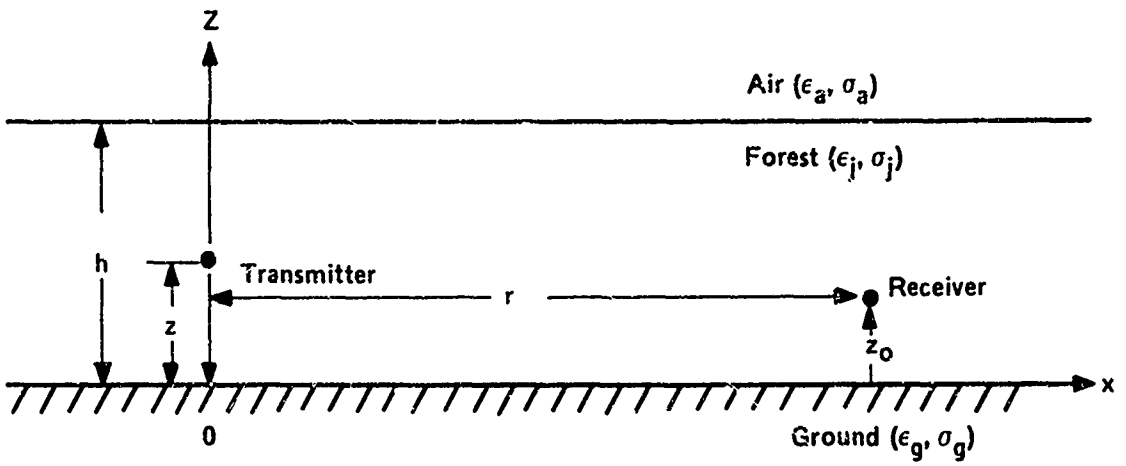

Figure 2.1 Sketch of Homogeneous Slab Model of Forest

The rms electric field between two short dipoles in the homogeneous slab model, excluding the case of very low antennas (heights $\lesssim \lambda/10$) which may involve antenna impedance changes, may be written as [Sachs and Wyatt, 1966; Sachs, 1966; Tamir, 1967]

$$E_{rms} = \frac{9 \times 10^{10} \sqrt{P}}{\sqrt{2}\, \pi f r^2 |\eta_j^2 - 1|} F(z)\, F(z_o)\ \mu v/m \qquad (2.1)$$

where f is the frequency in MHz, r is the range, h is the slab or effective forest height, P is the transmitter power in

kilowatts, z and z_o are the transmitter and receiver antenna heights above ground, $\eta^2 = \varepsilon + 18\, i\sigma/f$ is the refractive index, σ is the conductivity in mmhos/m, ε is the dielectric constant, and the subscript, j, indicates the forest or jungle (slab) medium. Other symbols are identified in Figure 2.1. Further, for both horizontal and vertical polarization (transmit and receive antennas are assumed to have the same polarization) and for both antennas within the slab

$$F(z) = e^{-\alpha_L (h - z)} \left| \frac{1 + \Gamma_{V,H} e^{-2k_o z \sqrt{1 - \eta_j^2}}}{1 - \Gamma_{V,H} e^{-2k_o h \sqrt{1 - \eta_j^2}}} \right|$$

For the case of one antenna above and one in the jungle, one obtains, for vertical polarization

$$F(z) = \left| k_o (z - h)(1 - \eta_j^2)^{\frac{1}{2}} + \eta^2 \frac{\left(1 + \Gamma_V e^{-2k_o h \sqrt{1 - \eta_j^2}}\right)}{\left(1 - \Gamma_V e^{-2k_o h \sqrt{1 - \eta_j^2}}\right)} \right| \sqrt{\frac{r}{k_o}} > z > h$$

and for horizontal polarization

$$F(z) = \left| k_o (z - h)(1 - \eta_j^2)^{\frac{1}{2}} + \frac{\left(1 + \Gamma_H e^{-2k_o h \sqrt{1 - \eta_j^2}}\right)}{\left(1 - \Gamma_H e^{-2k_o h \sqrt{1 - \eta_j^2}}\right)} \right| \sqrt{\frac{r}{k_o}} > z > h$$

where $\alpha_L = k_o \mathrm{Im}\left(\sqrt{\eta_j^2 - 1}\right)$. The subscript V and H correspond to vertical and horizontal polarization respectively, and for vertical polarization the reflection coefficient Γ is

$$\Gamma_V = \frac{\eta_g^2(1 - \eta_j^2)^{\frac{1}{2}} - \eta_j^2(1 - \eta_g^2)^{\frac{1}{2}}}{\eta_g^2(1 - \eta_j^2)^{\frac{1}{2}} + \eta_j^2(1 - \eta_g^2)^{\frac{1}{2}}}$$

and for horizontal polarization

$$\Gamma_H = \frac{(1 - \eta_j^2)^{\frac{1}{2}} - (1 - \eta_g^2)^{\frac{1}{2}}}{(1 - \eta_j^2)^{\frac{1}{2}} + (1 - \eta_g^2)^{\frac{1}{2}}} \quad .$$

Also, the expression for $F(z_o)$ is obtained directly from $F(z)$ simply by replacing z by z_o.

The experimental data to be used in checking these theoretical results, however, are customarily given in terms of basic transmission loss, L_b, referenced to isotropic antennas. Hence, the theoretical field of Eq. (2.1) is converted to basic transmission loss by [Norton, 1959]

$$L_b = 139 - 20 \log E + 20 \log f \qquad (2.2)$$

which is derived for 1 kw of power radiated into free space for short dipole antennas, and f is the frequency in MHz and E the rms field strength in μv/m.

To check the validity of the homogeneous slab model in describing the median field strength in a forested environment, and if valid to obtain the correct slab parameters, one assumes reasonable values for the slab parameters, computes the E_{rms} from Eq. (2.1) and then the basic path loss from Eq. (2.2), and compares the theoretical results with experimental data. If the agreement is not satisfactory, the assumed slab parameters are adjusted and the process repeated until satisfactory agreement, if possible, is obtained.

A large amount of experimental data from two tropical forested environments are available and encompass many antenna heights, frequencies, ranges, and both horizontal and vertical polarizations. A large data base was required to obtain a statistically reliable mean value of path loss for each operating frequency, polarization, antenna height, etc., due to signal variability caused by terrain and/or vegetation variations within the environment. The number of statistical samples for any given operational configuration can be effectively increased by accepting the range dependence of field strength, $1/r^2$ in Eq. (2.1), which has been experimentally established for HF and VHF frequencies in forested environments [Jansky & Bailey, 1966], and normalizing all measurements to a common range according to this dependence. This has been done [Hicks, et al., 1969] and experimental results so normalized are employed here.

The initial objective here, as mentioned, was to obtain frequency dependent parameters for the homogeneous slab in order to obtain better agreement between theory and experiment than was afforded by frequency independent parameters. To this end, several combinations of the equivalent electrical and height parameters of the homogeneous slab were employed

and, with the aid of a digital computer, the basic path loss was computed for several frequencies, antenna heights and both polarizations using Eqs. (2.1) and (2.2).

The results can be presented in a variety of ways. An example of the theoretical path loss for horizontal polarization at different frequencies as a function of the slab conductivity, σ_j is given in Figure 2.2. The transmit and receive antenna heights were 13 feet and 15 feet respectively, $\varepsilon_g = 15$, $\sigma_g = 10$ mmhos/m, $\varepsilon_j = 1.01$ and $h_j = 100$ feet. For present purposes, the most interesting feature of Figure 2.2 is probably the slope of the path loss vs. conductivity curves at the various frequencies. At 2 MHz the slope is small, indicating that the path loss is nearly independent of σ_j for the antenna heights, etc., employed in the computation. The slopes generally increase with increasing frequency from 2 MHz to the 400 MHz limits used, and the curves are nearly linear although some curvature is apparent in the frequency range of 12 MHz to 100 MHz. The small slopes of these curves in the lower HF frequency range indicate that values of σ_j over a fairly wide range of values would be equally suitable as a practical slab model parameter. This has the advantage of making selection of σ_j for use in a model at these frequencies (at least for the antenna heights, etc., used in the illustration) a noncritical function. This is a disadvantage, however, in that since σ_j is not unique, σ_j is not identifiable with any unique environmental parameters which, in turn, implies that σ_j cannot be determined by physical aspects of the environment. This, however, does not imply that other homogeneous slab parameters cannot be obtained which can be related to the environment. In fact, it would be most fortunate if all except a single parameter, identifiable with the environment, were arbitrary. A brief examination of the remaining parameters, ε_j and h_j, however, shows that this is not the case

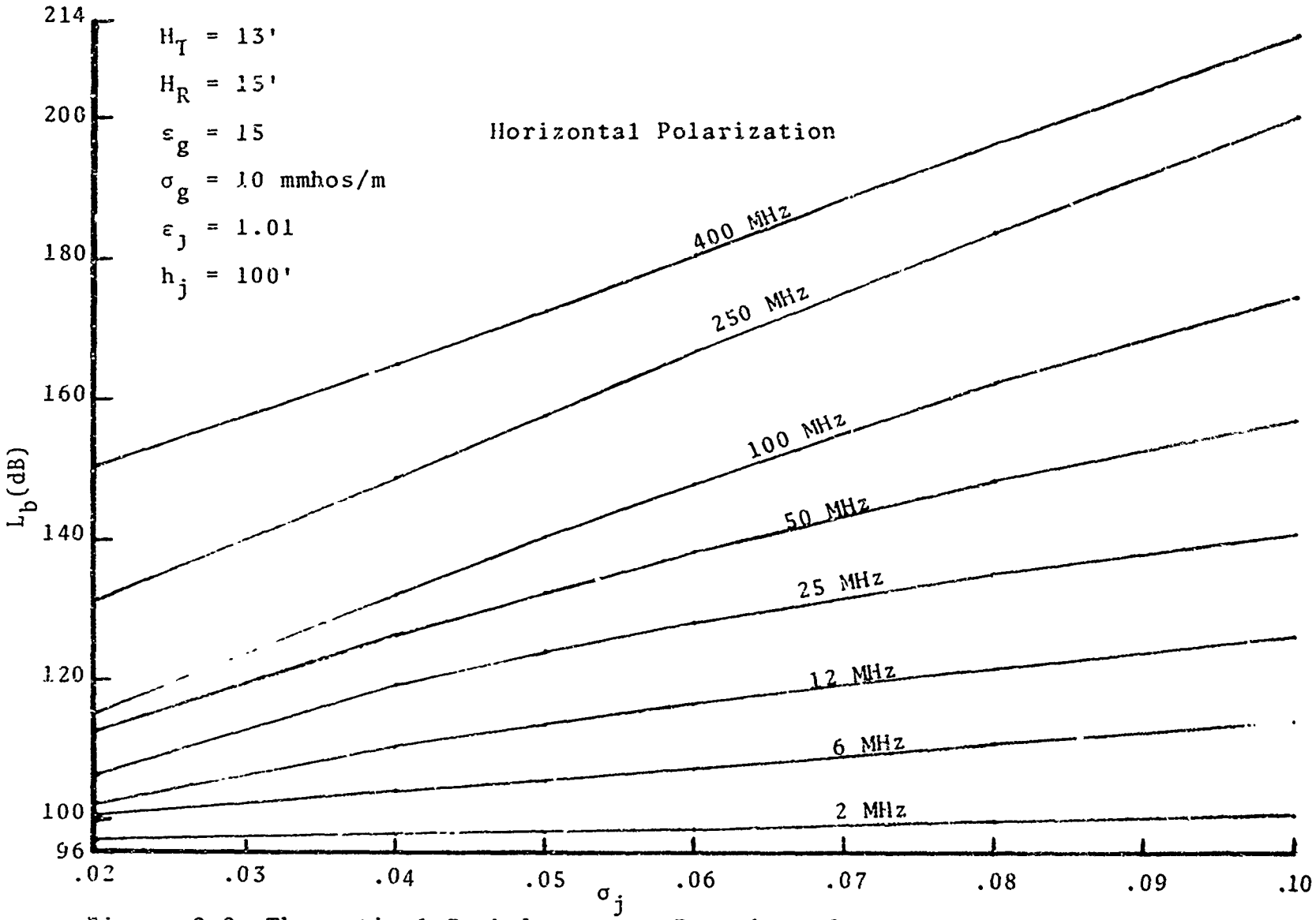

Figure 2.2 Theoretical Path Loss as a Function of Frequency and Slab Conductivity

and, further, that a unique set of homogeneous slab parameters cannot be specified.

Figure 2.3a is a plot of the theoretical and experimental path loss (Area II) as a function of σ_j for 25 MHz, three combinations of antenna heights, horizontal polarization, and different values of ε_j and h_j. Figures 2.3b and c are similar plots for 50 MHz and 100 MHz. Other frequencies and parameter values could have been illustrated, but those of Figure 2.3 are sufficient for present purposes. In this regard, note that for the higher antenna heights (transmitter height = 120 ft., receiver height = 115 ft.) the theoretical values of h_j and, to a lesser degree, ε_j, are fairly critical, while σ_j is, again, quite arbitrary. As the antenna heights are lowered, however, it can be seen that the experimental and theoretical values of path loss for different antenna heights, but at a fixed frequency, generally do not agree (theoretical and experimental curves do not intersect) at the same σ_j. Further, the values of h_j and ε_j can not be changed by much to improve this agreement because they have been found to be fairly critical from the results at the higher antenna heights. Hence, only σ_j (and to some extent, ε_j) can apparently be changed with antenna height to improve the agreement, but these cannot be allowed to change with height in the homogeneous slab model by definition. Hence, extension to a slab model which is nonhomogeneous in the z-direction (electrical parameters vary with height) is indicated. Such a nonhomogeneous model will, presumably, permit $\sigma_j(z,f)$, and therefore a set of nonhomogeneous slab parameters, to be uniquely determined.

Of equal importance, however, is the question as to whether such parameters, if indeed unique, can be related sufficiently to the physical factors of the forest environment

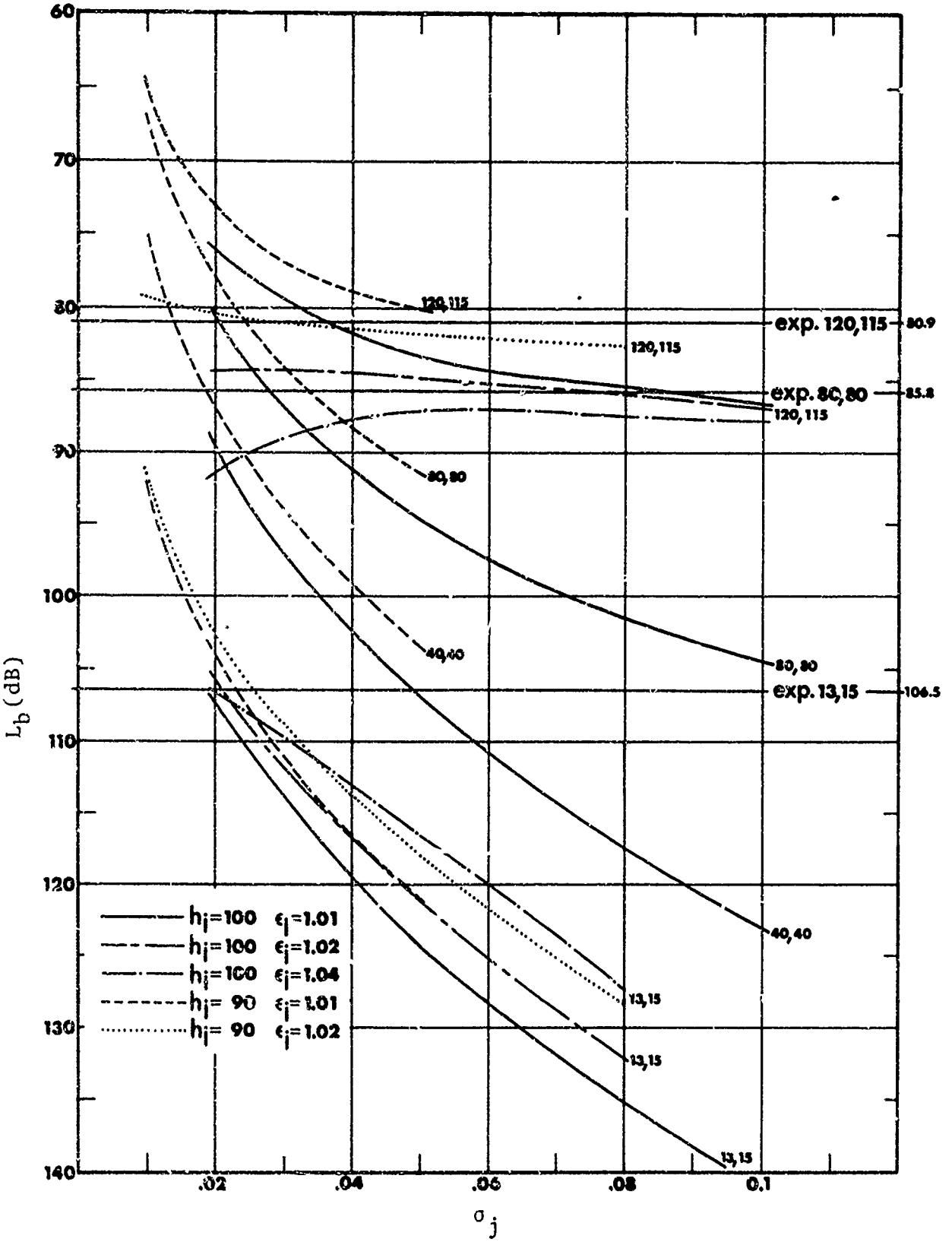

Figure 2.3a Theoretical and Experimental Path Loss at 25 MHz as a Function of Antenna Heights, Conductivity, and Permitivity

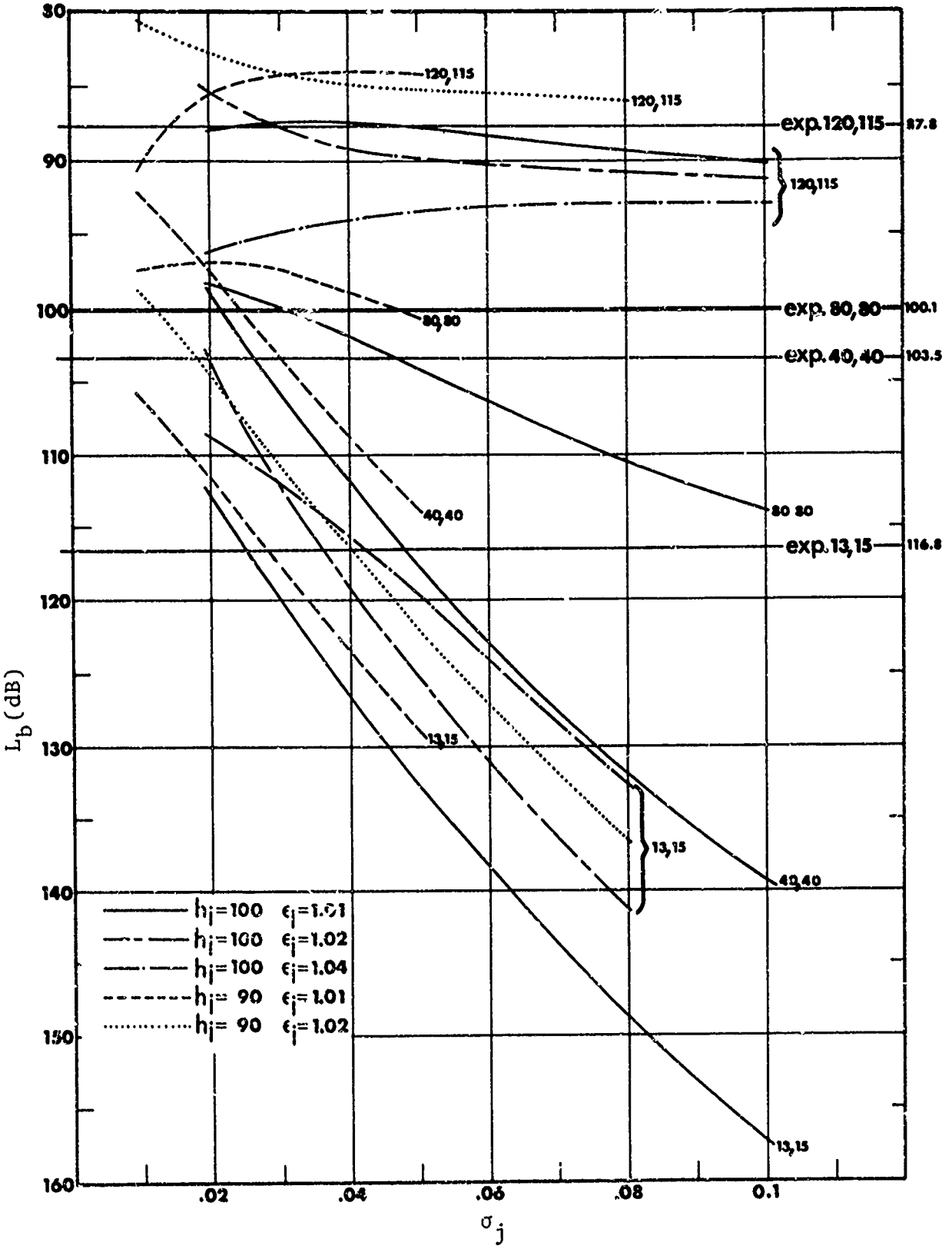

Figure 2.3b Theoretical and Experimental Path Loss at 50 MHz as a Function of Antenna Heights, Conductivity, and Permitivity

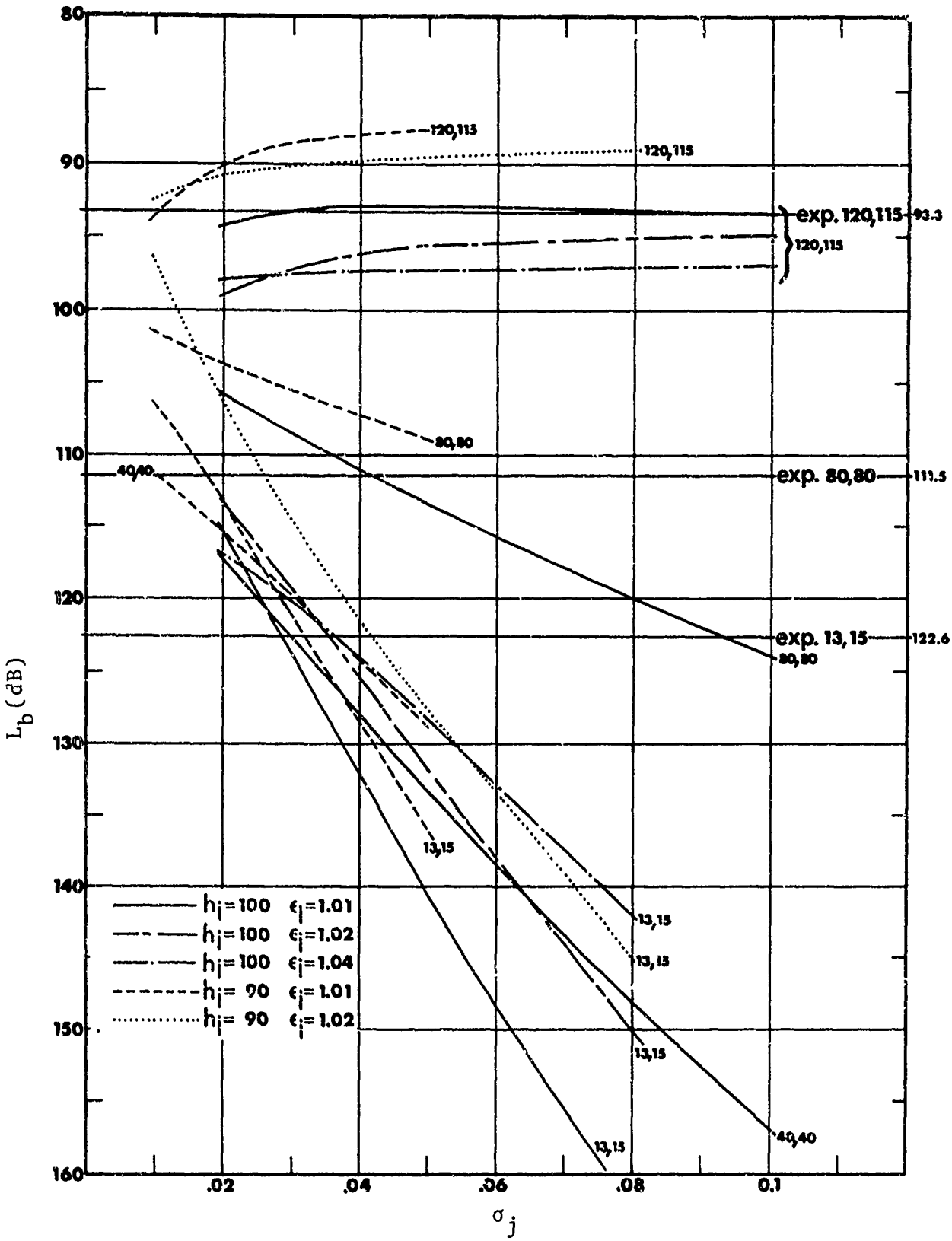

Figure 2.3c Theoretical and Experimental Path Loss at 100 MHz as a Function of Antenna Heights, Conductivity, and Permitivity

(tree height, tree density, etc.) so that slab parameters may ultimately be predicted from knowledge of environmental factors. This can be answered with definiteness only after the parameters of the nonhomogeneous model are determined and comparison is made between theoretical and experimental factors of the model and forest. Some insight into this may be gained, however, by examination of some environmental features. Robertson [1969] measured tree heights and diameters-at-breast-height (DBH) for trees whose diameters $\geq$ 6", over a large region ($\approx$ 1000' x 1000') in Area II of Thailand. The empirical relation for biomass, or mass in kilograms of a single tree, is $w = 0.2\,(DBH)^{2.5}$ [Robertson, 1969]. Now, if the distribution of this biomass with height for a single tree is known, the distribution of biomass with height for the large region surveyed (which is presumably representative of the forest) can be determined by straightforward averaging. Unfortunately, the biomass distribution with height for single trees, in general, is not known. However, it seems obvious in most cases that the biomass of a tree decreases with height. Hence, two distributions of biomass with height for a single tree (constant and linearly decreasing) have been assumed and the resultant distribution of biomass with height for the region surveyed by Robertson [1969] in Area II has been computed using each.

These distributions are shown in Figure 2.4. Note that this tree survey was made in the same region in which the propagation measurements discussed above were made. Also, the survey included only trees whose DBH $\geq$ 6", and the results were extrapolated to smaller trees in arriving at Figure 2.4. Further, the presence of vines and undergrowth has been ignored in computing the biomass distribution of Figure 2.4, which tends to underestimate the true biomass near the ground by about 10% of the total [Robertson, 1969]. However, it seems clear from Figure 2.4 that the biomass density of the forest

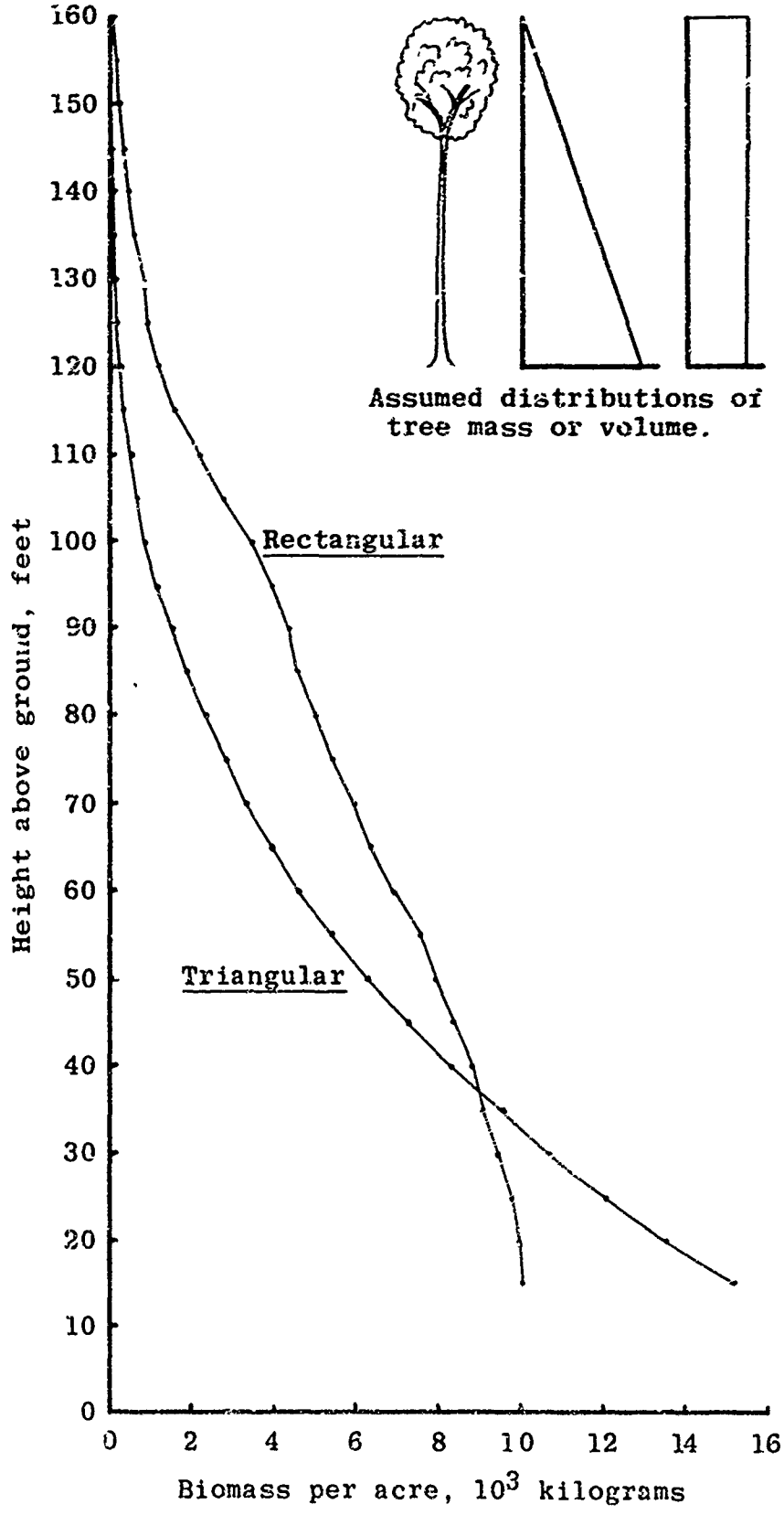

Figure 2.4 Distribution of Forest Biomass With Height

decreases with height, as could be expected on the basis of a single tree (the assumed constant distribution of biomass for a single tree is expected to yield the smallest, or limiting, case). The decrease in biomass density with height is consistent with the fact that η_j^2 must be a function of height. This consistency strongly suggests that there is a direct connection between the forest biomass density and the electrical parameter $\eta_j^2 = f(z)$, which would permit prediction of slab (nonhomogeneous) parameters on the basis of more readily determined environmental factors. The functional form of $\eta_j^2 = f(z)$ may be established by adjustment of variables appearing in the theoretical results of a nonhomogeneous slab model until these results conform to experimental data. This functional form of η_j^2 should then be examined and related, if possible, to parameters of the forest environment, such as biomass density.

Thus, extension to a nonhomogeneous slab model will not only provide a more accurate model but it may also provide the final factor (the law governing the nonhomogeneity) needed to permit propagation prediction from knowledge of environmental factors. Hence, the development of a nonhomogeneous slab model has been undertaken. The theoretical results for the nonhomogeneous model are derived in Appendix A for the case of horizontal polarization with the antennas immersed in the foliage. The results have been presented in a form similar to those for the homogeneous model for ease of comparison, and results of the two are repeated here, for horizontal antennas in the foliage, and compared. The general expression for E_{rms} may be given as

$$E_{rms} = \frac{9 \times 10^{10} \sqrt{P}}{\sqrt{2}\, \pi f r^2} |F(z)||F(z_o)| \mu v/m$$

where, for the homogeneous case (Eq. 2.1)

$$F(z) = \frac{e^{-k_o(h-z)\sqrt{1-\eta_j^2}}\left[1 + \Gamma_H e^{-2k_o z\sqrt{1-\eta_j^2}}\right]}{\sqrt{1-\eta_j^2}\left[1 - \Gamma_H e^{-2k_o h\sqrt{1-\eta_j^2}}\right]}$$

and for the nonhomogeneous case (Eq. A-2)

$$F(z) = \frac{e^{-k_o\int_z^h \left[1-\eta_j^2(a)\right]^{\frac{1}{2}}da}\left[1 + \Gamma_g(o)\, e^{-2k_o\int_o^z \left[1-\eta_j^2(a)\right]^{\frac{1}{2}}da}\right]}{\left[1-\eta_j^2(h)\right]^{\frac{1}{4}}\left[1-\eta_j^2(z)\right]^{\frac{1}{4}}\left[1 - \Gamma_g(o)\, e^{-2k_o\int_o^h \left[1-\eta_j^2(a)\right]^{\frac{1}{2}}da}\right]}$$

where, in both cases, $F(z_o)$ is equal to $F(z)$ with z replaced by z_o. It is easily seen here that when $\eta_j(z) = \eta_j(h) = \eta_j(o) = \eta_j(a) = \eta_j$, which defines the homogeneous case (i.e., η_j is a constant independent of z), that the nonhomogeneous model reduces to the homogeneous model, as expected. Specifying the functional form of $\eta_j^2(z)$ for the nonhomogeneous case clearly permits an additional degree of freedom relative to the homogeneous case and should be quite useful for determining the equivalent slab parameters and for correlating these with environmental factors.

Further effort is needed to develop the equations for vertical polarization and for antennas of arbitrary location, which involves straightforward extensions of the theory given in Appendix A, and to compare the results with experimental propagation and environmental data.

3. FREQUENCY AND DISTANCE FADING STATISTICS IN A TROPICAL FOREST CHANNEL AT VHF

Radio transmission at HF frequencies and above in tropical forest channels generally consist of a fairly direct signal (lateral wave) plus a number of relatively delayed signals which are caused by scattering from trees in the general vicinity of the antennas [Hicks and Robertson, 1969]. The tropical forest channel is thus a multipath channel at HF and above. The instantaneou. received signal is, of course, the vector (amplitude and phase) sum of all the multipath signals arriving at the receive antenna at that instant. The relative phases and, probably to a lesser degree, the amplitude of the multipath signals change in some random manner as either the antenna position in the forest is changed, or as the transmission frequency changes over some finite bandwidth. The resultant complex signal, generally referred to as the channel transfer function and denoted by H(f,x) here, is thus a random process characterizing the frequency, f, and spatial, x, variability of the signal. Note that the channel transfer function has most often been discussed in relation to dynamic channels such as the troposphere, ionosphere, and others and thus written as H(t) to denote the frequency and time variability of such channels. The time variations of tropical forest channels, however, caused by wind-induced tree motion, are sporadic and generally small at HF and VHF relative to the spatial variability and are thus assumed negligible relative to the spatial variations (i.e., the channel is assumed to be static). Hence, the channel transfer function is denoted here as H(f,x), which shows distance, but no time dependence.

The statistical properties of the signal, or channel transfer function, are important in the design and operation of

both narrowband and wideband systems. The probability density function of the short spatial variations of the envelope is needed in establishing the power margin for narrowband and wideband (for flat – flat-fading) systems, and is a first requisite in computing bit error rates in wideband digital systems [Stein and Jones, 1967].* Probability density functions of short spatial fades at VHF for a tropical forest environment (Area II) have been reported earlier [Robertson et al., 1970] and a few additional distributions are presented later in this report. The normalized distance (or time if the terminals are in motion) and frequency cross covariances of the transfer function are needed in designing spatial and frequency diversity schemes for both narrowband and wideband systems, and for determining pulse length and bandwidth limitations of digital systems to avoid spatial (or time if the terminals are in motion) and frequency-selective fading.

The time dependence introduced here is not the same as the time dependence caused by wind-induced tree motion. The latter has been neglected, as mentioned above, while the former is introduced through terminal motion (e.g., mobile applications) and is directly dependent upon the spatial variations.

The character of these normalized cross covariances is the major topic of this section. In particular, the normalized distance and frequency covariances of both the envelope and the complex signal are obtained from experimental data from a tropical forest environment (Area II). These data were

---

* Note that other factors, namely the mean propagation loss, long spatial variability, and indigenous and/or system noise are also needed in establishing power margins and signal-to-noise ratios in general. These factors have been discussed in previous ARC reports [see Jansky & Bailey, 1966; Hicks et al., 1970] and elsewhere and are not a subject of this section.

obtained using sweep-frequency techniques (4 MHz sweep) and include frequencies of 50, 100 and 150 MHz, various antenna heights (dipole antennas) and horizontal and vertical polarization.

The distance and frequency envelope covariances are also discussed for some limited measurements at 400 MHz, some with a 10 MHz sweep width, and some with directive antennas.

The envelope covariances are discussed first, followed by the complex covariances, a few probability distributions of the envelope, and ending with a general discussion and conclusions.

3.1 Envelope Frequency and Distance Correlations

The majority of the experimental data acquired for computing the frequency and distance correlation functions for the tropical forested channel are of the signal envelope as a function of swept-frequency and distance. The envelope gives only the magnitude of the complex signal, but because of the relatively complicated problems associated with obtaining the phase of the complex signal, envelope statistics are often used to approximate the channel characteristics. The complex signal response was also obtained for the tropical forested channel for a few operating configurations but, because of their added complexity in data collection and analysis, they are discussed in the next section.

This section is devoted to a discussion of the envelope data. A brief review of the operational configurations and experimental procedures is given first, followed by the data reduction and analysis procedures and a discussion of the results.

3.1.1 Experimental Data and Measurement Procedures

The experimental equipment and procedures used in obtaining the envelope versus swept-frequency and distance data have been discussed earlier [Robertson, et al., 1970]. A number of frequency correlation functions were also computed and discussed there, but a constant mean was assumed in the analysis. In the present case a more realisitic linear changing mean is assumed and additional analyses are also performed. A brief review of the operational parameters of frequency, antenna heights, etc., used and the experimental procedures is given for continuity.

The propagation measurements were made over relatively smooth terrain in a tropical rain forest near Songkhla in Southern Thailand, designated as Area II. The data were photographs of the scope face of a spectrum analyzer which displayed the received signal envelope as a function of swept frequency. The frequency sweep width was generally 4 MHz, centered about the test frequency, with a limited number of tests being made with a 10 MHz sweep width. The test frequencies were for the most part 50, 100 or 150 MHz, with a limited number of tests also made at 400 MHz. The transmitting antenna heights were either 40 or 80 feet and the receive antenna heights were 6 feet. Half-wave dipole antennas were employed with the exception that a limited number of tests were also made with antennas having greater directivity. The antennas were aligned for maximum gain along the line-of-sight direction between transmitter and receiver. The receive antennas were located at various positions in the environment, identified as field points. The distance from the transmitter to these field-points and the general vegetation and terrain characteristics of each have been discussed earlier [Robertson et al., 1970].

A complete set of data representing one operating configuration of center frequency, polarization, antenna height, etc., generally consisted of 101 photographs of the amplitude versus swept-frequency trace taken sequentially at equally spaced distance increments of length $\lambda/10$, over a total distance of 10λ (λ = wavelength). In some runs the direction of receive antenna motion was radial from the transmitter and in others it was transverse. The antennas were stationary and wind effects small while each photograph was taken. Each run, which may be viewed as an ensemble of amplitude versus frequency functions taken over distance, provides the samples used to compute the frequency and distance correlation functions (one each) representative of that run, or operation configuration.

3.1.2 Reduction and Analysis of Envelope Data

To facilitate analysis on a digital computer, the analogue trace of each amplitude versus frequency-sweep photograph was sampled in amplitude at each 0.25 MHz for the data taken with a 4 MHz sweep-width and at each 0.2 MHz for the 10 MHz sweep-width data. These sample intervals appeared, visually, to more than satisfy the Nyquist criterion.

It was frequently necessary during data recording to adjust a step-attenuator at the spectrum analyzer input to maintain a satisfactory sensitivity and/or to keep the trace within the scale of the spectrum analyzer scope face. All such adjustments, which were constant for each photograph, were recorded and subsequently removed from the data.

A calibration photograph, to permit corrections for any inherent non-flat character of the sweep, was frequently

taken with the receiver very near the transmitter to avoid distortions due to the environment. Other than rounding of the leading and trailing edges of the sweep, caused by equipment response, the sweep was generally quite flat. The calibration photo was used where available, however, to correct the data and where not available the sweep was assumed to be flat. In all cases, however, the rounded edges of the sweep were avoided by utilizing data from only the central 3.5 MHz of the 4 MHz sweep and the central 8 MHz of the 10 MHz sweep.

In computing correlations, the variations about the mean value are normally used. Hence, it is customary to remove the mean, if not already zero. The amplitude traces for the 4 MHz sweep generally revealed a linear changing mean and the mean of the 10 MHz traces appeared to be fairly constant. Hence, a least square fit for a linear changing mean was computed from the digitized values (appropriately adjusted for gain and calibration as discussed above) of the central 3.5 MHz data of each 4 MHz sweep and was removed from the sweep. A constant mean was computed from the digitized values (appropriately adjusted) of the central 8 MHz for each 10 MHz sweep and was removed from each.

The resultant digitized envelope values of each photograph are zero-mean and may be called $d(f_i)$, where f_i identifies frequency at which the i^{th} envelope sample is taken and $i = 1, 2, 3, \ldots\eta$ where $\eta = 15$ for the 3.5 MHz sweep width data and $\eta = 39$ for the 8 MHz sweep width data. For each run or set of the data representing one operating configuration, there are generally 101 such photographs as mentioned above. Hence, a sample of the envelope at frequency f_i from the j^{th} photograph may conveniently be called $d(f_i; x_j)$ where $j = 1, 2, 3, \ldots N$, (N is usually 101) and x_j identifies the position at which the photograph was taken. The resultant ensemble of digitized

envelope values for each run are assumed to represent a stationary, ergodic process.

The general expression for the normalized frequency-distance cross-covariance (or correlation coefficient) of the envelopes may be written as [Bendat and Piersol, 1966].

$$r(\Delta f;\Delta x) = \frac{\overline{H(f;x)H^*(f+\Delta f;x+\Delta x)} - \overline{H(f;x)}\;\overline{H^*(f+\Delta f;x+\Delta x)}}{\sqrt{\overline{|H(f;x)|^2} - \overline{|H(f;x)|}^2}\;\sqrt{\overline{|H(f+\Delta f;x+\Delta x)|^2} - \overline{|H(f+\Delta f;x+\Delta x)|}^2}} \tag{3.1}$$

where the overbar denotes the ensemble average and the asterisk denotes complex conjugate. In the present case involving only the envelopes, the correlation coefficients are computed from Eq.(3.1) by replacing H and H* by $|H|$.

In terms of the digitized envelope values where $|H(f_i;x_j)| \equiv d(f_i;x_j)$ for convenience, the frequency correlation coefficients $r(q)$, are computed from Eq.(3.1) by letting $x = 0$. The terms of Eq.(3.1) are then

$$\overline{d(f_i;x_j)\,d(f_{i+q};x_j)} = \frac{1}{N(\eta-q)} \sum_{j=1}^{N} \sum_{i=1}^{\eta-q} d(f_i;x_j)\,d(f_{i+q};x_j) \tag{3.2}$$

$$\overline{d(f_i;x_j)} = \frac{1}{N(\eta-q)} \sum_{j=1}^{N} \sum_{i=1}^{\eta-q} d(f_i;x_j) \tag{3.3}$$

$$\overline{d(f_{i+q};x_j)} = \frac{1}{N(\eta - q)} \sum_{j=1}^{N} \sum_{i-1}^{\eta-q} d(f_{i+q};x_j) \qquad (3.4)$$

$$\overline{d(f_i;x_j)^2} = \frac{1}{N(\eta - q)} \sum_{j=1}^{N} \sum_{i=1}^{\eta-q} [d(f_i;x_j)]^2 \qquad (3.5)$$

$$\overline{d(f_{i+q};x_j)^2} = \frac{1}{N(\eta - q)} \sum_{j=1}^{N} \sum_{i-1}^{\eta-q} [d(f_{i+q};x_j)]^2 \qquad (3.6)$$

where, for simplicity in notation, $\Delta f = 0.25\ q$ MHz for the 3.5 MHz sweep data and $\Delta f = 0.20\ q$ MHz for the 8 MHz sweep data, and $q = 0,1,2,\ldots,\eta-1$.

The distance correlation coefficients, r(p) are computed from Eq.(3.1) by letting $\Delta f = 0$. The terms of Eq.(3.1) are then

$$\overline{d(f_i;x_j)\,d(f_i;x_{j+p})} = \frac{1}{\eta(N-p)} \sum_{j=1}^{N-p} \sum_{i=1}^{\eta} d(f_i;x_j)\,d(f_i;x_{j+p}) \qquad (3.7)$$

$$\overline{d(f_i;x_j)} = \overline{d(f_i;x_{j+p})} = \frac{1}{\eta(N-p)} \sum_{j=1}^{N-p} \sum_{i=1}^{\eta} d(f_i;x_j) = 0 \qquad (3.8)$$

$$\overline{d(f_i;x_j)^2} = \frac{1}{\eta(N-p)} \sum_{j=1}^{N-p} \sum_{i=1}^{\eta} [d(f_i;x_j)]^2 \qquad (3.9)$$

$$\overline{d(f_i; x_{j+q})^2} = \frac{1}{n(N-p)} \sum_{j=1}^{N-p} \sum_{i=1}^{n} [d(f_i; x_{j+p})]^2 \qquad (3.10)$$

Employing Eqs.(3.1) and (3.7) - (3.10) gives the distance correlation coefficients at values of $\Delta x = p\ \lambda/10$, and $p = 0, 1, 2, \ldots, N - 1$.

3.1.3 Presentation and Discussion of Results

The computed values of the envelope frequency correlation coefficients (connected by smooth curves) are shown in Figures 3.1a-n. The particular operating configuration is identified on each plot. The first number in the top line of the identification is frequency in MHz, the second symbol is either H or V for horizontal or vertical polarization, and the third number is the transmitting antenna height in feet. The direction of receiving antenna motion relative to the line-of-sight to the transmitter is identified as "radial" or "transverse," and the field point locations are identified as FP-10, Y-20, Y-25, or Z-29. With the exception of the 400 MHz special runs, whose identification is as above, the special runs are further identified with receiver (Rx) or transmitter (Tx) directive antenna (either a 6-element Yagi "beam" or a two element array having a "cardioid" pattern) and by the sweep width (8 MHz).

The curves show the frequency correlations to generally fall off quite rapidly. A quasi-periodic component, with period of ≈ 1 - 2 MHz, is also evident in many of the frequency correlations (e.g., see Fig.3.1e, 100 H 40 Radial at Y-20). A periodic component in the correlation is evidence of the same in the data [Lee, 1960] and, due to the Fourier transform relation between frequency correlation and multipath intensity

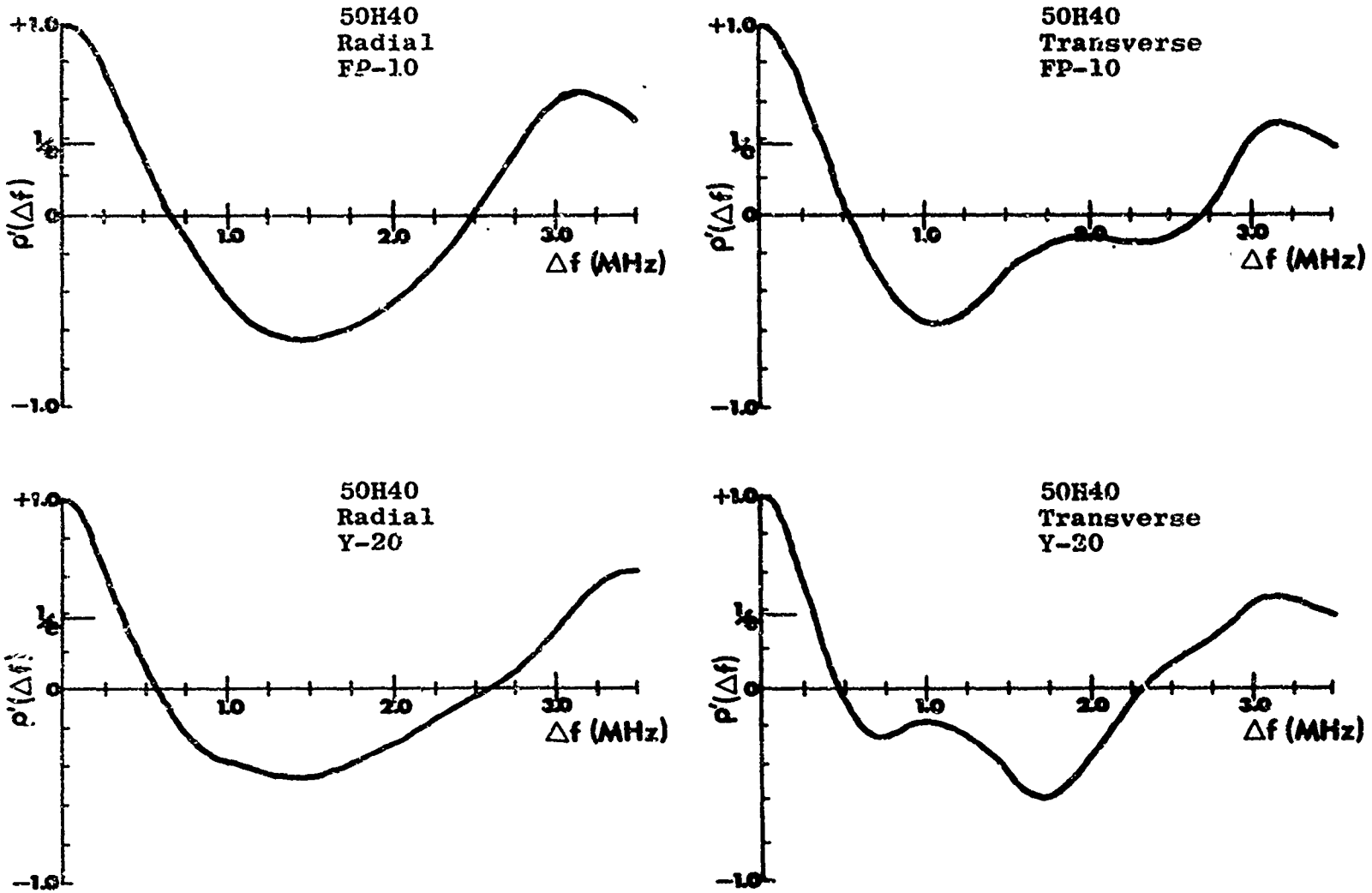

Figure 3.1a Frequency Correlation Functions of the Envelope

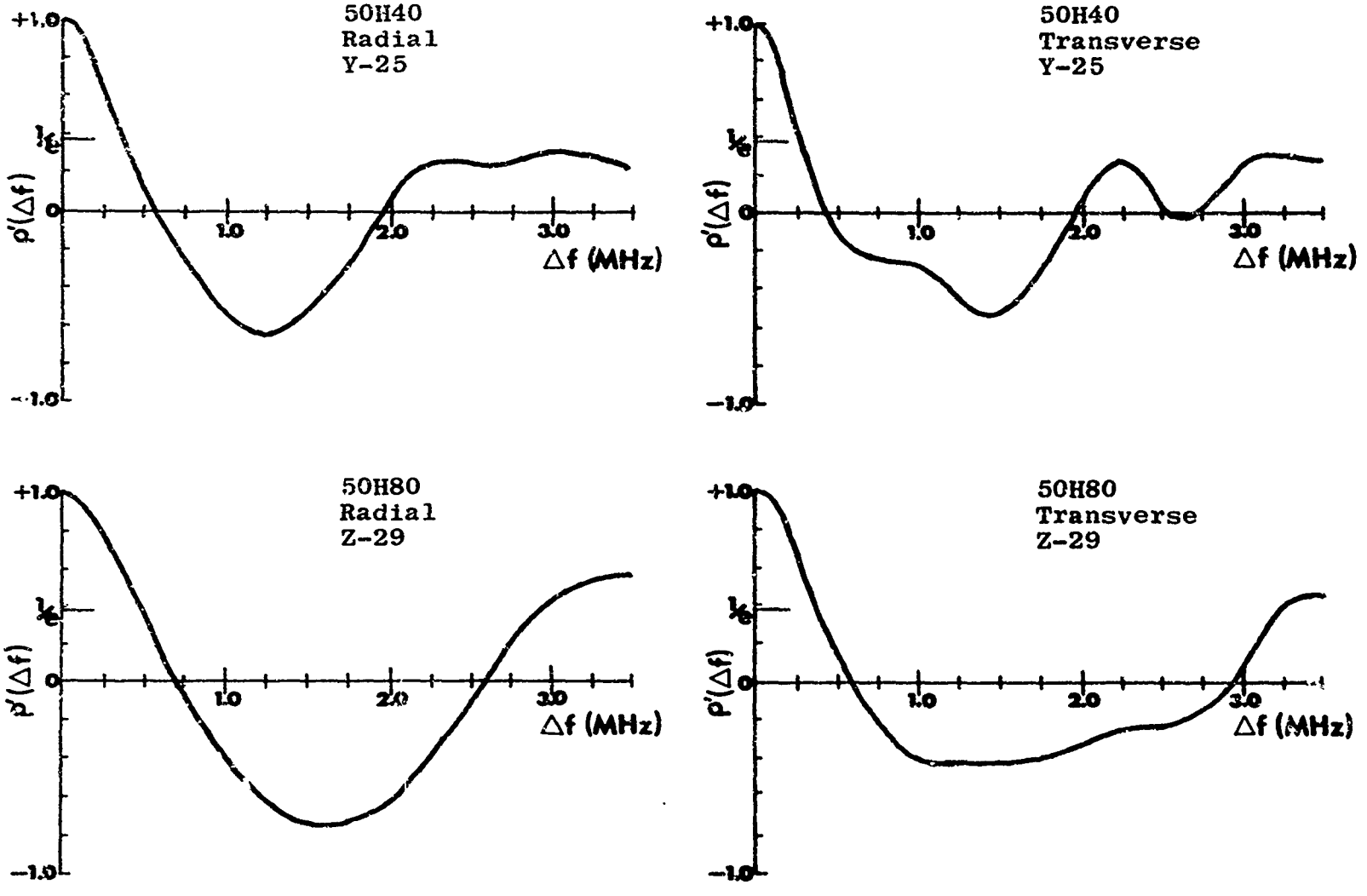

Figure 3.1b Frequency Correlation Functions of the Envelope

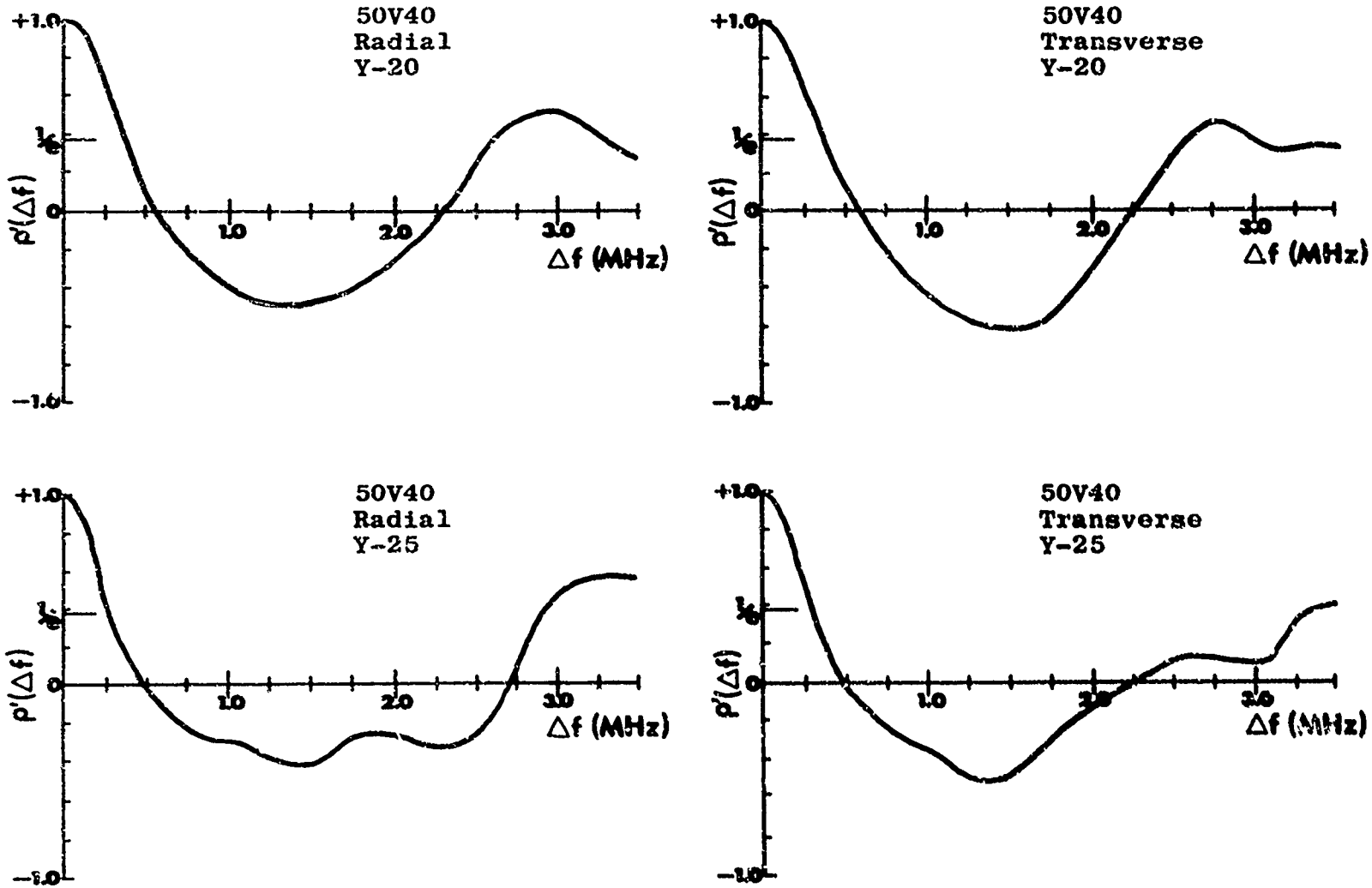

Figure 3.1c Frequency Correlation Functions of the Envelope

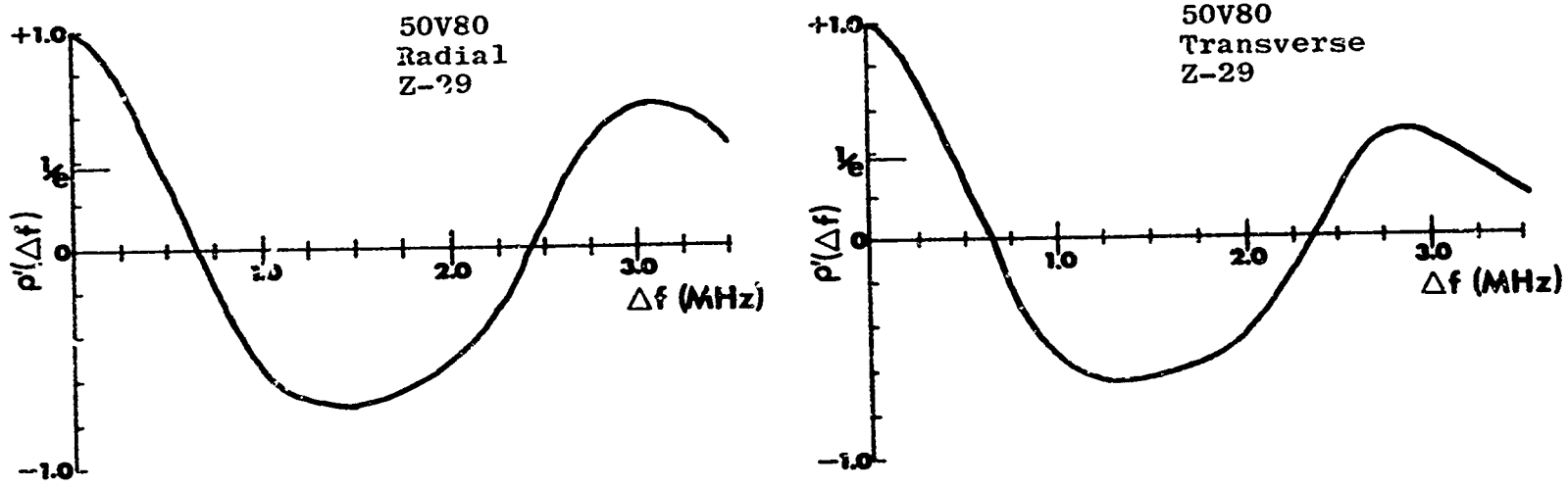

Figure 3.1d Frequency Correlation Functions of the Envelope

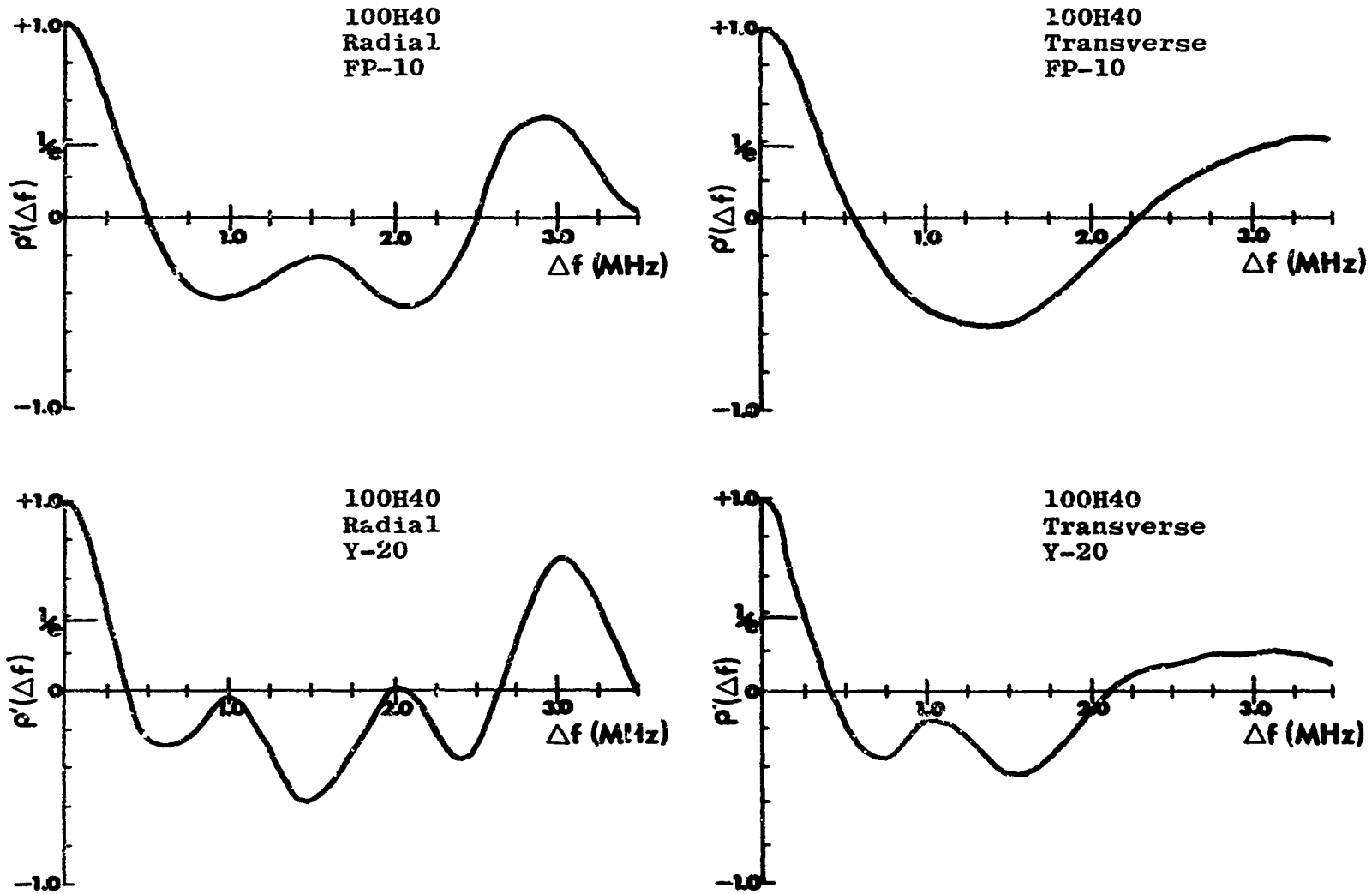

Figure 3.1e Frequency Correlation Functions of the Envelope

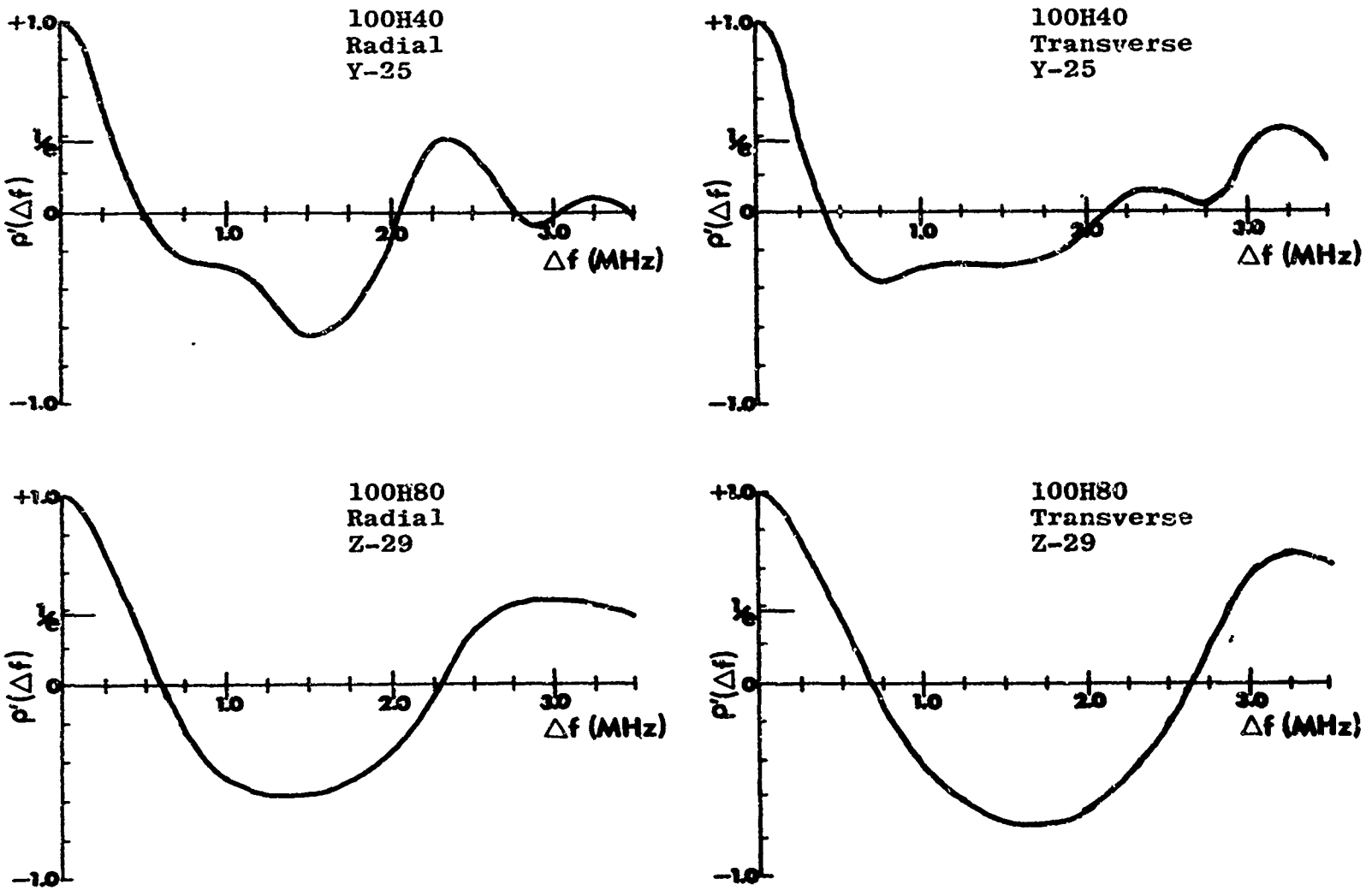

Figure 3.1f Frequency Correlation Functions of the Envelope

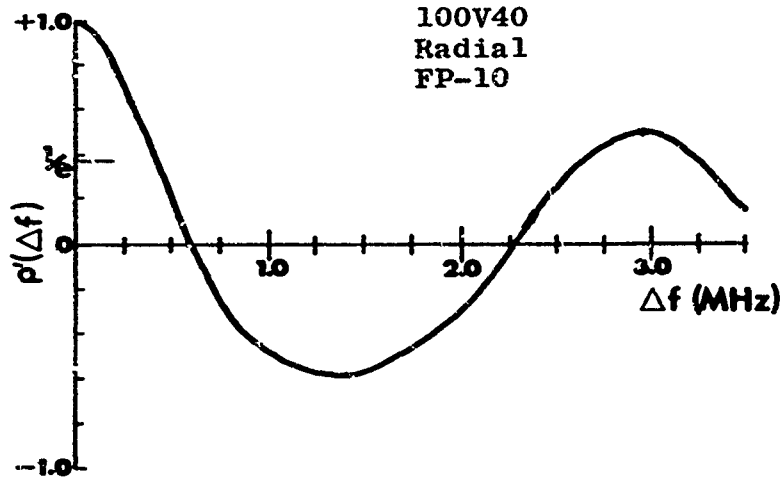

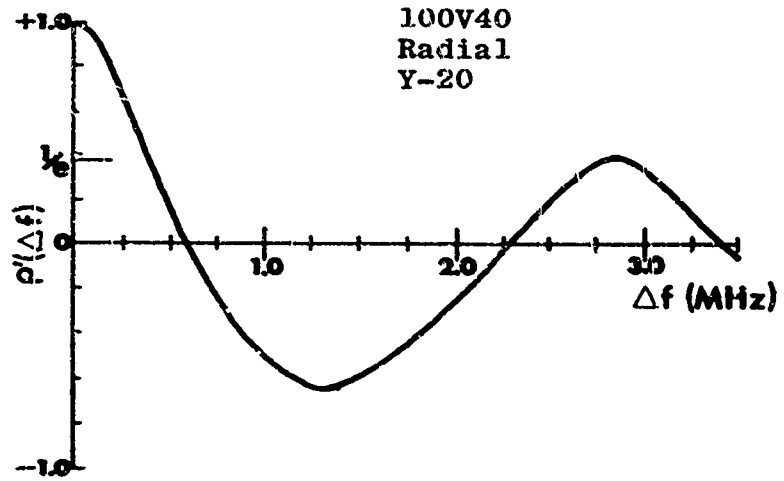

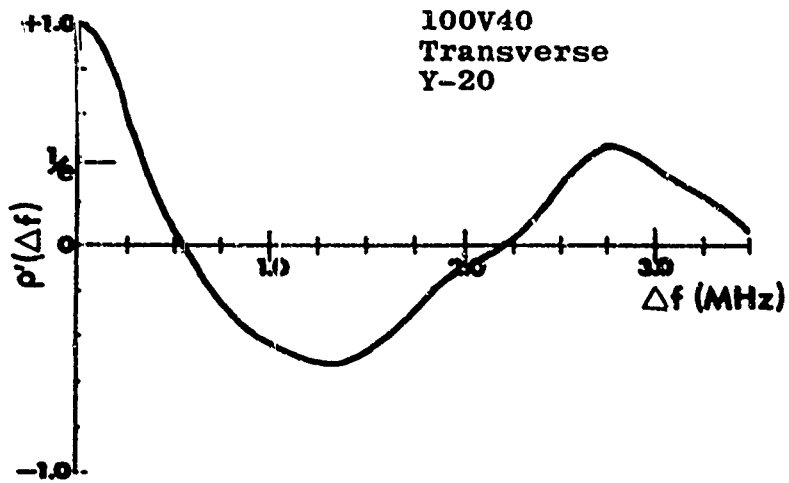

Figure 3.1g Frequency Correlation Functions of the Envelope

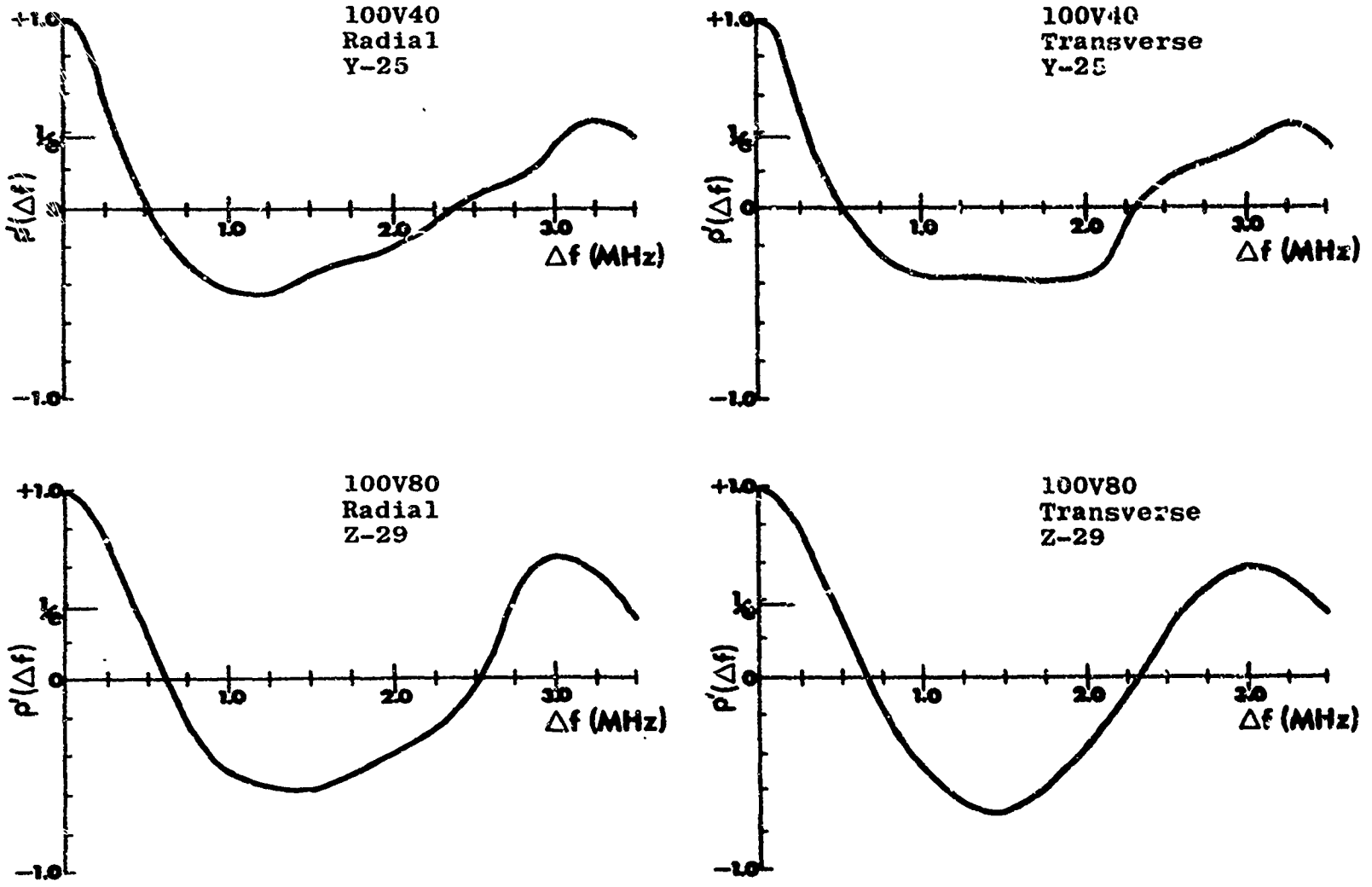

Figure 3.1h Frequency Correlation Functions of the Envelope

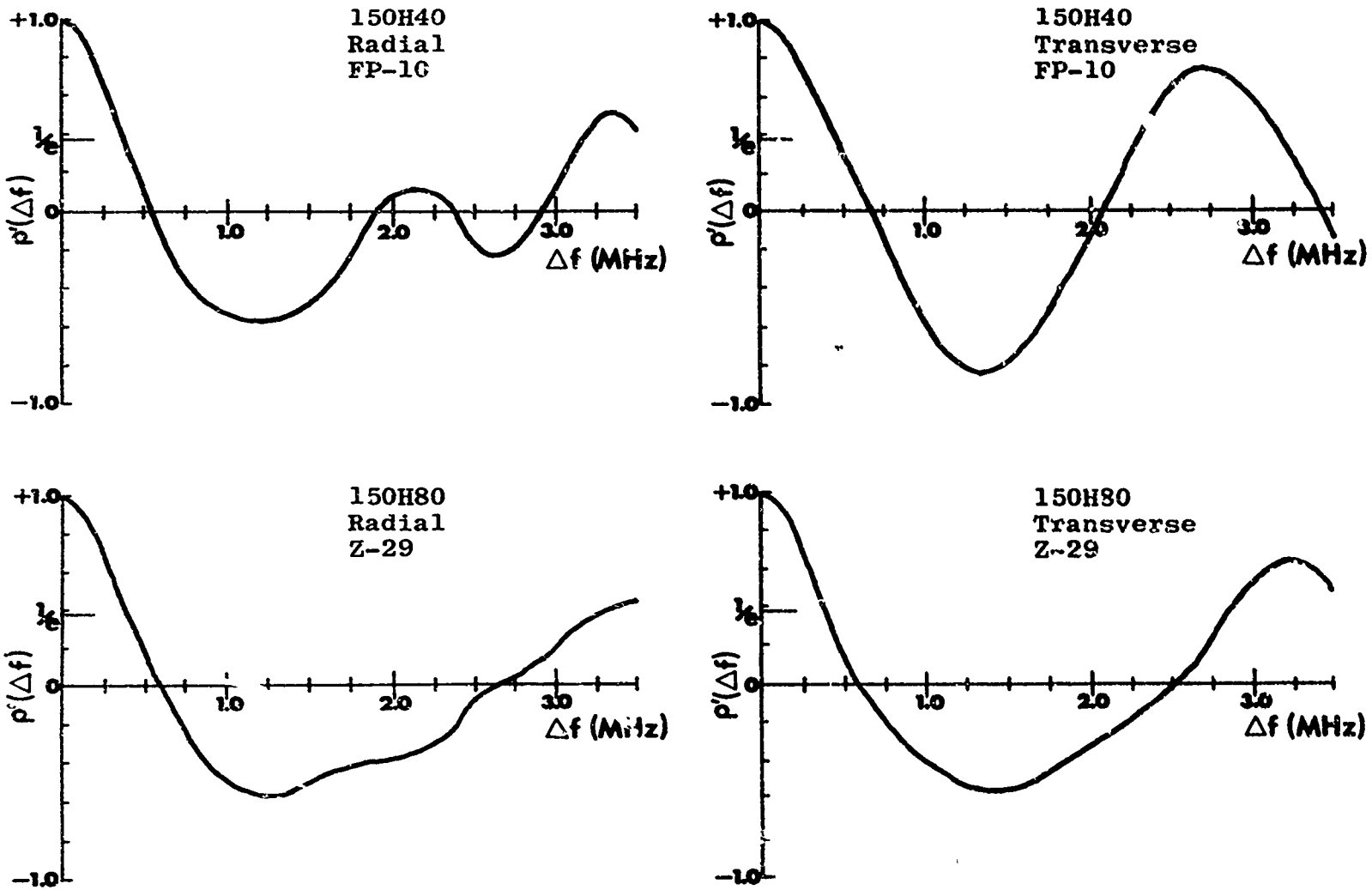

Figure 3.1i Frequency Correlation Functions of the Envelope

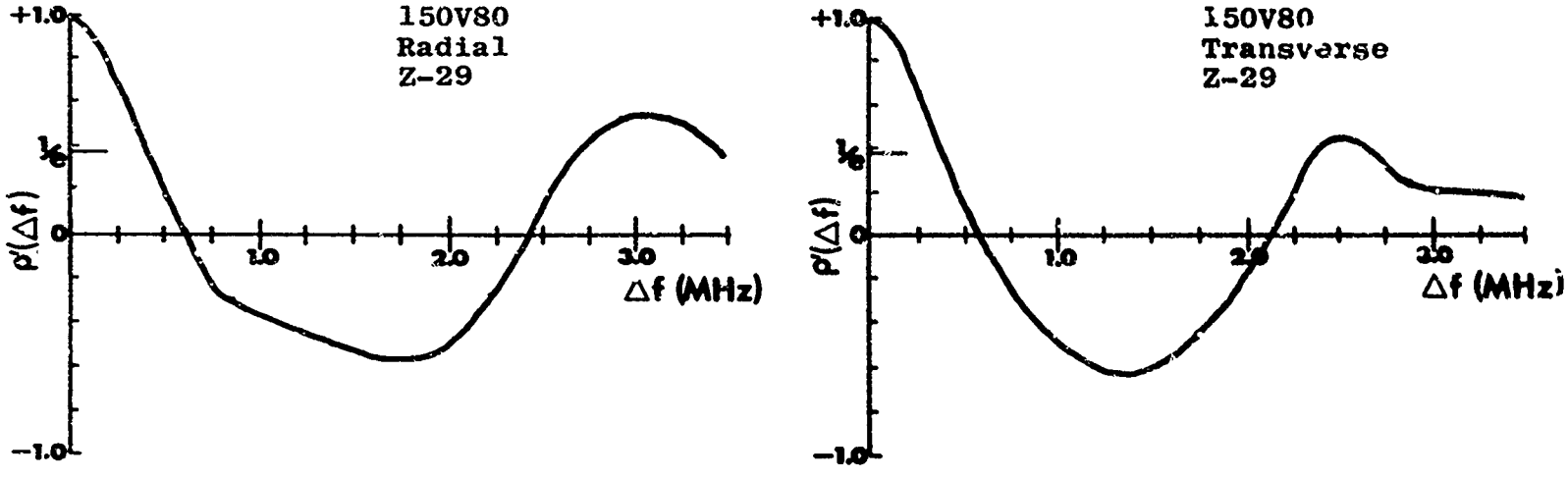

Figure 3.1j Frequency Correlation Functions of the Envelope

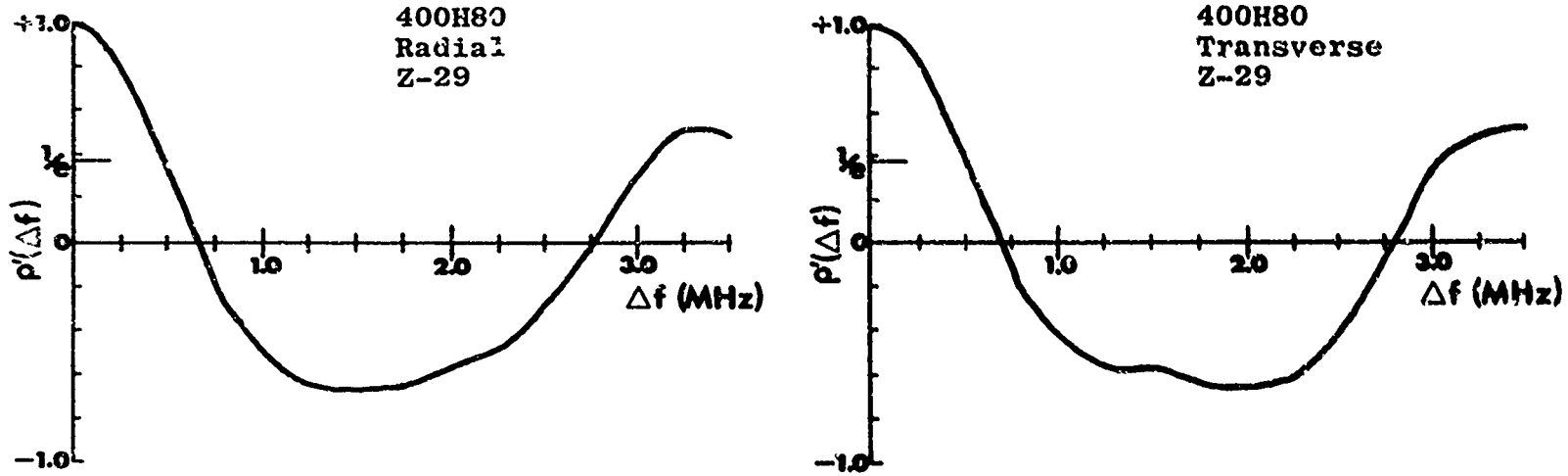

Figure 3.1k Frequency Correlation Functions of the Envelope

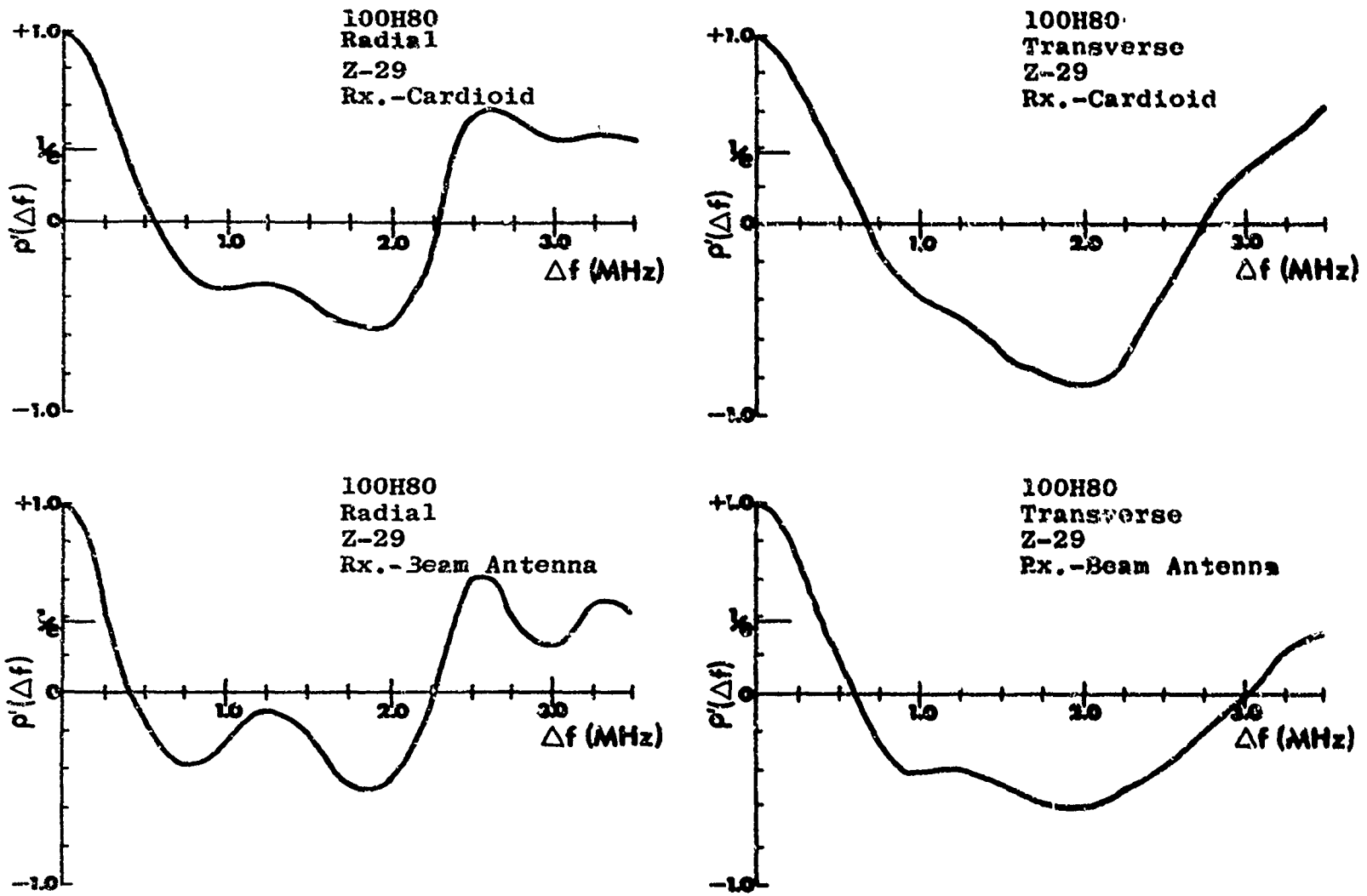

Figure 3.11 Frequency Correlation Functions of the Envelope

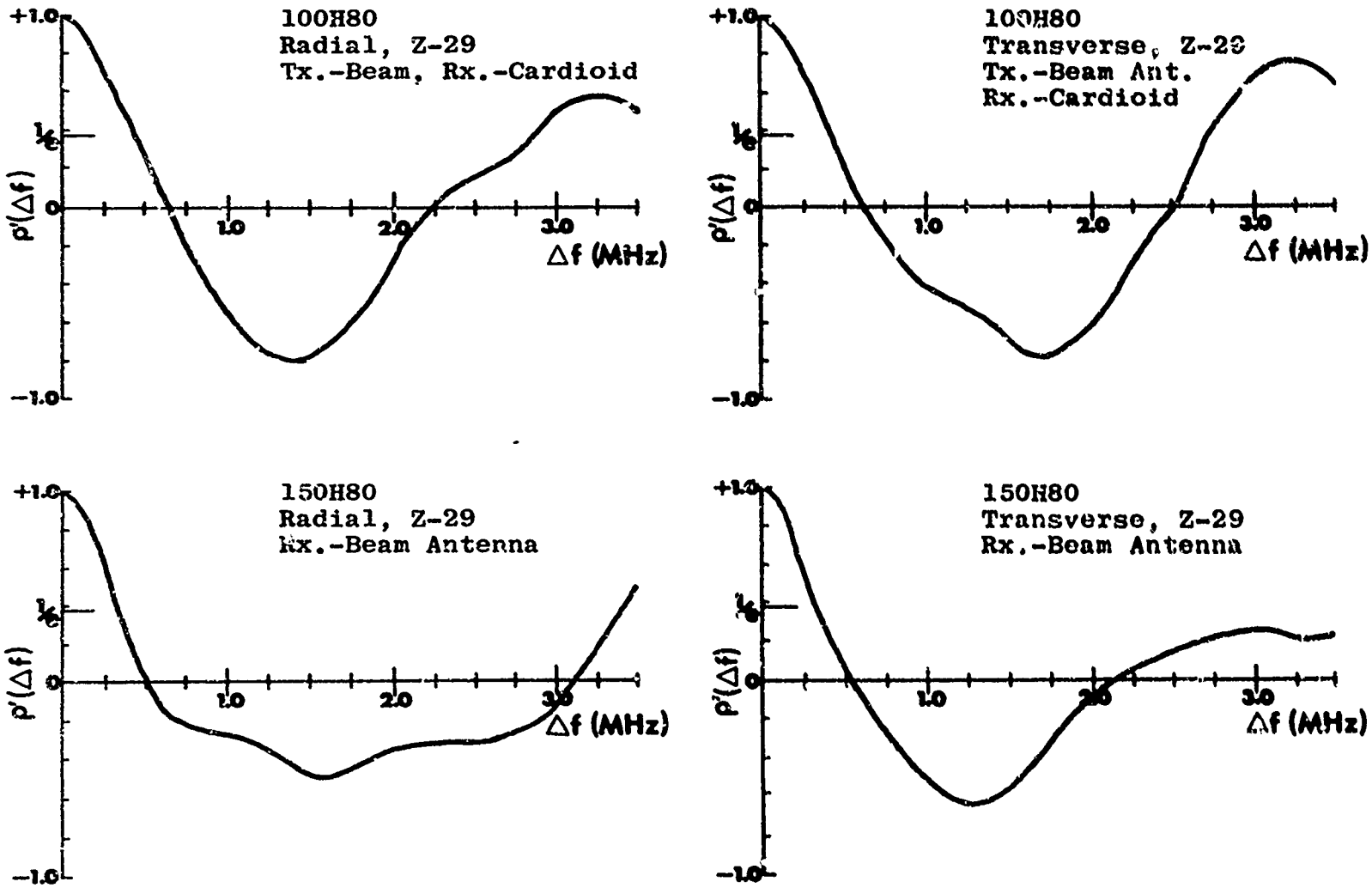

Figure 3.1m Frequency Correlation Functions of the Envelope

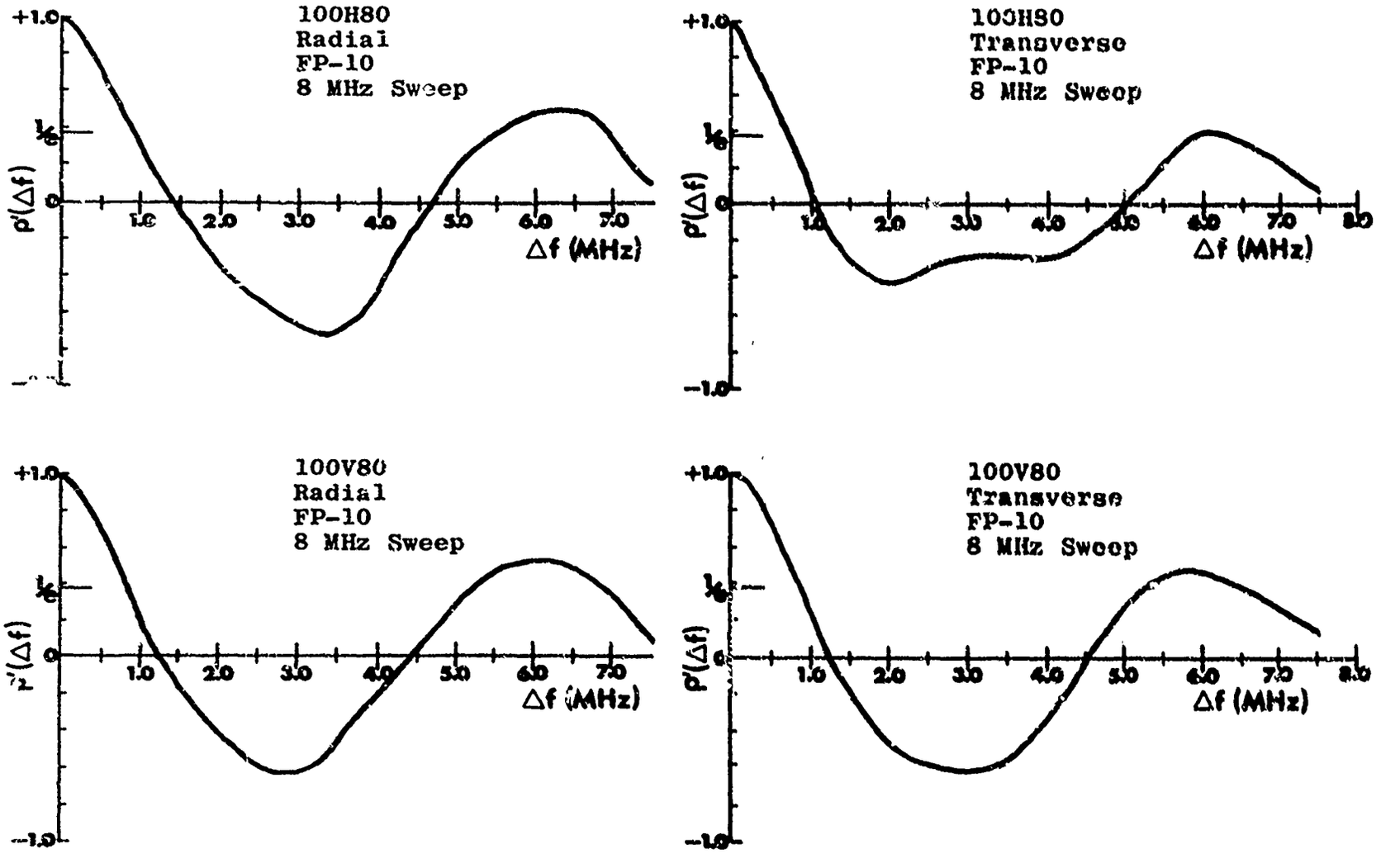

Figure 3.1n Frequency Correlation Functions of the Envelope

profile [Schwartz, Bennett and Stein, 1966], indicates a dominant multipath with, in the present case, a relative delay of 1/period ≈ 0.5 to 1 μsec. Note also that the correlations tend to become positive near the maximum lag after having been negative. This is true for both the 3.5 and 8 MHz sweep-width results and may be interpreted as indicating quasi-periodic components with periods of ≈ 3 and 6 MHz. Such periodic components of longer period indicate relatively distinct multipaths of shorter relative delay and are generally of lesser significance than the multipaths of longer delays, other things being equal.

Another characteristic of the frequency correlations, and probably of greater significance, is the frequency separation at which the correlations drop to 1/e, which is termed the "coherent bandwidth." The coherent bandwidth provides an order-of-magnitude estimate of the maximum operational bandwidth permissible if frequency-selective fading and intersymbol interference and, hence, irreducible error rates are to be avoided in digital transmissions [Schwartz, Bennett and Stein, 1966]. The coherent bandwidth also provides an order-of-magnitude estimate of the minimum frequency separation required for frequency diversity with either narrowband or wideband transmissions in the environment. For frequency diversity with wideband systems the frequency separation would, of course, have to be proportionately wider to accommodate the information bandwidths. For complete decorrelation of fading on the two diversity channels, frequency spacing an order-of-magnitude larger than the coherent bandwidth has been suggested [Stein and Jones, 1967].

Values of the coherent bandwidth from the envelope frequency correlations are presented in Table 3.1. The minimum coherent bandwidth is shown to be 0.29 MHz, the maximum is

Table 3.1
Coherent Bandwidths From Frequency Correlations of the Envelope

Freq. (MHz)	Polarization	FIELD POINT FP-10	Y-20	Y-25	Z-29[1]	AVERAGES FP-10	Y-20	Y-25	Z-29	All Field Points	Both Polarizations
50	H[2]	[4]R 0.45 [5]T 0.38	R 0.37 T 0.31	R 0.37 T 0.30	R 0.50 T 0.39	0.42	0.34	0.34	0.44	0.38	0.38
50	V[3]		R 0.37 T 0.40	R 0.31 T 0.32	R 0.49 T 0.46	-	0.38	0.32	0.48	0.39	
100	H	R 0.36 T 0.40	R 0.29 T 0.29	R 0.33 T 0.29	R 0.42 T 0.51	0.38	0.29	0.31	0.46	0.36	0.38
		R 0.91 T 0.74 }[6]			R 0.35 T 0.47 }[8]	0.82[7]			0.41[7]		
					R 0.30 T 0.41 }[9]				0.36[7]		
					R 0.45 T 0.42 }[10]				0.44[7]		
100	V	R 0.41	R 0.40 T 0.34	R 0.33 T 0.32	R 0.44 T 0.47	0.41	0.37	0.32	0.46	0.39	
		R 0.90 T 0.90 }[6]				0.90[7]					
150	H	R 0.39 T 0.47			R 0.41 T 0.39	0.43			0.40	0.42	0.41
					R 0.36 T 0.35 }[9]				0.36[7]		
150	V				R 0.41 T 0.40				0.40	0.40	
400	H				R 0.48 T 0.49				0.48[7]		
						0.41	0.34	0.32	0.44		0.39

1 Transmitter antenna height = 80 feet for this field point, 40 feet for all others.
2 H = Horizontal
3 V = Vertical
4 R denotes radial.
5 T denotes transverse.
6 Tests using 8 MHz bandwidth.
7 Special runs, not included in overall average.
8 Receiver antenna had a cardiod pattern.
9 Receiver antenna was a 6-element Yagi beam antenna.
10 Transmitter was beam antenna and receiver was antenna with cardiod pattern.

0.50 MHz, and the average (excluding the special runs) is 0.38 MHz. Some trends of the coherent bandwidth with frequency, polarization, radial and transverse motions of the antenna, etc., may be suggested, but these do not appear to be significant in view of the limited observations. For example, the most suggestive trend apparent is that the coherent bandwidth is different for different receiver locations in the forest. In this regard, note that the coherent bandwidths at FP-10 and Z-29 are generally somewhat larger than those at Y-20 and Y-25. A partial explanation of this might be the fact that the forest at FP-10 is less dense and the canopy height less than at the other three field points. This, of course, does not account for the relatively larger coherent bandwidths at Z-29, but the transmitter antenna was higher for the measurements at this point which may also partially account for the larger coherent bandwidths there. As is the case in general, however, too few observations, field points and antenna heights in the present example were examined to be conclusive about the effects on coherent bandwidth.

The fact that the coherent bandwidth was not increased by use of directive antennas should, perhaps, be discussed a bit since employing directional antennas is a fairly standard technique for reducing multipaths (which generally improves coherent bandwidth). Evidence indicates that the multipaths in the forested environment originate from the near vicinity of the antenna terminals (excluding mountains, airplanes, etc.) [Hicks and Robertson, 1969]. Thus, multipaths at either terminal contribute to the overall interference, and if multiple scattered signals are negligible (i.e., only single scattering is effective) then the resultant coherent bandwidth will be limited primarily by the terminal end having the worst multipath environment. Hence, employing a directive antenna at one end of the forested transmission link, when both ends are in a multipath environment, does not necessarily improve the coherent

bandwidth of the link. Employing a directive antenna at both ends presumably should improve the coherent bandwidth. The fact that it did not do so in the single such test performed in the present case is attributed to the fact that the cardioid pattern of the 2-element array eliminates multipaths from, roughly, only the back direction which, apparently, is not sufficient to seriously affect the longer delayed multipaths and, hence, coherent bandwidth, in the configuration tested.

The computed values of the envelope distance correlation coefficients (also connected by smooth curves) are shown in Fig. 3.2a-n. The nomenclature identifying the operational configurations is the same as in Fig. 3.1. The abscissa, or distance axis, of the correlations are expressed in units of wavelength because the correlations appear to be frequency dependent. In nearly all cases for radial motion, except those for the directive antennas, there is a quasi-periodic component in the correlations with period of $\approx 0.5\lambda$ to 0.75λ, with the periodicity being far more pronounced for horizontal than for vertical polarization. The correlation distance, or the distance at which the correlation falls to 1/e, for radial receive antenna motion is, excluding the directive antennas, $\approx 0.1\lambda$ for horizontal and $\approx 0.25\lambda$ to 0.75λ for vertical polarization.

For transverse receive antenna motion, excluding directive antennas, there is no periodic component for horizontal polarization, and the 1/e point is $\approx \lambda/2$ or greater, but for vertical polarization the periodic component is of about the same strength as it was for radial motion, with the period being somewhat longer ($\approx 0.5\lambda$ to 1λ), but the 1/e point is about the same.

The use of the directive antennas, one of which was always the receiving antenna, resulted in greatly reducing or eliminating the quasi-periodic component from the correlations and in increasing the correlation distance to, usually, $> \lambda$.

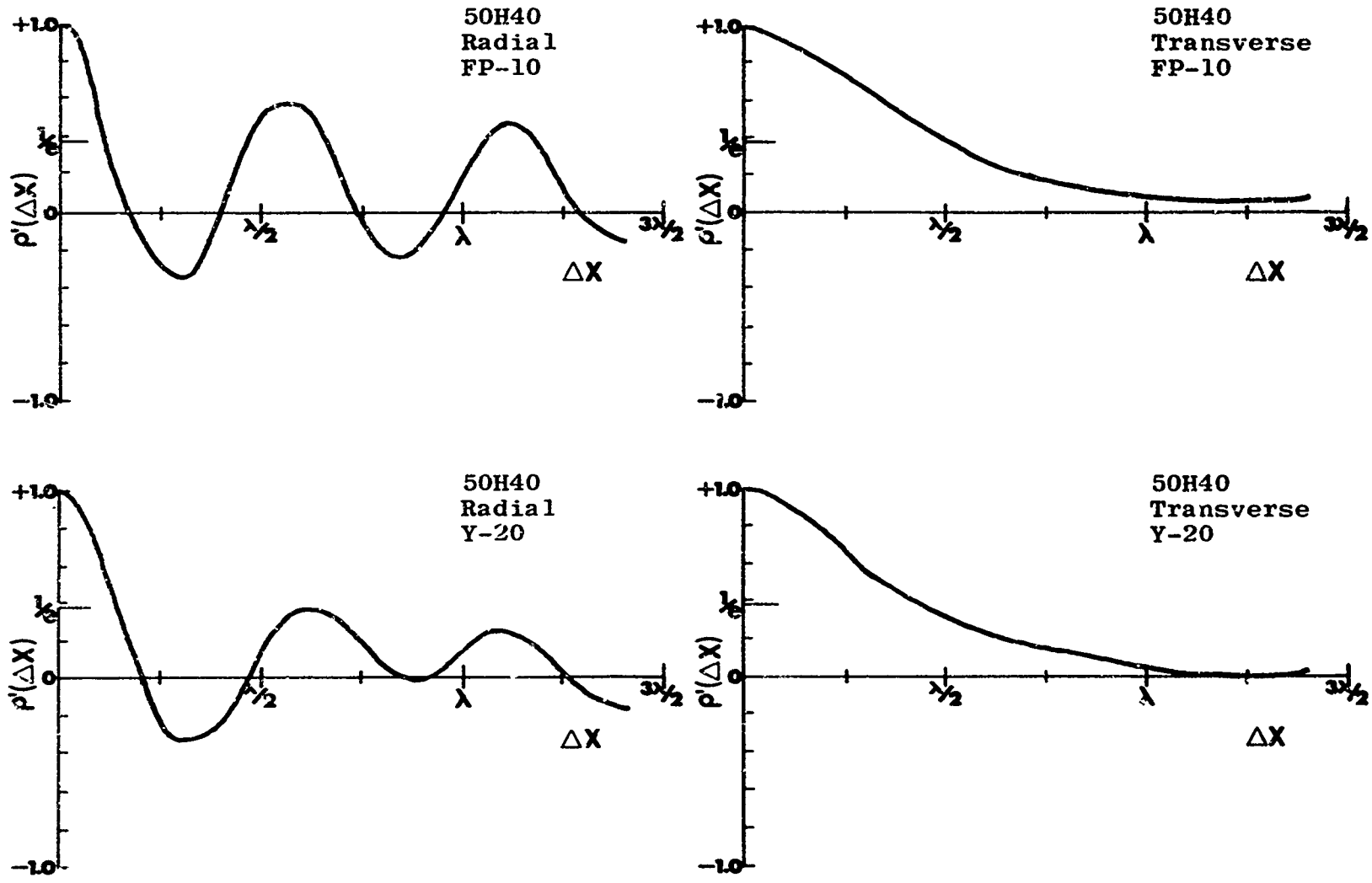

Figure 3.2a Distance Correlation Functions of the Envelope

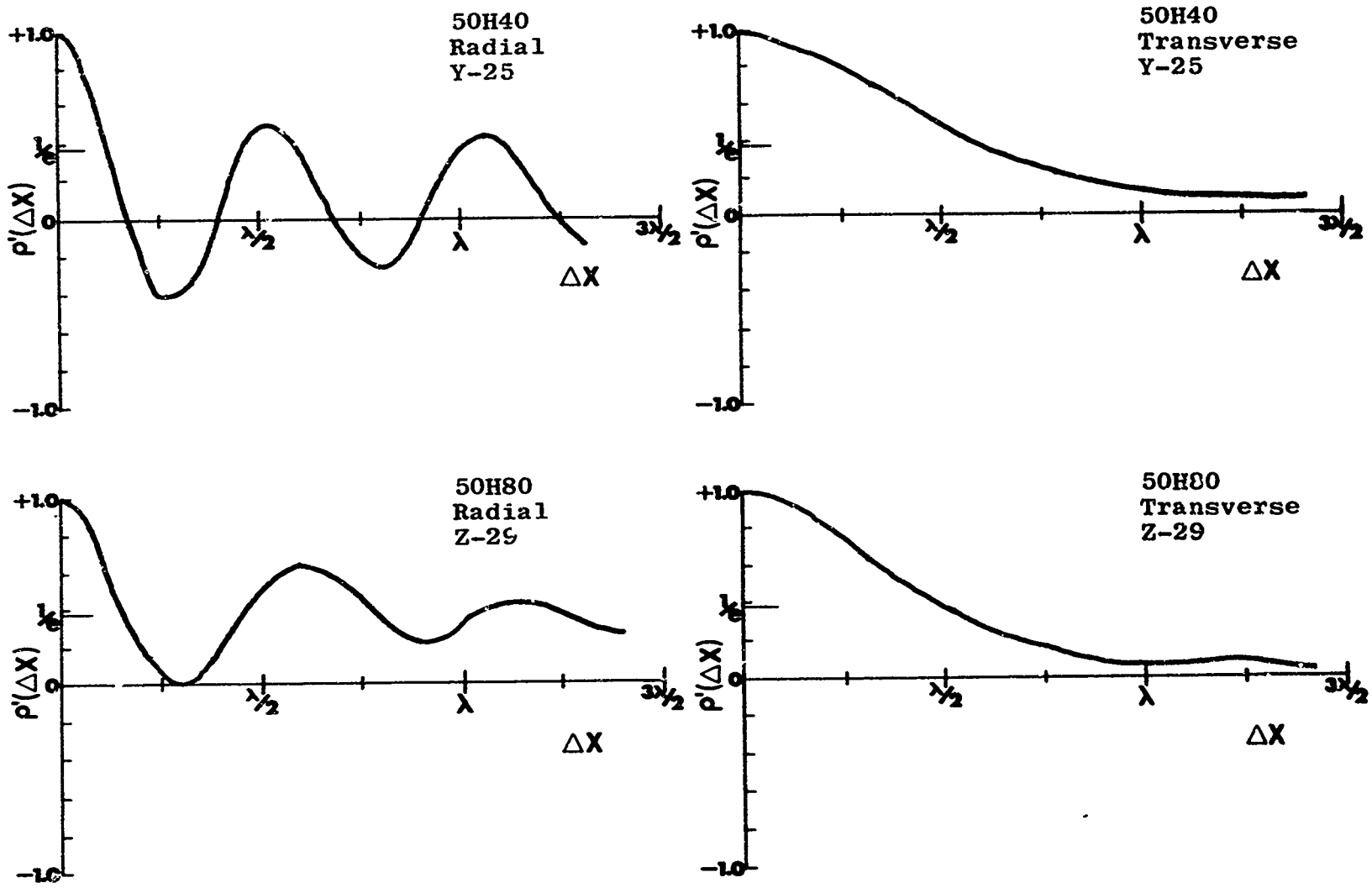

Figure 3.2b Distance Correlation Functions of the Envelope

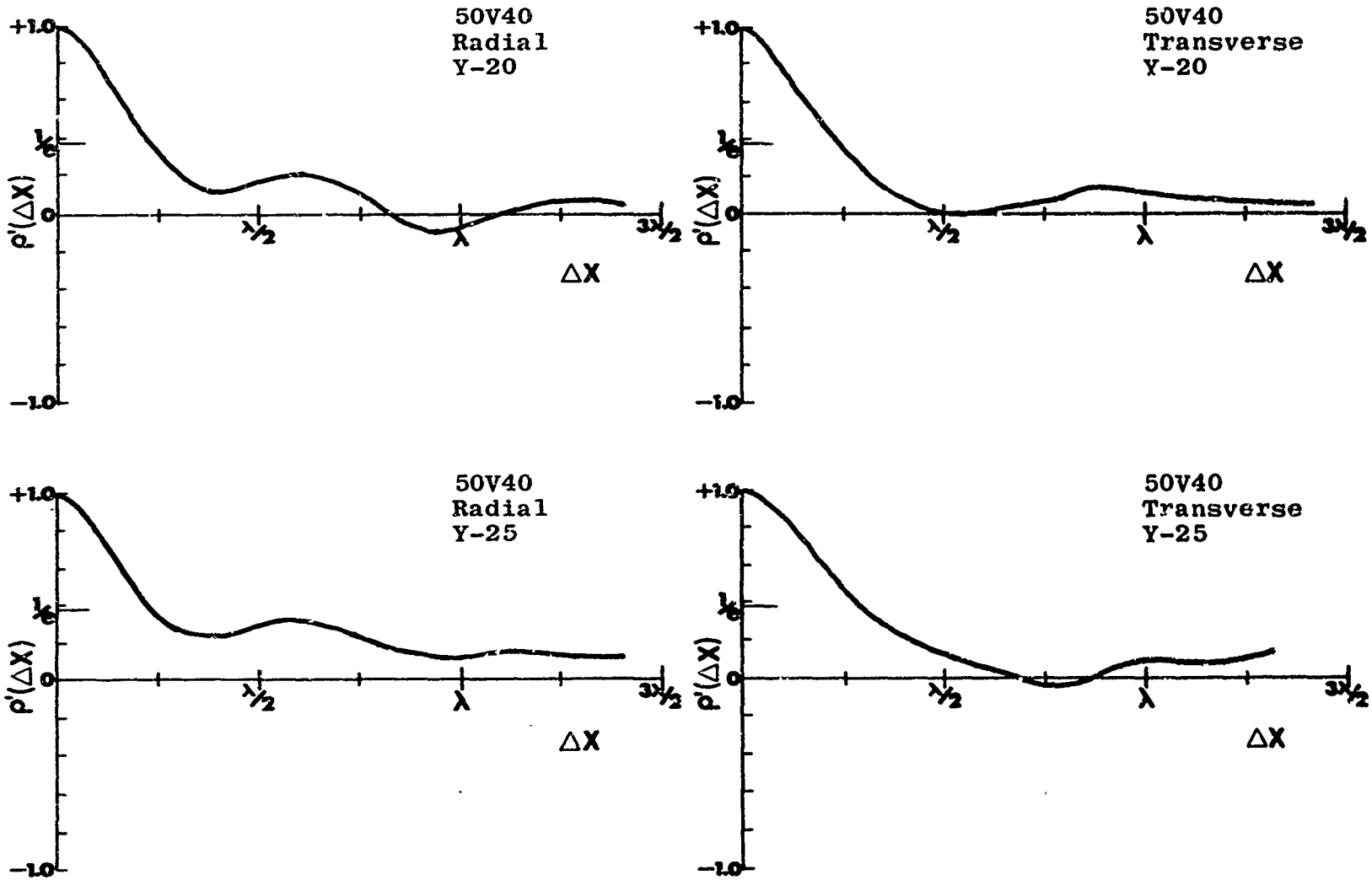

Figure 3.2c Distance Correlation Functions of the Envelope

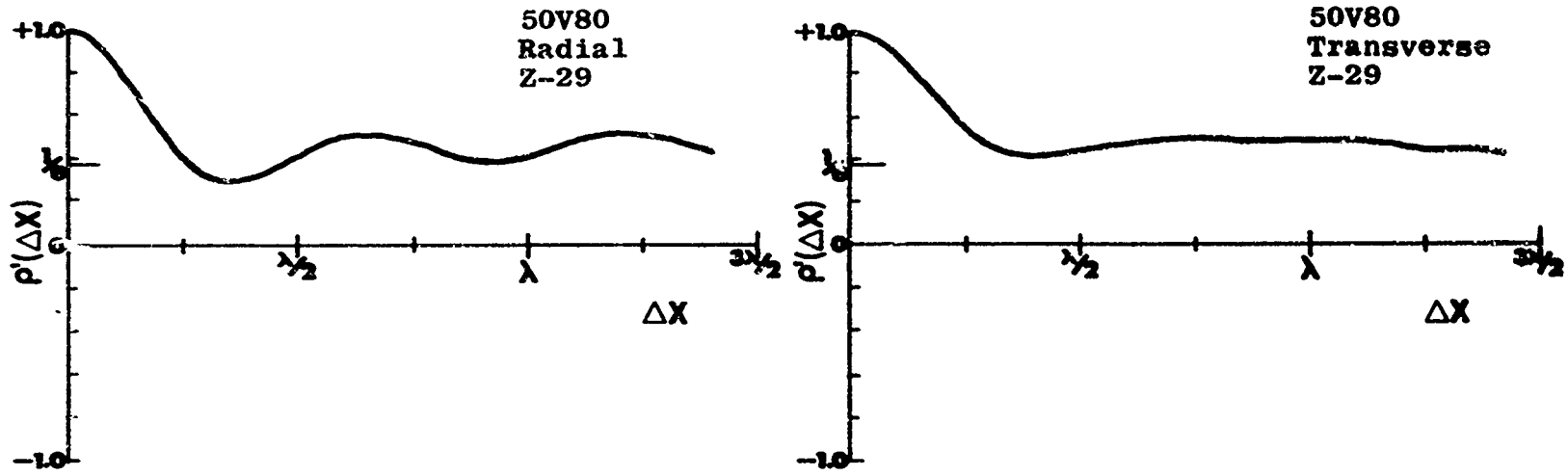

Figure 3.2d Distance Correlation Functions of the Envelope

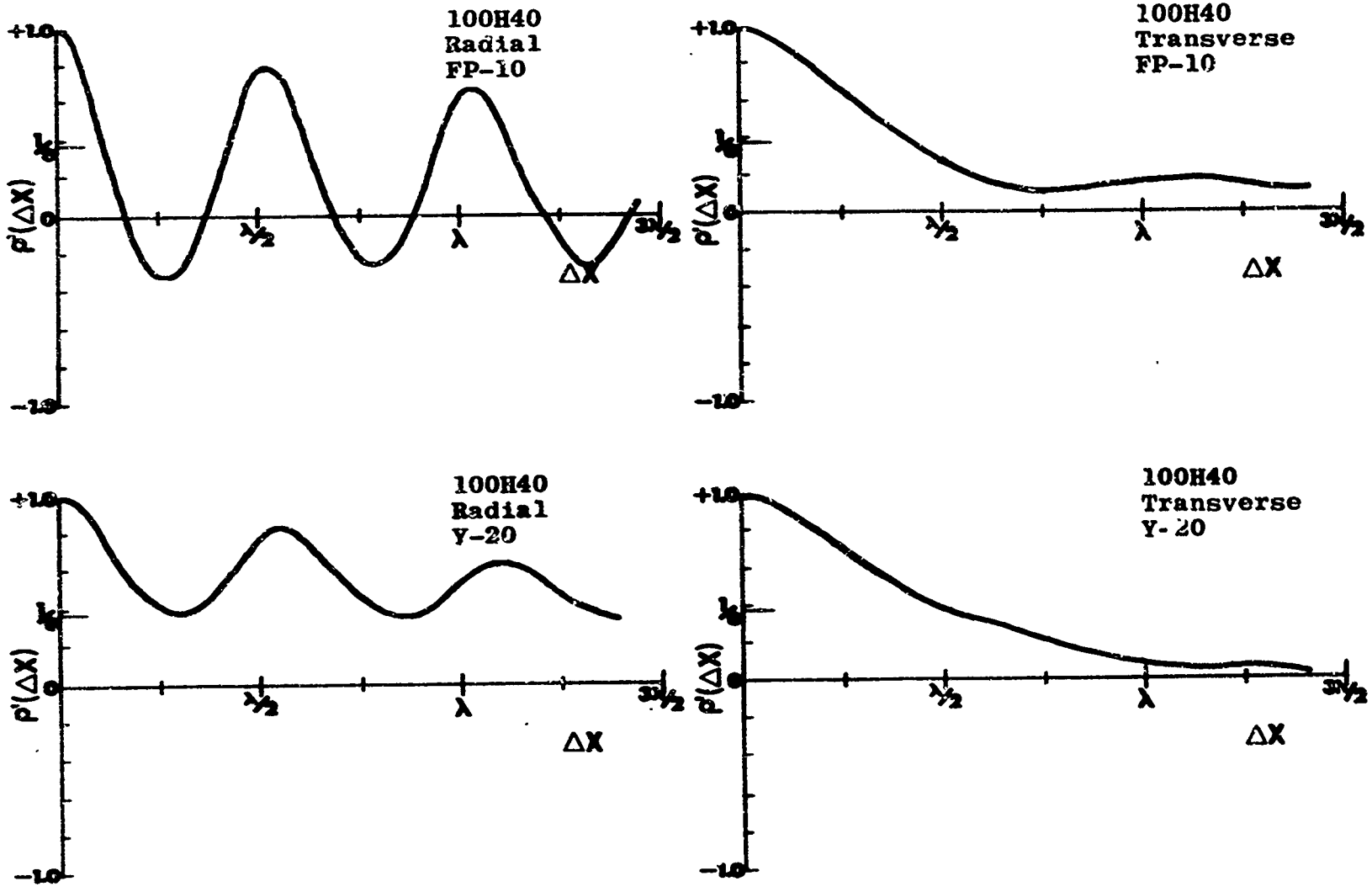

Figure 3.2e Distance Correlation Functions of the Envelope

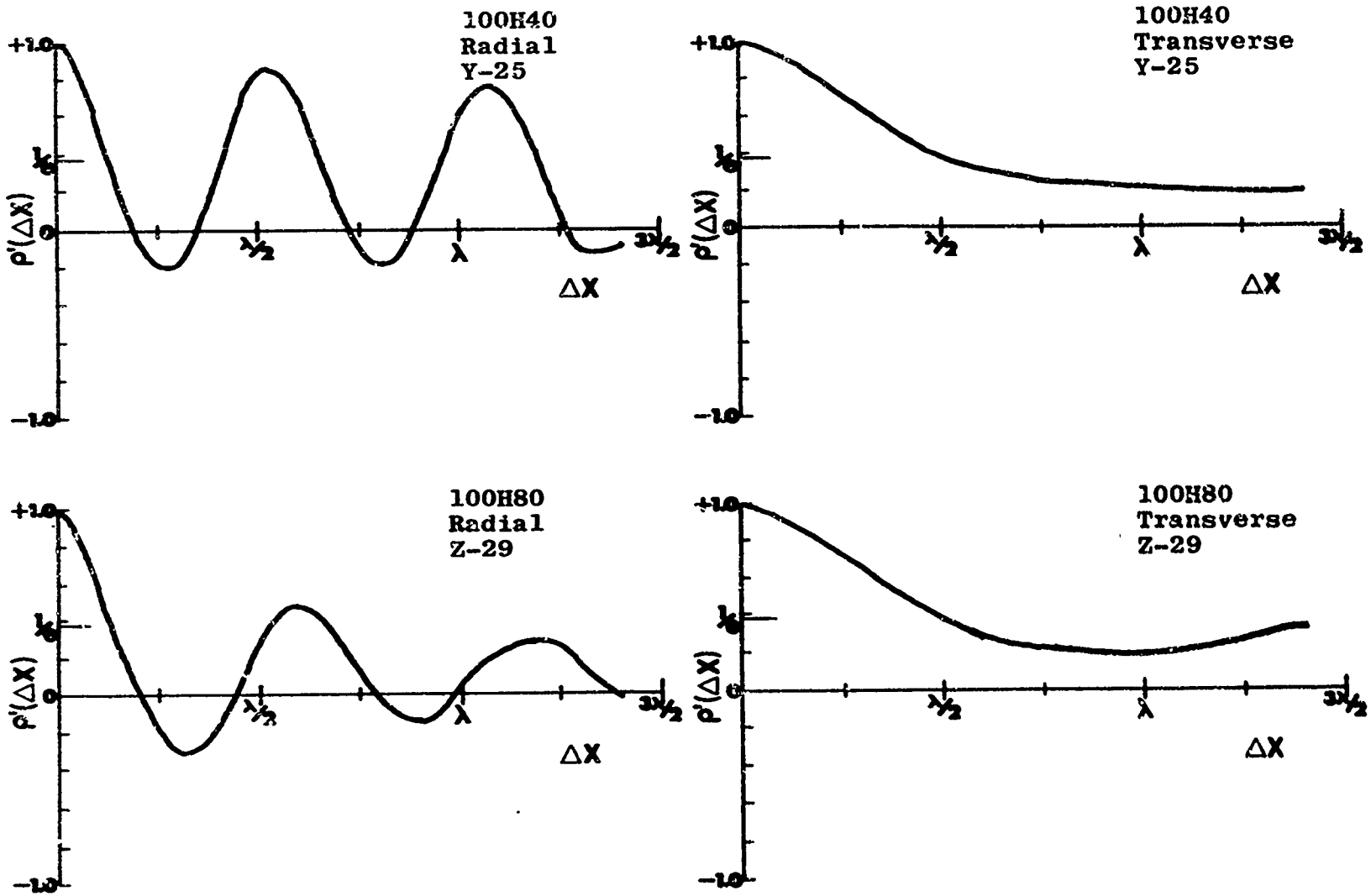

Figure 3.2f Distance Correlation Functions of the Envelope

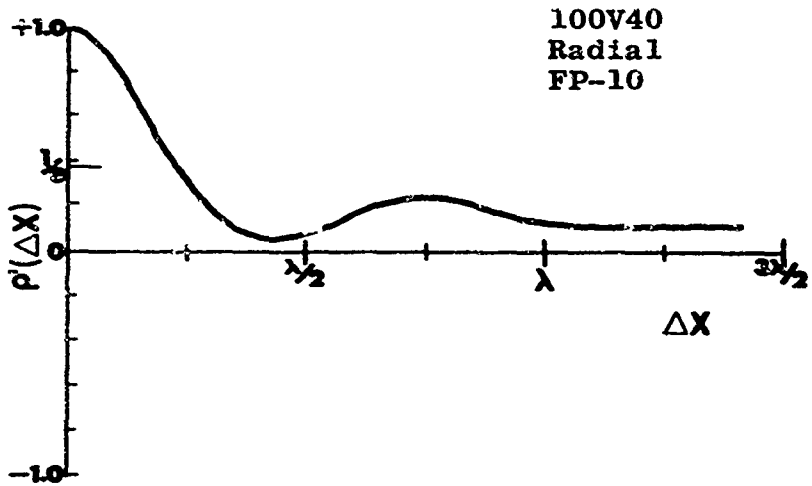

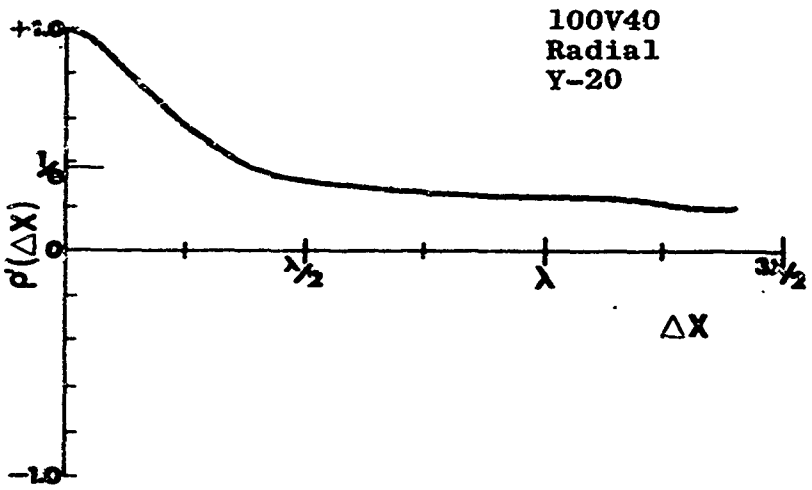

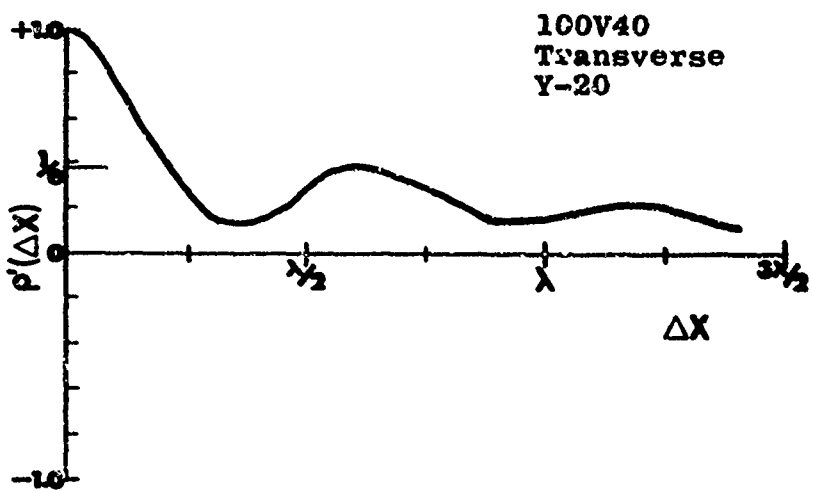

Figure 3.2g Distance Correlation Functions of the Envelope

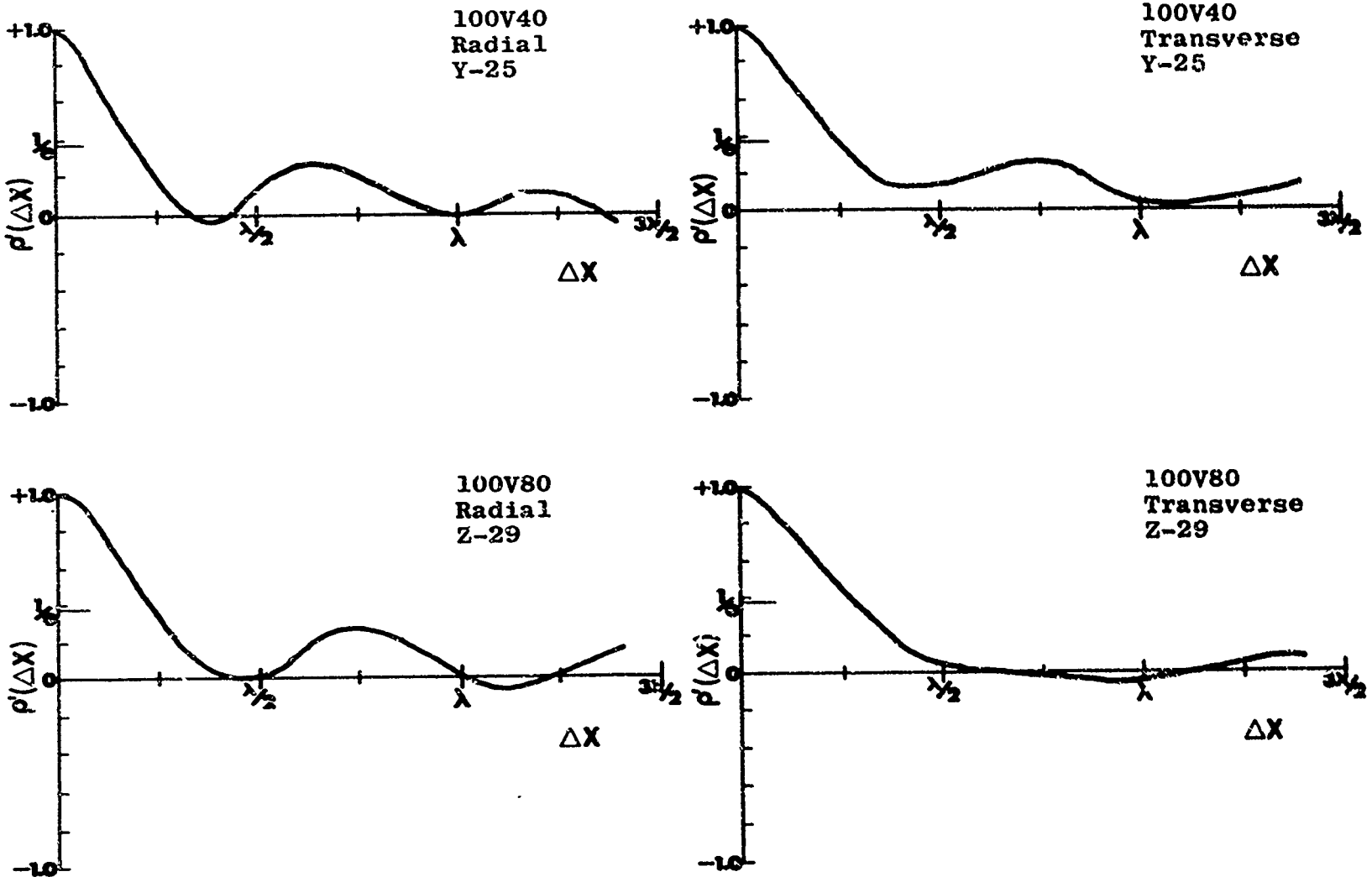

Figure 3.2h Distance Correlation Functions of the Envelope

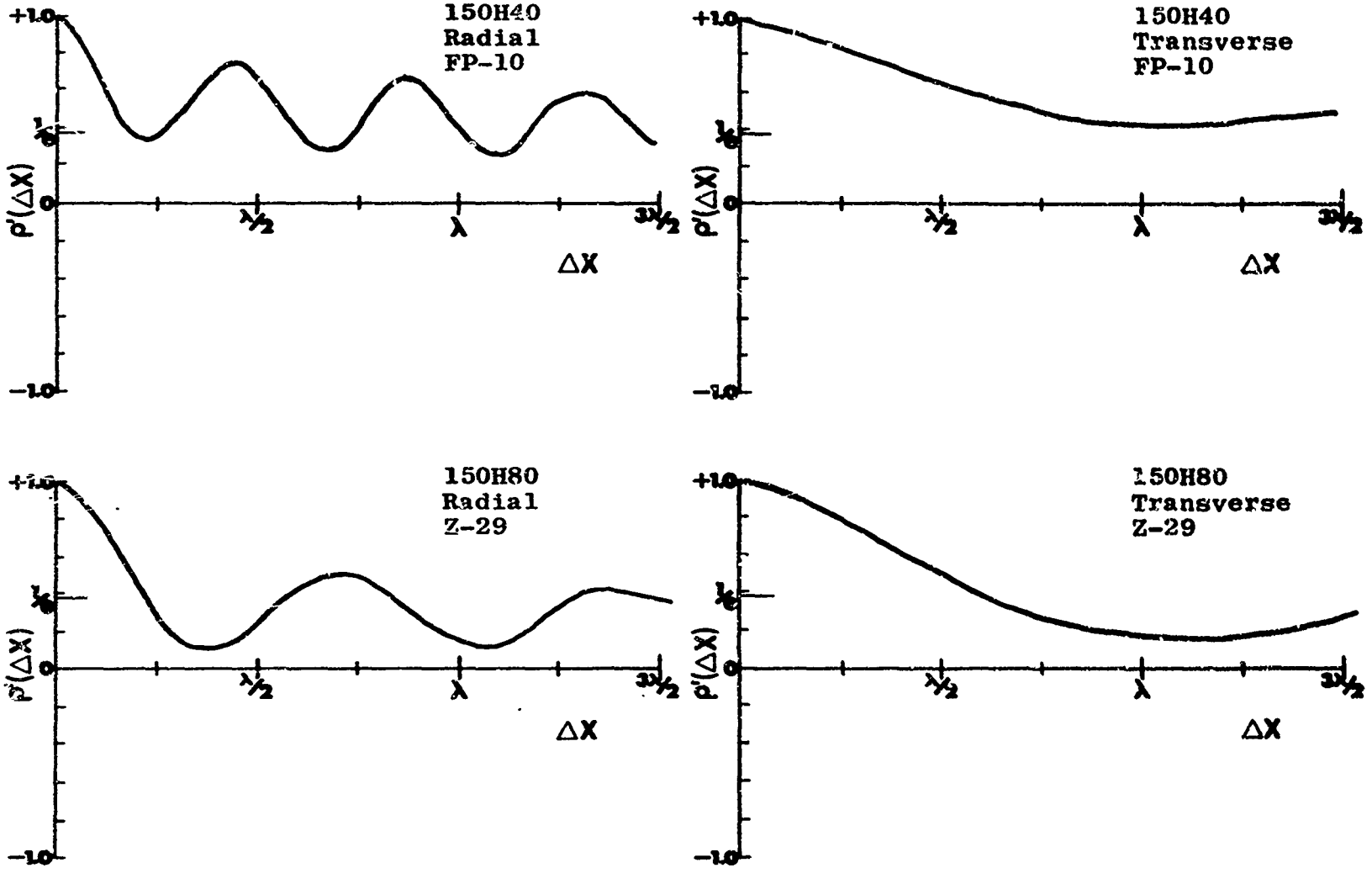

Figure 3.2i Distance Correlation Functions of the Envelope

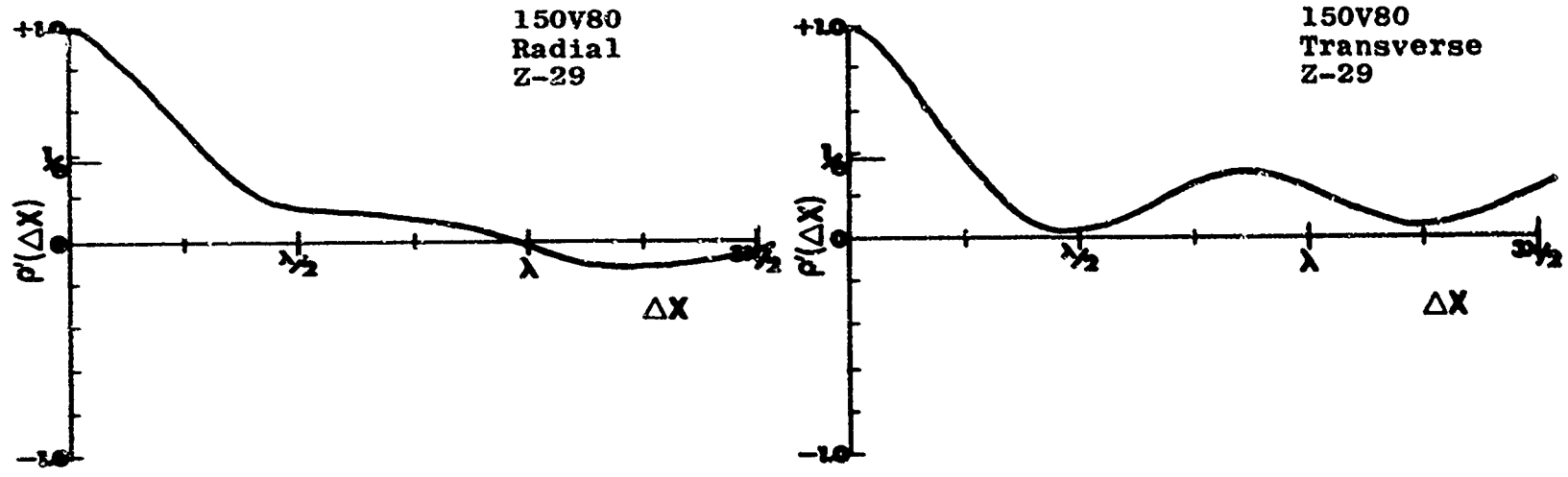

Figure 3.2j Distance Correlation Functions of the Envelope

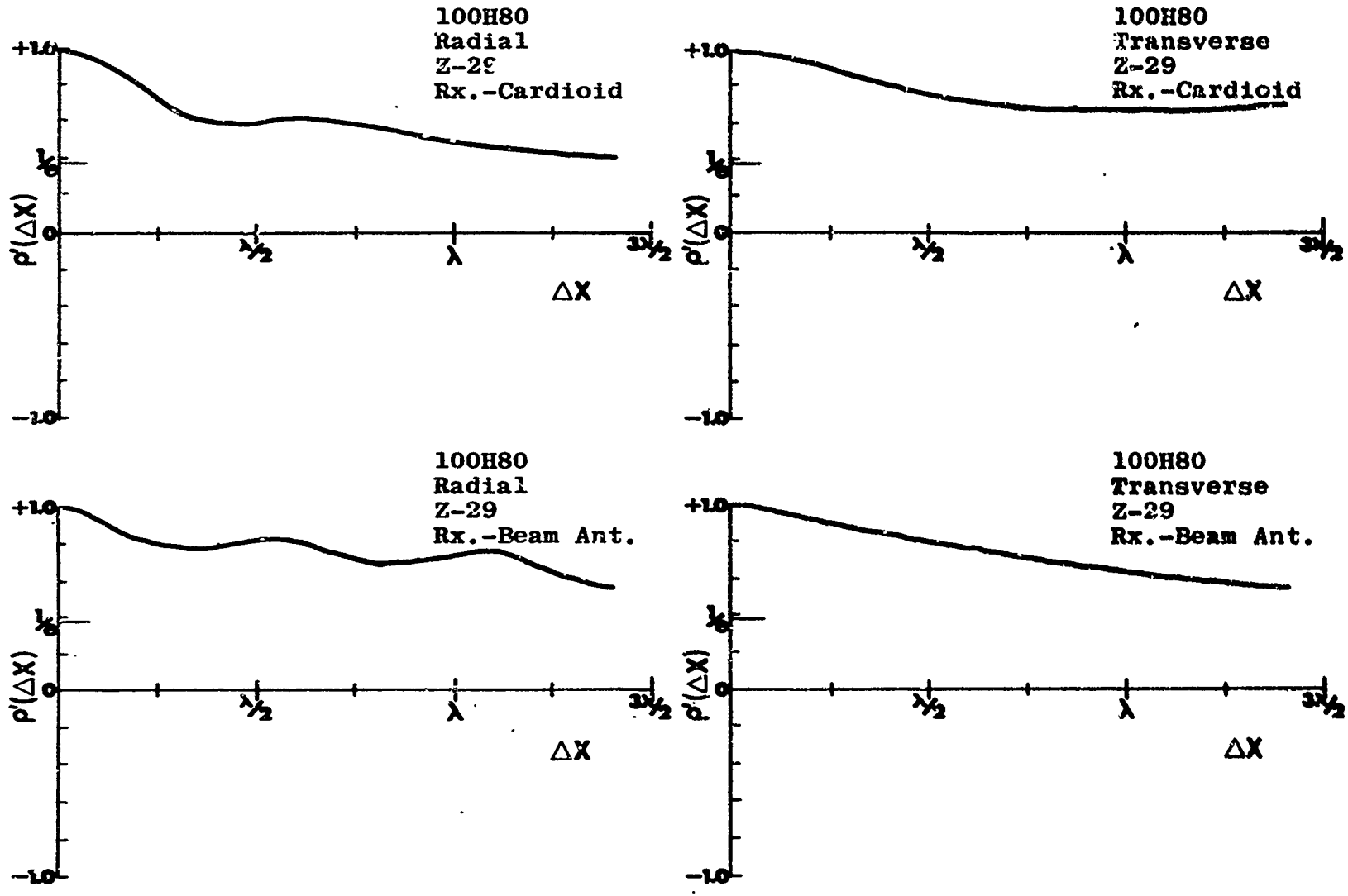

Figure 3.2k Distance Correlation Functions of the Envelope

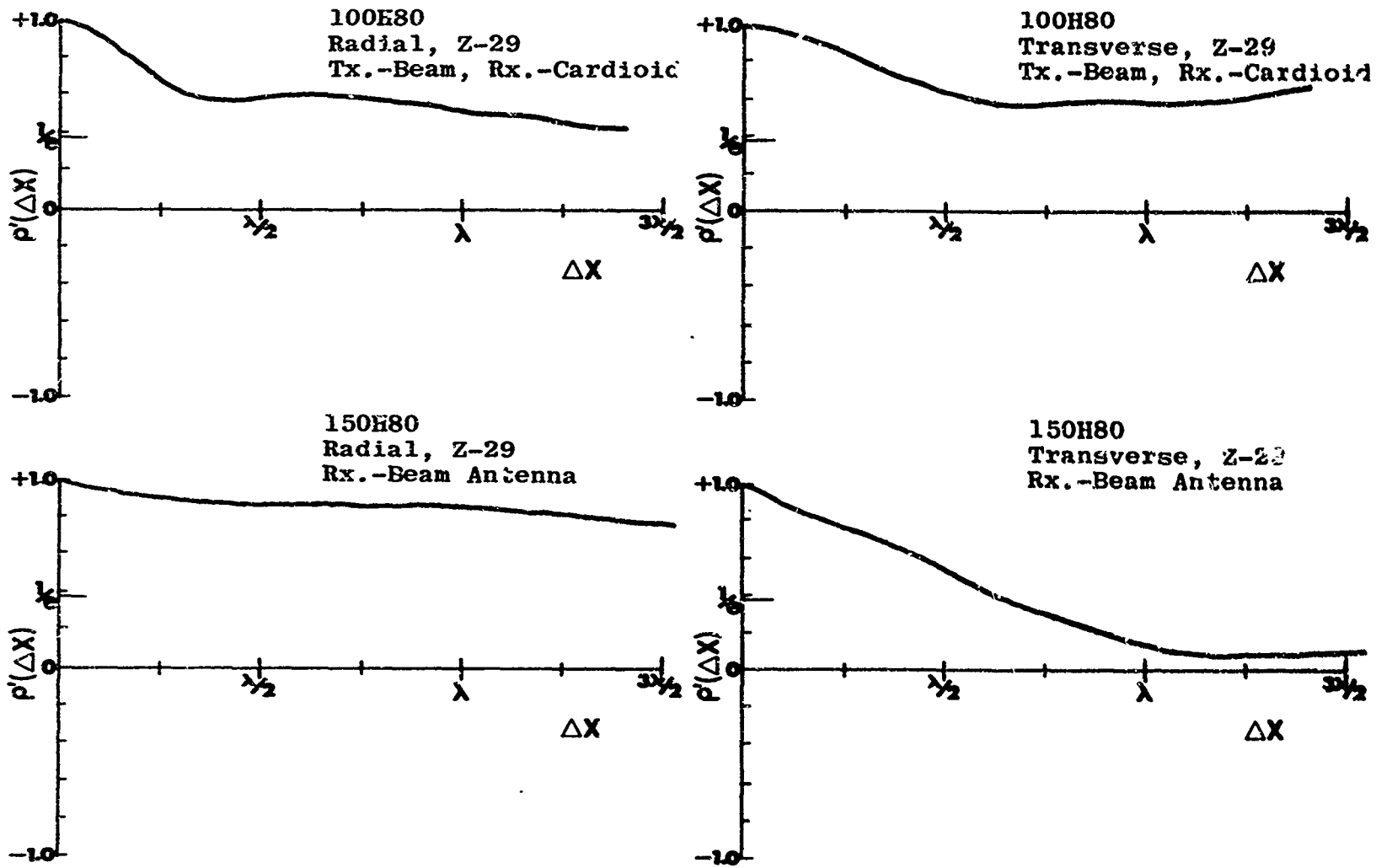

Figure 3.21 Distance Correlation Functions of the Envelope

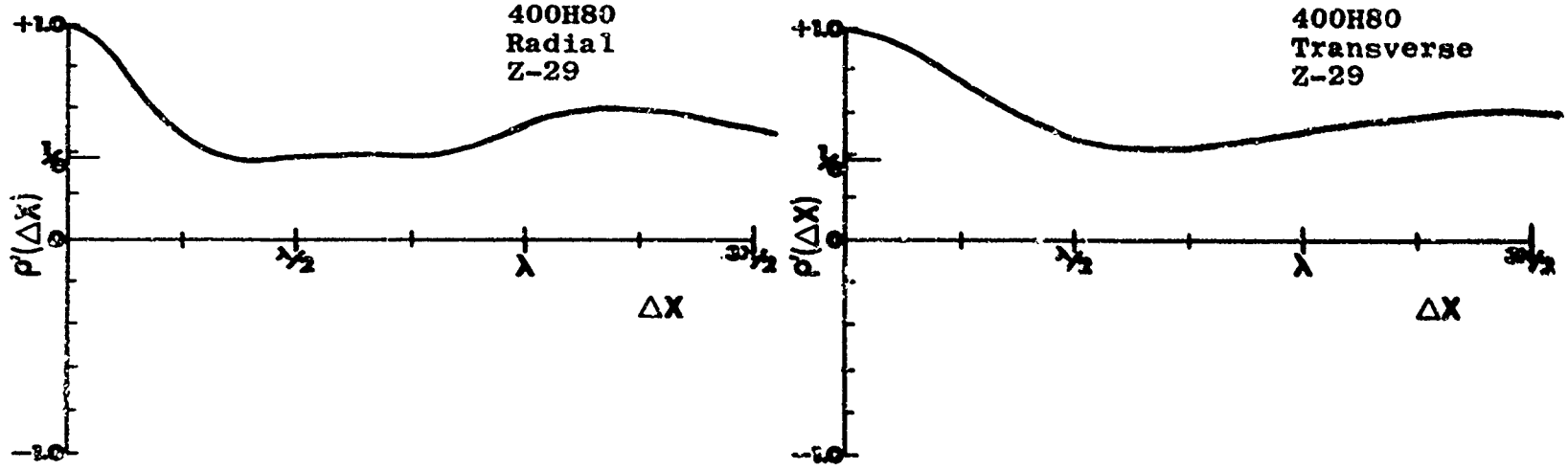

Figure 3.2m Distance Correlation Functions of the Envelope

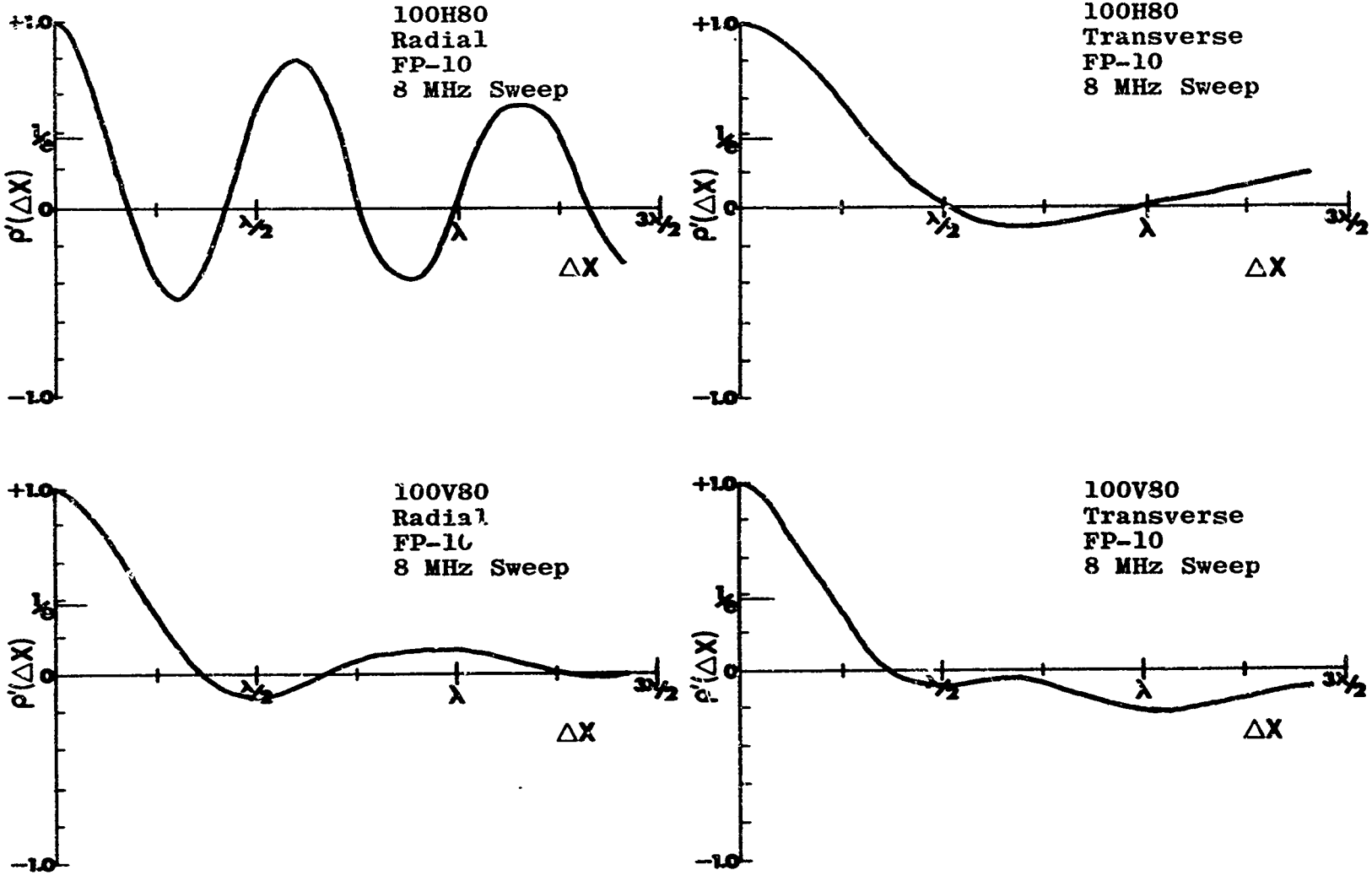

Figure 3.2n Distance Correlation Functions of the Envelope

All of the above characteristics of the distance correlations may be simply accounted for in terms of a qualitative scatter model wherein the scatter, or multipaths, originate from the vicinity of the terminals, as mentioned above in relation to the coherent bandwidths for the directive antennas. First, recall that for horizontal polarization the probability density function of the envelopes is generally Rician at VHF [Robertson, et al., 1970] which indicates a dominant signal plus lesser multipaths. Intuitively this dominant signal is also the most direct lateral wave. Also, the horizontal dipole, oriented for maximum gain toward the transmitter, discriminates against multipaths from the transverse direction (dipole ends). Hence, radial motion of the horizontal polarized receive antenna will observe interference between the direct component and multipaths from behind, above, and forward of the antenna, but not from the sides. The phase relation between the direct signal plus forward multipaths does not change significantly with the receiver antenna motion over short distances, but interference between the direct signal (plus forward multipaths) and those from above and behind the receive antenna results in standing waves with fairly short periods along the radial direction. The lower limit on the period is $\lambda/2$, which is for paths interfering from opposite directions and is analogous to the standing wave resulting from interference on transmission lines. Hence, the quasi-cyclic nature of the correlations for radial motion with horizontal polarization indicates interference between forward and primarily backward, or backscatter, multipaths. The absence of the short quasi-periodic component for transverse motion with horizontal polarization is attributed to the horizontal antenna discriminating against multipaths from the transverse directions, along with the intuitive expectation that the interference between the forward and backward multipaths does not change rapidly (the path lengths do not change significantly) with limited transverse motion.

For vertical polarization, however, the probability density function of the envelopes is generally Rayleigh [Robertson, et al.,1970], which indicates a more uniform set of multipaths as opposed to having a dominant one. Further, the vertically polarized antenna discriminates against signals from above and, hence, does not favor multipaths from either the radial or transverse direction. Thus, receive antenna motion in the radial or transverse direction should be similar, as it is.

The directive antennas discriminate against multipaths from, primarily, the backward (behind the receiver) and side directions. Hence, interference between signals from opposite directions, as analogous to that on transmission lines, is greatly reduced, which virtually eliminates the possibility of short quasi-cyclic variations for either transverse or radial receive antenna motion.

It should, perhaps, be mentioned that only the receiver was moved in these investigations, but it is expected that similar results would be obtained for either, or both, antennas in motion. Also, the distance fading and correlation distance may be transformed to time fading and correlation time for mobile applications by the transformation of (fades or correlation/distance) (velocity) = (fades or correlation)/unit time.

3.2 Complex Frequency and Distance Correlations, Intensity Profiles and Probability Distribution of the Envelope

The procedures followed in obtaining the complex signal were similar in principle to those employed with the envelope data. Yet, they are sufficiently different in detail to warrant separate discussion. The analysis of the complex data to obtain the correlations is also quite similar to that

done with the envelope data. However, it is possible to utilize the complex frequency correlations, through Fourier transforms, to obtain the intensity profiles of the multipaths which, without employing questionable assumptions, cannot generally be accomplished with the envelope data alone [Stein and Jones, 1967]. The analysis of the complex data includes computation of intensity profiles, and also first order probability functions. First, the experimental procedures, which have been discussed previously [Robertson, et al., 1969] are briefly reviewed, and the analyses are discussed in the next section.

3.2.1 Experimental Data and Measurement Procedures

The propagation measurements were made in Area II. The data are photographs of the scope face of a dual beam oscilloscope displaying the amplitude and relative phase of the received signal as a function of swept frequency. The frequency sweep-width was 4 MHz, centered about the test frequency. The test frequencies were 50, 100 or 150 MHz and both horizontal and vertical polarization were used. The transmitting antenna height was either 80 or 95 feet and the receive antenna height 6 feet. Half-wave dipole antennas were used for transmitting and receiving and were aligned for maximum gain along the line-of-sight between transmitter and receiver. The relative phase of the received signal is referenced to the signal phase at a directive (Yagi) antenna, generally elevated to near the tree-top level in the general vicinity of the receiver. The receiver was a vector voltmeter, which yielded the signal amplitude and relative phase for display on the oscilloscope.

It should, perhaps, be mentioned that positioning the reference antenna to obtain a flat amplitude versus swept-frequency spectrum from the reference antenna (which indicates

a lack of interfering multipaths at the reference antenna and thus a reliable reference) was usually a laborious trial-and-error procedure. This was not unexpected, since multipaths are expected to originate from the general vicinity of either terminal. The reference antenna, however, was made directive in an effort to reduce the multipaths originating from near the receiver and thereby aid in the search for a distortionless reference signal. This directivity probably helped, but still three to four hours of searching with the reference antenna while monitoring its amplitude versus swept-frequency response was often required to obtain a reliable reference. However, with sufficient searching, a reference whose amplitude ripple on the swept-frequency trace was < 3dB, which was assumed satisfactory, was obtained. The procedure of locating a satisfactory reference was repeated for each run.

A complete set of data representing one run, or operating configuration of center frequency, polarization, transmitting antenna height, etc., consists of a series of photographs of the amplitude and relative phase versus swept-frequency traces, taken sequentially at equally spaced distance intervals. In some runs the receive antenna motion was radial from the transmitter and in others it was transverse. The antennas were stationary and the wind effects were small while each photograph was taken. The distance separation between adjacent photographs was 6" at center frequencies of 100 and 150 MHz and 12" at 50 MHz. The receive antenna was mounted on a motor-driven unit, used to move the antenna between photographs, which operated over the length of a transportable bench 40 feet long. A stable receive antenna mounting, as was afforded by this method, was required in order to prevent variations in the data which could be caused by antenna motion (even slight) during a frequency sweep, which had to be relatively slow to accommodate phase determination by the vector voltmeter.

Each run may be viewed as an ensemble of amplitude and relative phase versus frequency functions taken over distance, as was the case for the envelope data, and similarly provide the samples for computing the complex frequency and distance correlation functions (one each) representative of that run.

3.2.2 Reduction and Analysis of Complex Data

The first step in the reduction of the complex data was to digitize the amplitude and relative phase of each swept-frequency photograph by sampling at frequency intervals of 0.25 MHz. The digitized amplitude values for each photograph were then adjusted, if required, by the appropriate constant determined by any gain adjustments required between photographs during a run. It is noted that the amplitude response of the vector voltmeter provided a flat response to the transmitted sweep (when the signal was not influenced by the environment) and hence permitted use of data over the full 4 MHz sweep-width.

3.2.2.1 Complex Frequency and Distance Correlations and Envelope Correlations

Using the digitized values of the complex data above, the next step was to remove linear trends in the phase response with frequency and distance. These linear trends were present in the phase data because the test and reference antennas were at different ranges from the transmitter, which results in there being a time delay in signal arrival between the reference and test antennas. This, in turn, results in a linear change in phase as a function of frequency over each sweep. Further, because the test antenna is repositioned between swept-frequency

photographs for a run, the time delay is different for each photograph for radial runs which, because the photographs are equally spaced, introduces a linear trend in phase with distance. These linear trends in the phase and the method of their removal are discussed in greater detail in Appendix B. It is noted here, however, that their removal simply refers the phase of all data points within a run to a common (zero) phase origin representative of the phase of the most direct, or earliest, signal. Intuitively, this most direct signal is the (nonscattered) lateral wave and is also the most dominant of the several multipaths. A dominant, steady signal plus less intense multipath signals implies a Rician distribution to the envelopes, which is, indeed, generally the case for horizontal polarization at VHF in the forested environment [Robertson, et al., 1970]. This steady component is generally removed from the data prior to (or during) the computation of the correlation function [Stein and Jones, 1967] since it represents a non-zero mean in the data. Having referenced all phases to the zero phase of this component facilitates the removal of this dominant component and is accomplished next by removing the constant complex mean from the data of each photograph.

The resulting digitized amplitude and phase samples of $H(f,x)$, with the constant complex mean removed, are designated $b(f_i; x_k)$ and $\phi(f_i; x_k)$, respectively, where $i = 1, 2, \ldots, 17$ identifies the sample position at each 0.25 MHz across each swept-frequency photograph, and $k = 1, 2, \ldots, N$ identifies the distance positions of the successive photographs.

The general expression for the normalized complex frequency-distance cross covariances has been given in Eq.(3.1). In terms of the digitized complex quantities, the complex frequency correlation coefficients, $r(q)$, are computed from Eq.(3.1) by letting $\Delta x = 0$, as

$$r(q) = \frac{R(q) - M_1 M_2^*}{\sqrt{\sigma_1^2}\ \sqrt{\sigma_2^2}} \tag{3.11}$$

where

$$R(q) = \frac{1}{N(17-q)} \sum_{k=1}^{N} \sum_{i=1}^{17-q} b(f_i;x_k)\, b(f_{i+q};x_k)\, e^{j[\phi(f_i;x_k) - \phi(f_{i+q};x_k)]} \tag{3.12}$$

$$M_1(q) = \frac{1}{N(17-q)} \sum_{k=1}^{N} \sum_{i=1}^{17-q} b(f_i;x_k)\, e^{j\phi(f_i;x_k)} \tag{3.13}$$

$$M_2(q) = \frac{1}{N(17-q)} \sum_{k=1}^{N} \sum_{i=1}^{17-q} b(f_{i+q};x_k)\, e^{j\phi(f_{i+q};x_k)} \tag{3.14}$$

$$\sigma_1^2(q) = \frac{1}{N(17-q)} \sum_{k=1}^{N} \sum_{i=1}^{17-q} \left| b(f_i;x_k)^2 - M_1(q) \right|^2 \tag{3.15}$$

$$\sigma_2^2(q) = \frac{1}{N(17-q)} \sum_{k=1}^{N} \sum_{i=1}^{17-q} \left| b(f_{i+q};x_k)^2 - M_2(q) \right|^2 \tag{3.16}$$

where, for simplicity in notation, $\Delta f = 0.25\ q$ MHz, $q = 0, 1, 2, \ldots, 16$ and $j = \sqrt{-1}$. Both the magnitude and phase of the frequency correlations are obtained from Eqs.(3.11)-(3.16). These equations are also employed, with $\phi = 0$, to compute the frequency correlation from the envelopes of the complex data, and a constant mean was removed from each envelope trace.

The complex distance correlation coefficients, r(p), are computed from Eq.(3.1) by letting $\Delta f = 0$, as

$$r(p) = \frac{R(p) - M_1 M_2^*}{\sqrt{\sigma_1^2}\ \sqrt{\sigma_2^2}} \tag{3.17}$$

where

$$R(p) = \frac{1}{17(N-p)} \sum_{k=1}^{N-p} \sum_{i=1}^{17} b(f_i; x_k) b(f_i; x_{k+p})\, e^{j[\phi(f_i;x_k) - \phi(f_i;x_{k+p})]} \tag{3.18}$$

$$M_1(p) = \frac{1}{17(N-p)} \sum_{k=1}^{N-p} \sum_{i=1}^{17} b(f_i; x_k)\, e^{j\phi(f_i; x_k)} \tag{3.19}$$

$$M_2(p) = \frac{1}{17(N-p)} \sum_{k=1}^{N-p} \sum_{i=1}^{17} b(f_i; x_{k+p})\, e^{j\phi(f_i; x_{k+p})} \tag{3.20}$$

$$\sigma_1^2(p) = \frac{1}{17(N-p)} \sum_{k=1}^{N-p} \sum_{i=1}^{17} \left| b(f_i; x_k)^2 - M_1(p) \right|^2 \tag{3.21}$$

$$\sigma_2^2(p) = \frac{1}{17(N-p)} \sum_{k=1}^{N-p} \sum_{i=1}^{17} \left| b(f_i; x_{k+p})^2 - M_1(p) \right|^2 \tag{3.22}$$

Employing Eqs.(3.17)-(3.22) gives the magnitude and phase of the complex distance correlation coefficients at values of

$\Delta x = \rho(a)$, where $a = 6''$ at frequencies of 100 and 150 MHz and $12''$ at 50 MHz, and $p = 0, 1, 2, \ldots, N - 1$.

3.2.2.2 Intensity Profiles

The Fourier transform of the complex frequency correlation function of the channel transfer function gives the intensity profile of the multipath channel [Stein and Jones, 1967]. The intensity profile is essentially a distribution of the relative energy in the various multipaths as a function of the multipath delays.

The Fourier transform, $A(\tau)$, of the complex frequency correlations discussed in the previous section were obtained with the aid of a digital computer. The relation used for this computation is [Jenkins and Watts, 1968]

$$A(\tau) = 1 + 2 \sum_{k=1}^{16} |\rho(k\Delta f)| \cos [2\pi k\Delta f\tau - \phi(k\Delta f)] \qquad (3.23)$$

where $|\rho(k\Delta f)|$ and $\phi(k\Delta f)$ are the magnitude and phase of the complex frequency correlation coefficients at lag $k\Delta f$, and values of τ were -0.5, -0.45, -0.40, ..., 0, +0.05, +0.1, +0.15, ..., +2.0 μsec. The intensity profiles were truncated at $\tau = -0.5$ because there appeared to be very little energy for negative τ's beyond this point. Intensity profiles, computed from Eq.(3.23), will be presented following the presentation of the complex frequency correlation function.

3.2.2.3 First Order Probability Function

The first order probability functions of a large amount of envelope data at VHF from the same forest environment discussed in this report (Area II) were presented in an earlier report [Robertson, et al.,1970]. However, those measurements were made at CW and hence were not amenable to frequency correlation analysis (second order probability) as are the swept-frequency data discussed in this report. It would seem worthwhile, however, to examine the first and second order probabilities from the same data. Hence, with the aid of a digital computer, the digitized envelope values of the complex data for each of seven runs were compared with fifteen predetermined amplitude levels. The number of envelope values exceeding each level were counted and normalized by the total number of envelope values. This results in a histogram representing the cumulative probability distribution, which was further normalized by dividing each envelope level by the median level. This normalized distribution was then plotted on Rician/Rayleigh probability graphs which allow the ratio of the steady-to-fluctuating components, γ_F, to be determined for each Rician or Rayleigh distribution [Robertson, et al., 1970]. The resulting γ_F of each run is listed on the complex frequency correlation curve for the corresponding run. These results are presented in the next section.

3.2.3 Presentation and Discussion of Results

The complex correlation coefficients (connected by smooth curves) are presented in Figures 3.3a-f. The nomenclature is the same as employed in the envelope correlations of Figures 3.1a-n, with the additional listing, when determined, of the ratio, γ_F, of the steady to the fluctuating signal components. These latter were determined from the probability

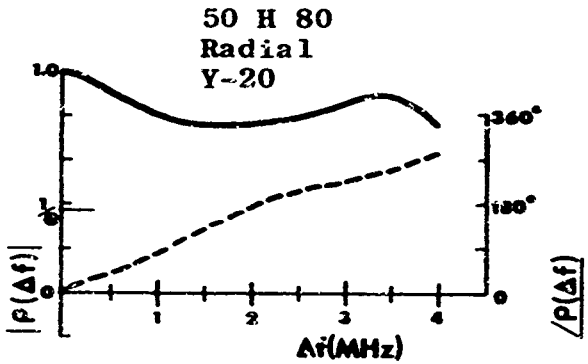

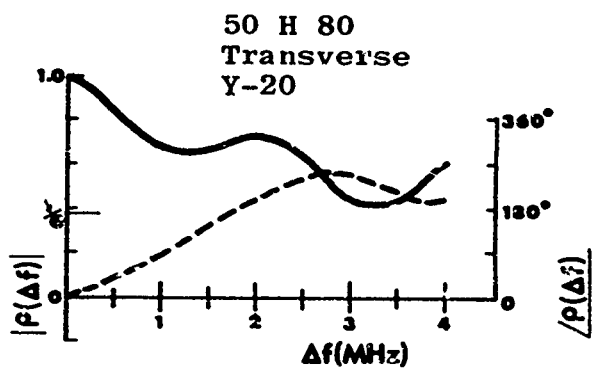

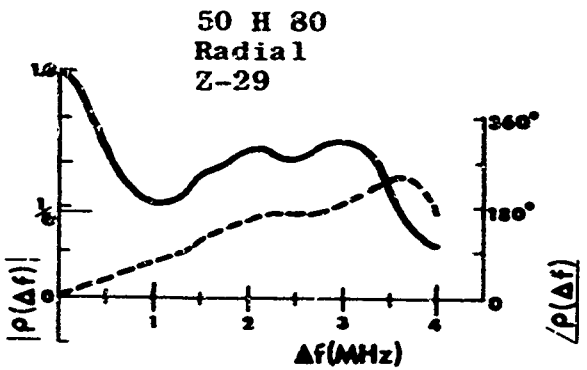

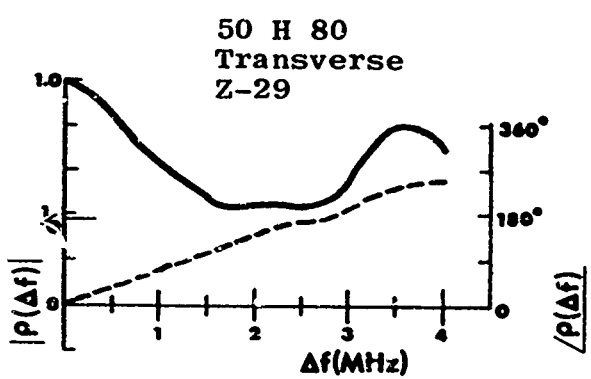

Figure 3.3a Complex Frequency Correlation Functions

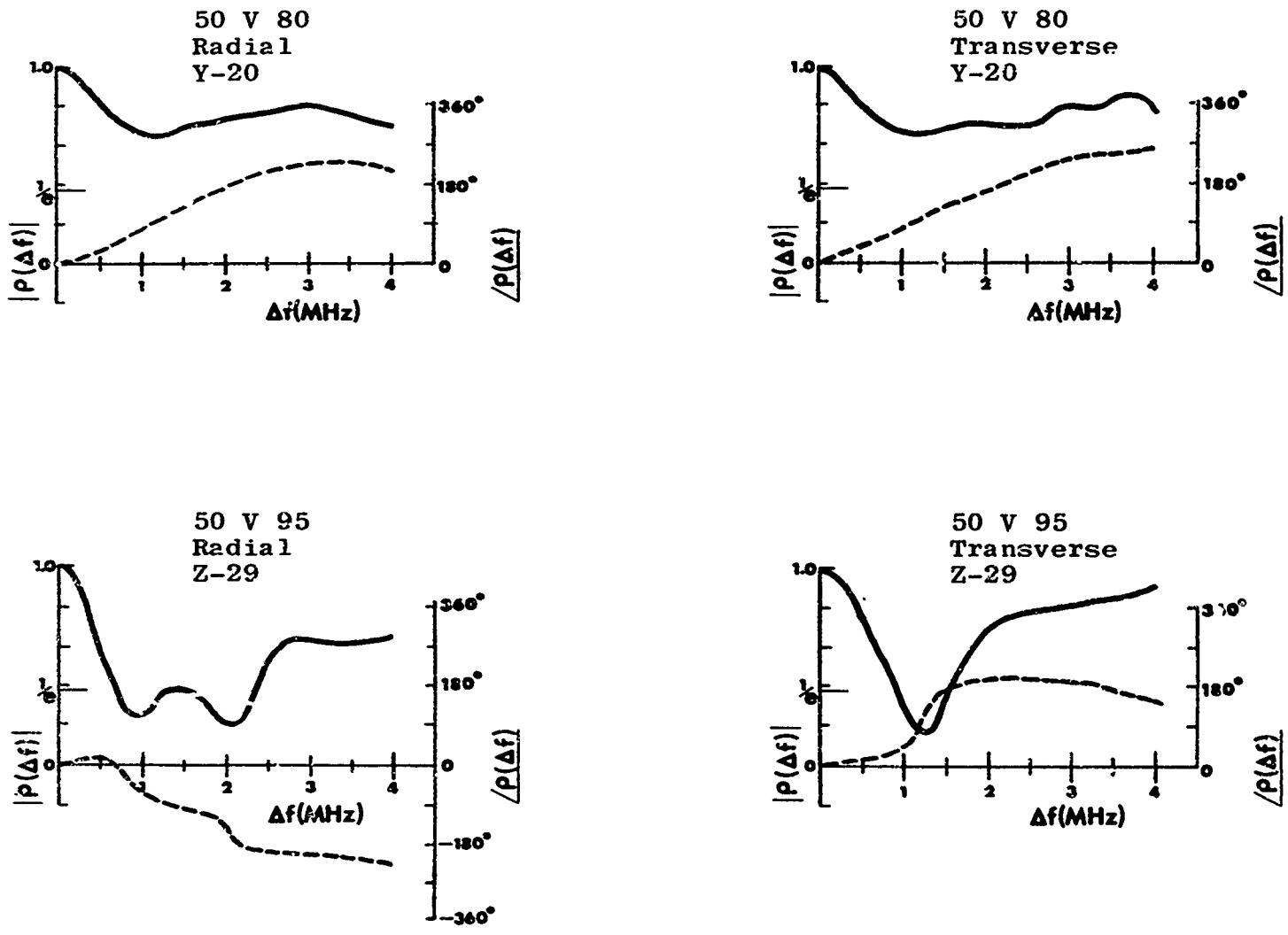

Figure 3.3b Complex Frequency Correlation Functions

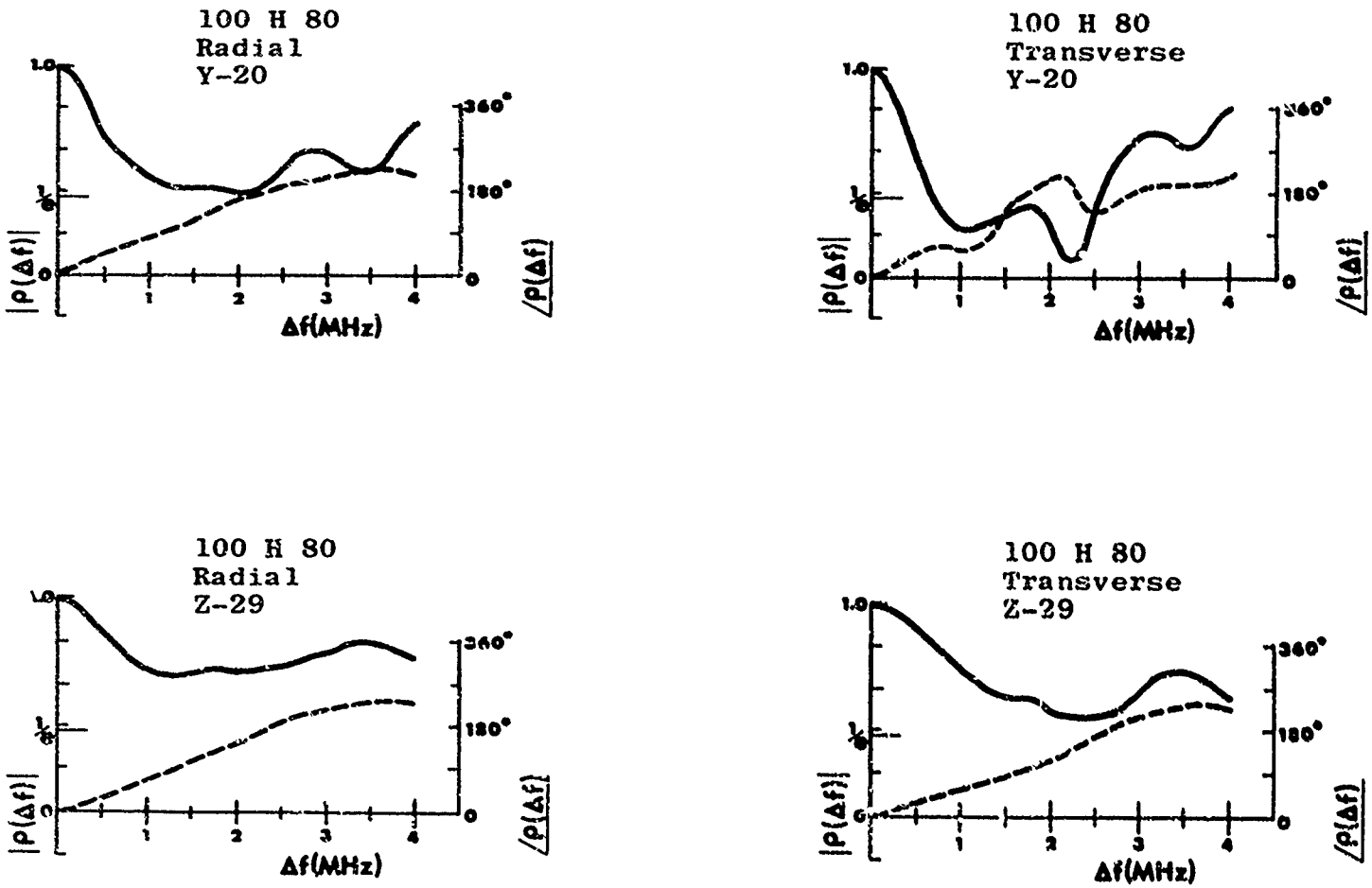

Figure 3.3c Complex Frequency Correlation Functions

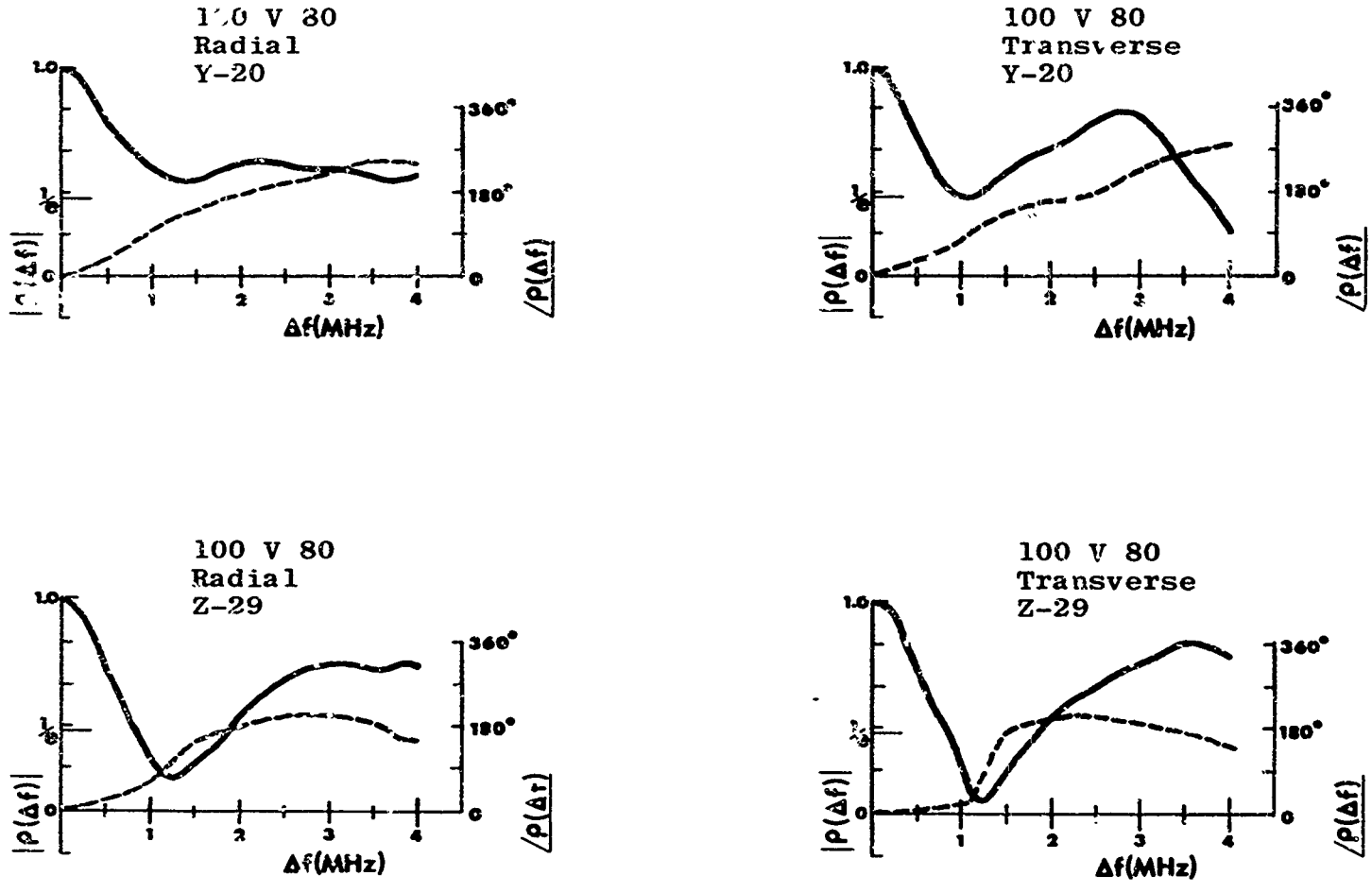

Figure 3.3d Complex Frequency Correlation Functions

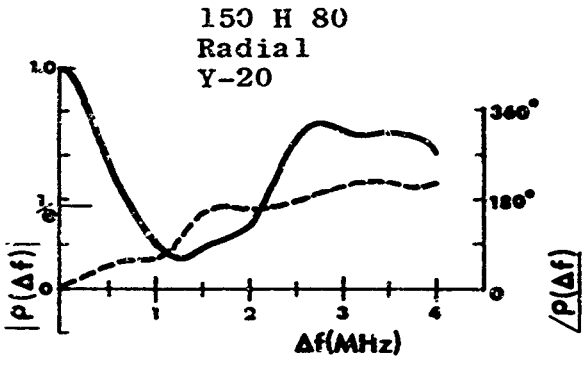

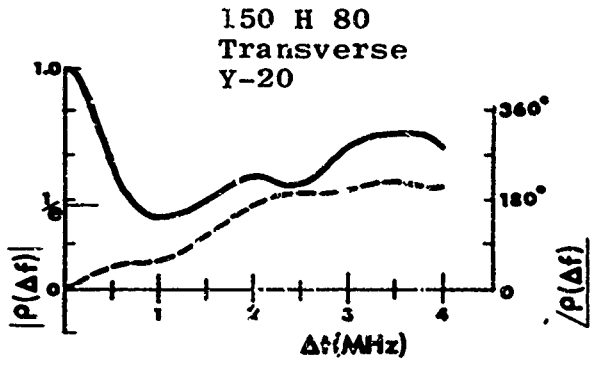

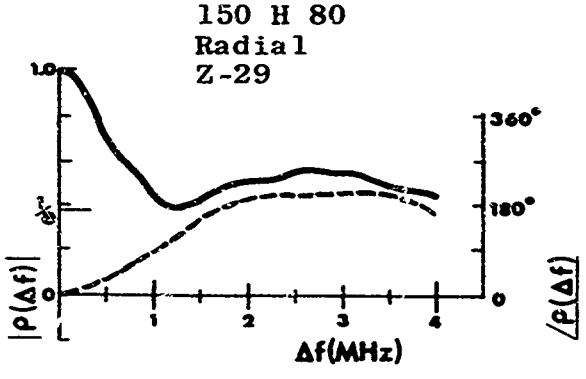

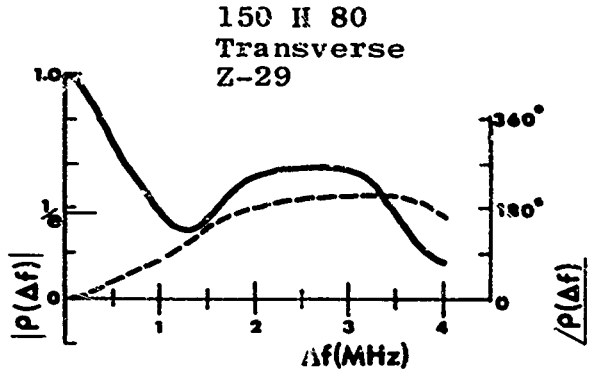

Figure 3.3e Complex Frequency Correlation Functions

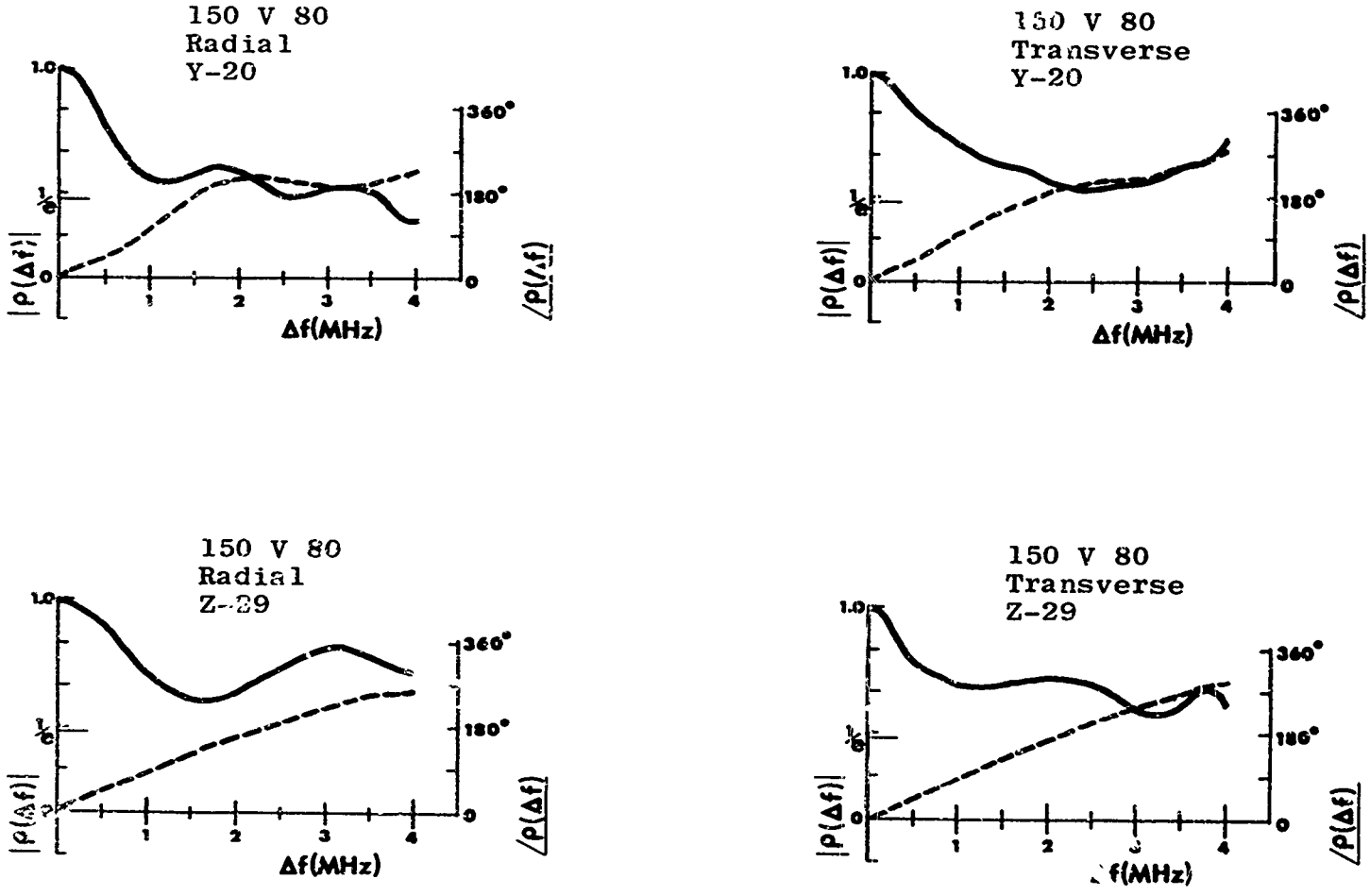

Figure 3.3f Complex Frequency Correlation Functions

distribution function of the envelopes of some of the complex data runs, and show $\gamma_F \leq 2$ dB which indicates that the envelope distribution is Rayleigh, or near Rayleigh, distributed for those cases examined.

Note that the phases of the complex frequency correlations generally have a linear changing mean. The linear mean in the phase is indicative of a time delay (see Appendix B) which, in the present instance, is the mean time delay of the multipaths relative to the most direct signal.

In an effort to reveal any dependence of the complex frequency correlations on polarization and/or frequency (the antenna heights and environmental features were not changed significantly) and to obtain an overall average of the complex frequency correlations, various averages of the correlations were computed. Figure 3.4 shows the average of all the complex frequency correlations for horizontal polarization as a function of frequency. This figure shows that for horizontal polarization the magnitude of the complex frequency correlation function tends to decrease less rapidly at 50 and 100 MHz than at 150 MHz. Figure 3.5 is the equivalent of Figure 3.4 but for vertical polarization, and shows the opposite of the behavior for horizontal polarization. Figure 3.6 is the average of all the complex frequency correlations over both polarizations as a function of frequency, and shows little dependence on frequency. Figure 3.7 shows the average of the frequency correlations over the three frequencies as a function of polarization, and also the average of all the complex frequency correlations. This figure shows little dependence of the correlations with polarization.

For comparison between the envelope and the complex frequency correlations, the envelope frequency correlations from the complex data are shown in Figure 3.8a-f. The character

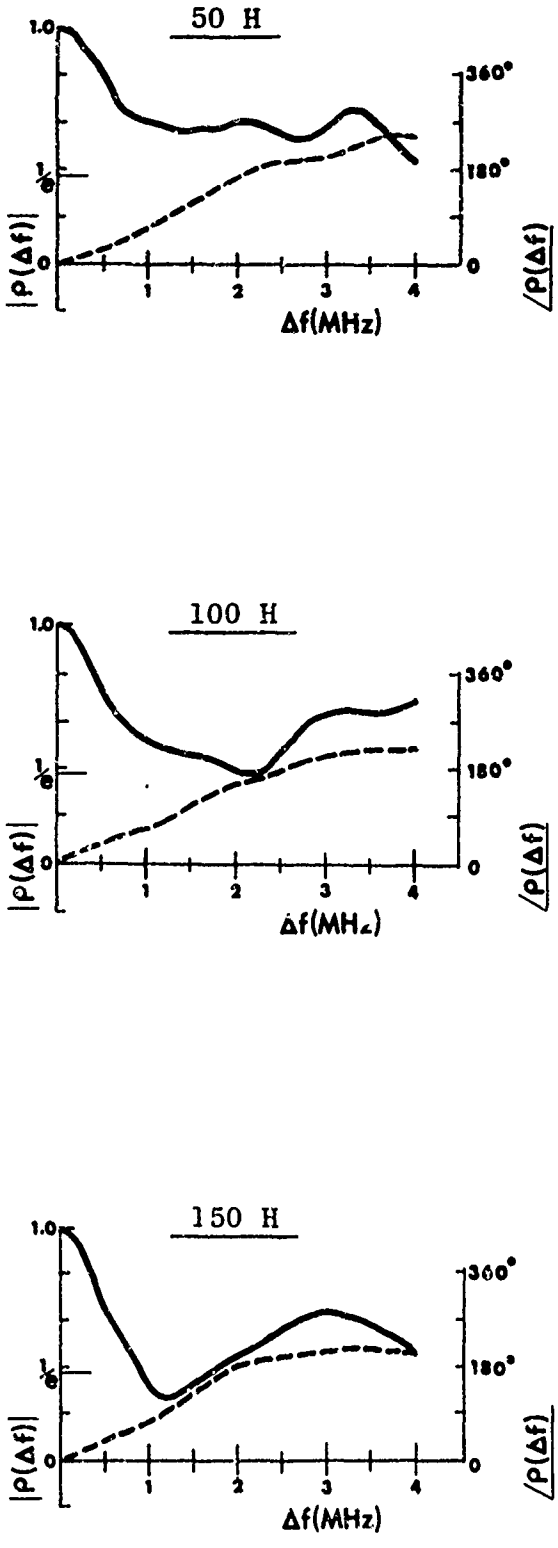

Figure 3.4 Average Complex Frequency Correlations for Horizontal Polarization as a Function of Frequency

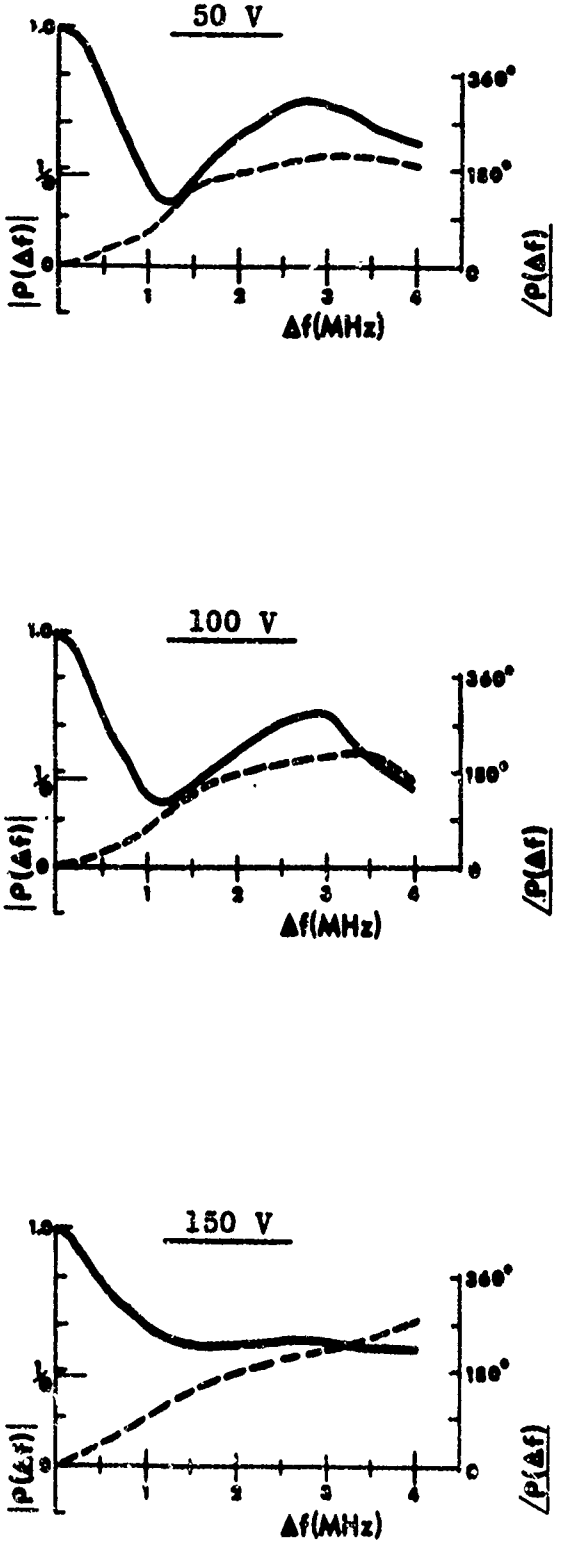

Figure 3.5 Average Complex Frequency Correlations for Vertical Polarization as a Function of Frequency

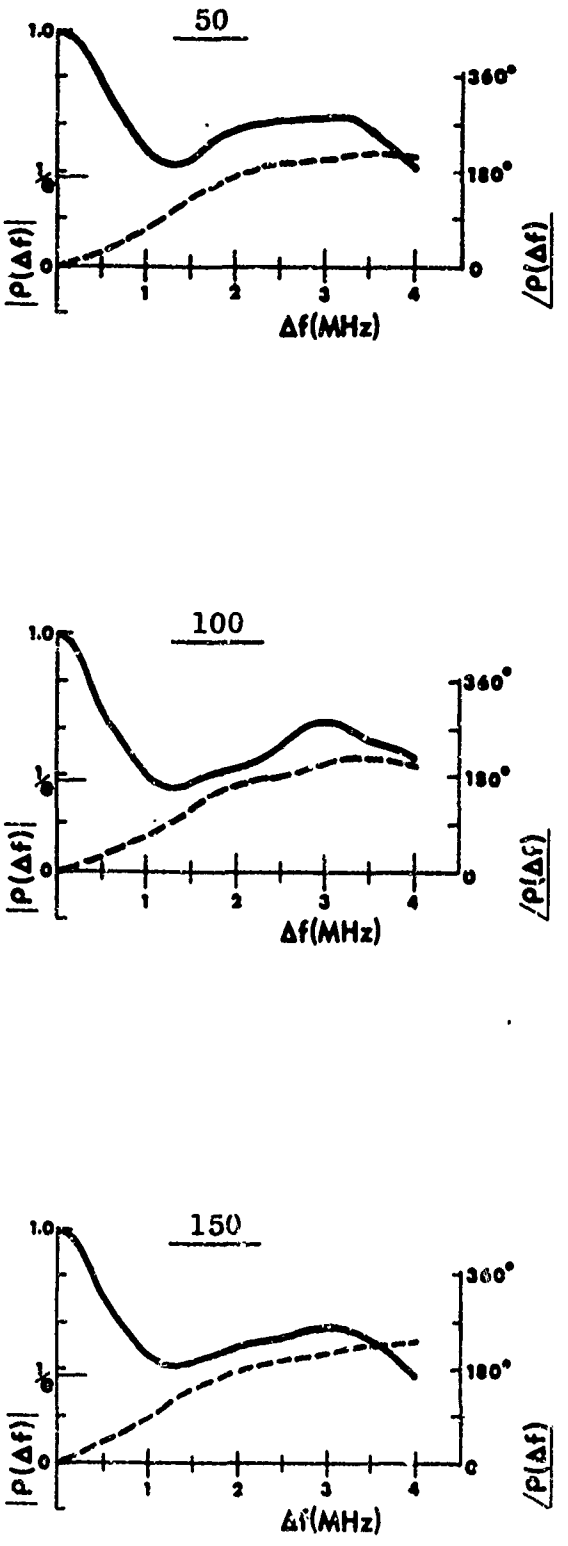

Figure 3.6 Average Complex Frequency Correlations as a Function of Frequency

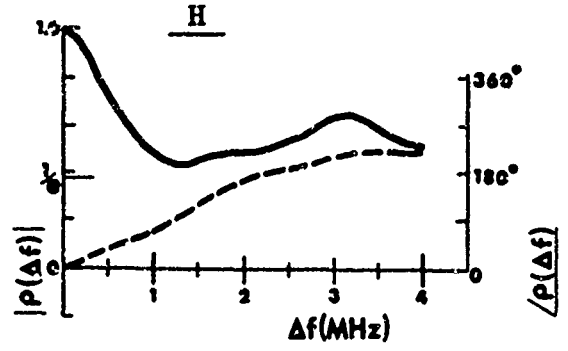

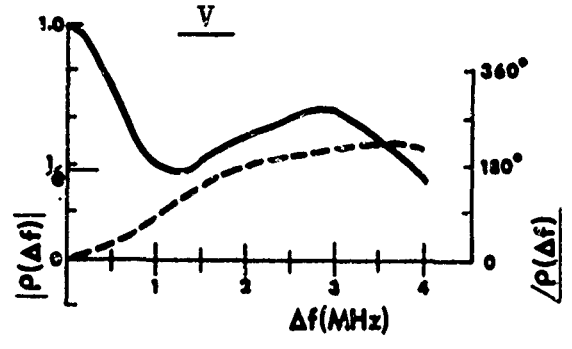

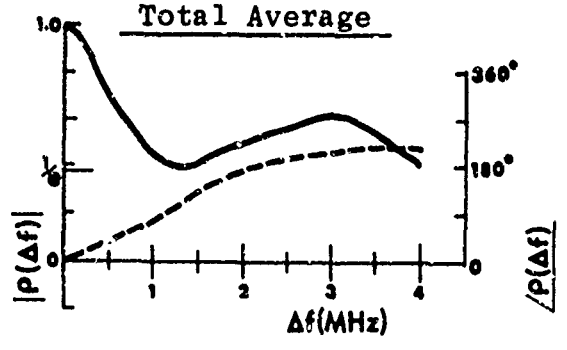

Figure 3.7 Average Complex Frequency Correlations as a Function of Polarization and Total Average

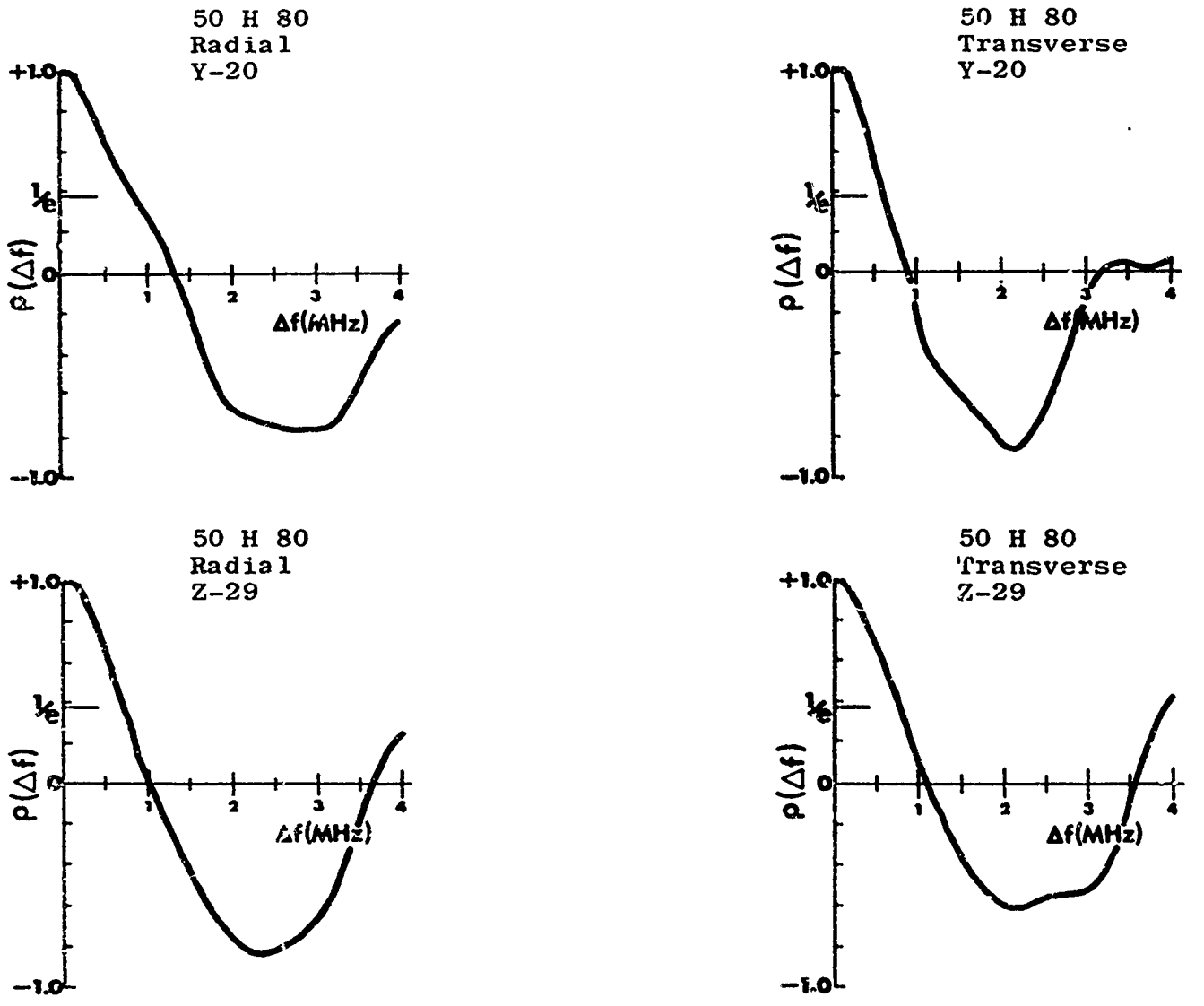

Figure 3.8a Frequency Correlation Functions of the Envelope From the Complex Data

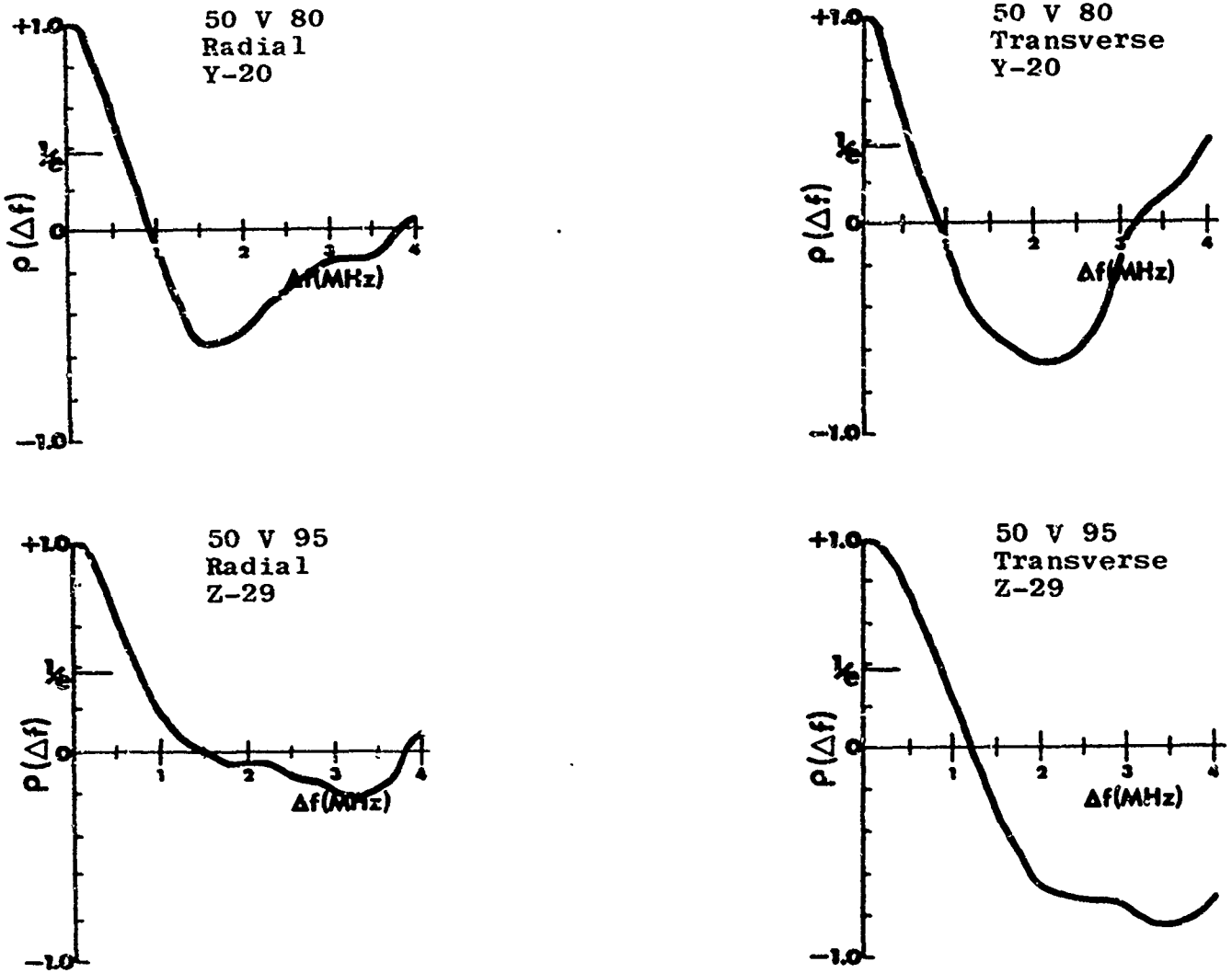

Figure 3.8b Frequency Correlation Functions of the Envelope From the Complex Data

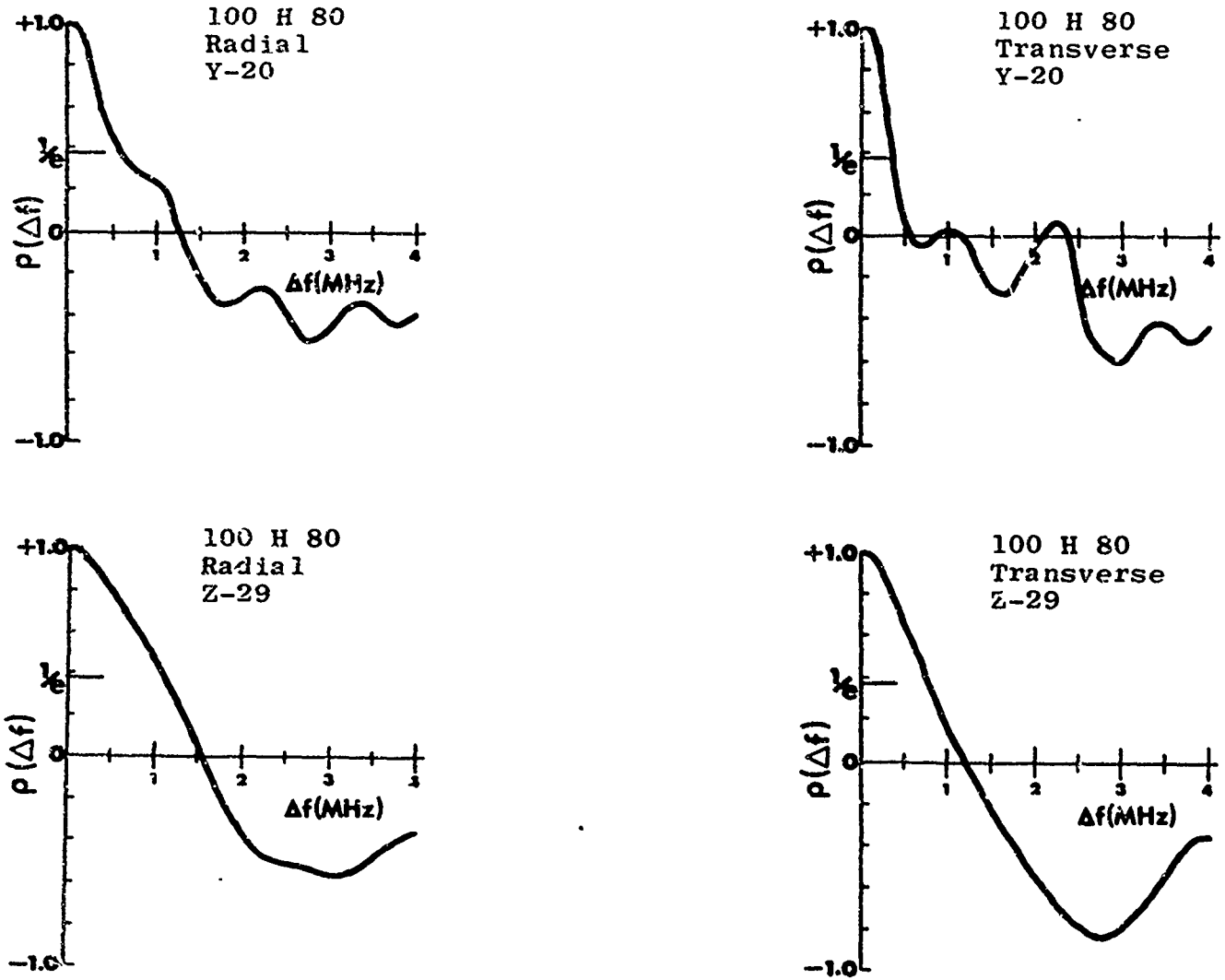

Figure 3.8c Frequency Correlation Functions of the Envelope From the Complex Data

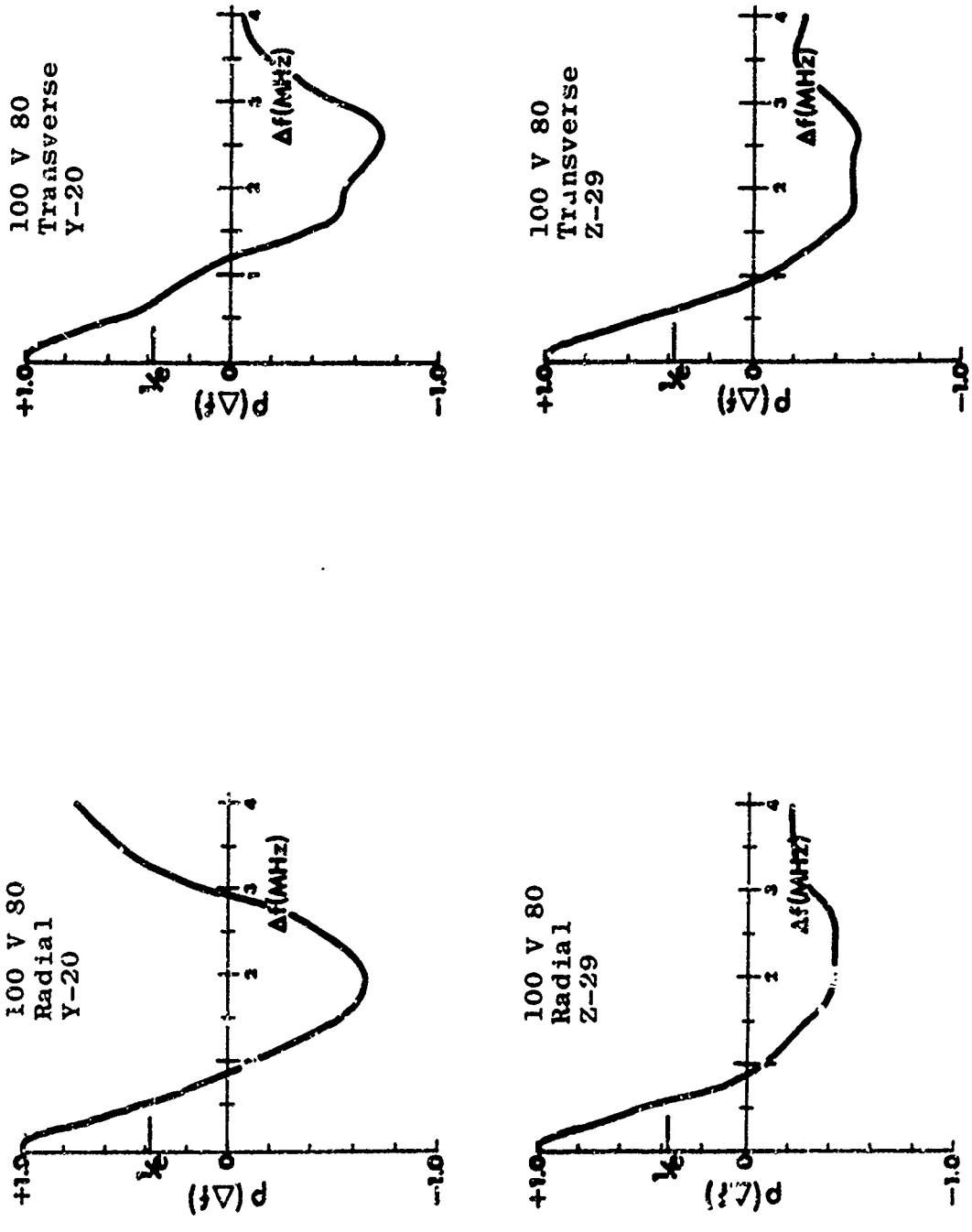

Figure 3.8d Frequency Correlation Functions of the Envelope From the Complex Data

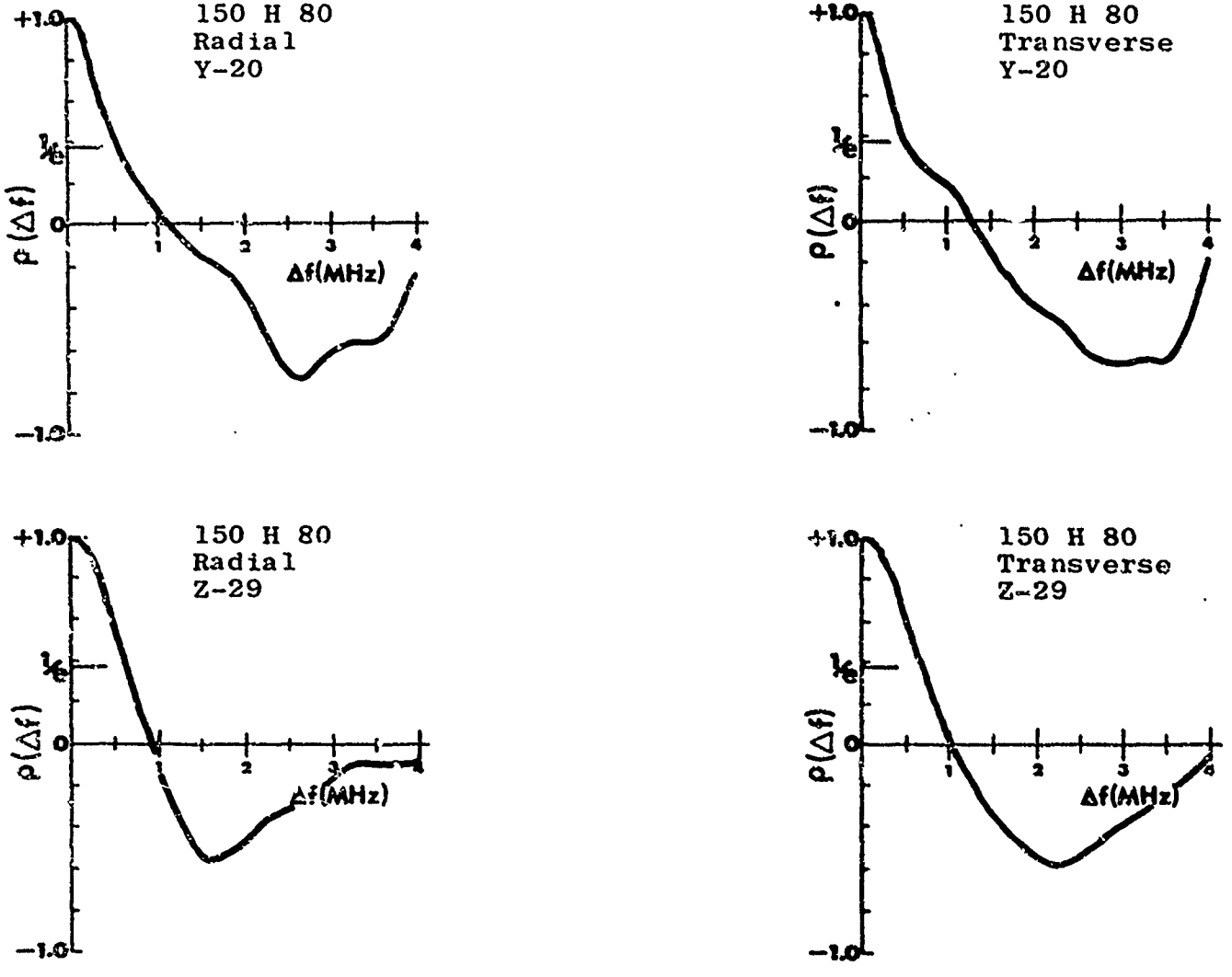

Figure 3.8e Frequency Correlation Functions of the Envelope From the Complex Data

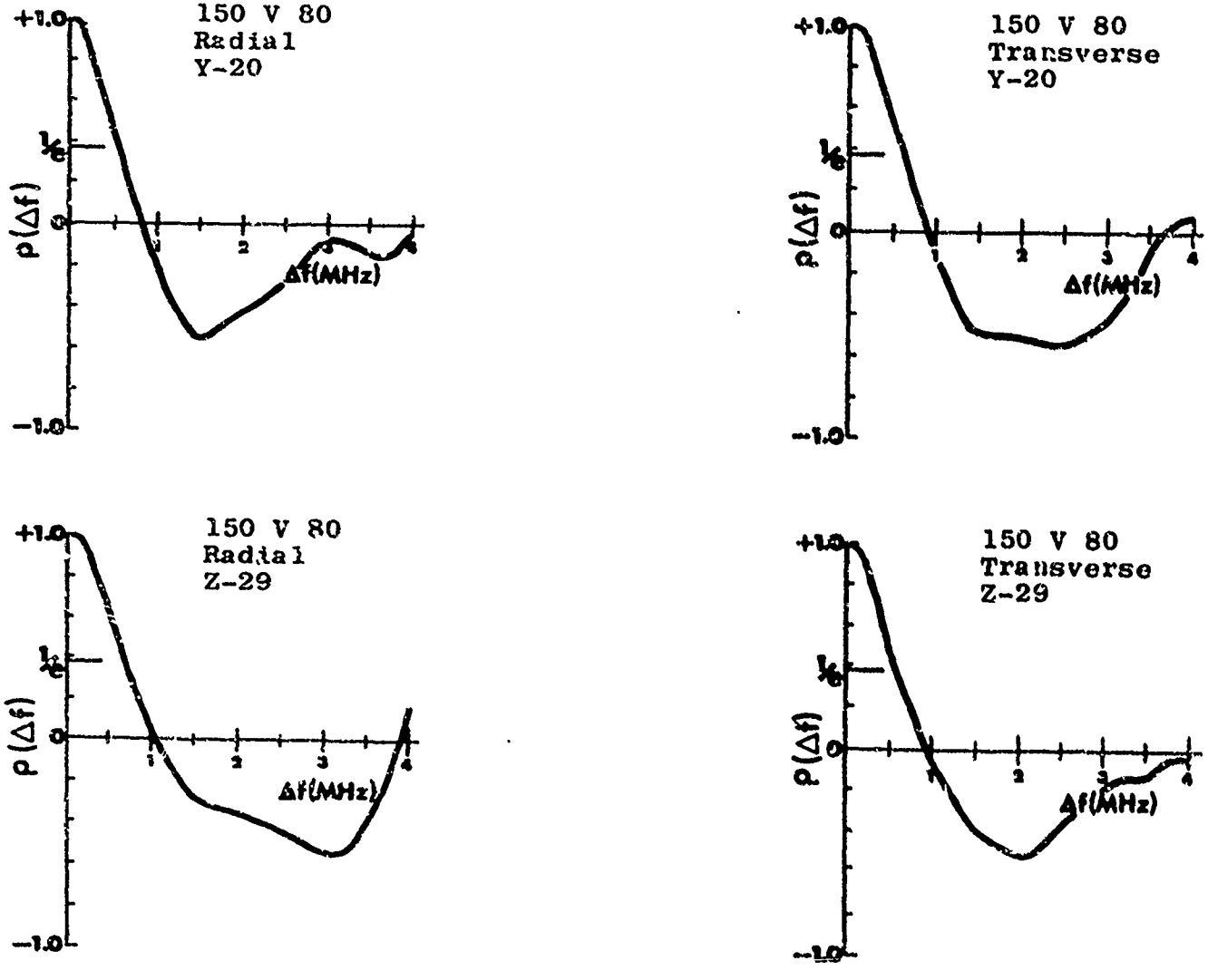

Figure 3.8f Frequency Correlation Functions of the Envelope From the Complex Data

of these envelope frequency correlations is quite similar at the shorter lags, but differs somewhat at the longer lags from the character of those discussed in Section 3.1.3. This difference is due primarily to the fact that here a constant mean was removed from the data of each swept-frequency photograph while a linear (least squares fit) mean was removed for those discussed in Section 3.1.3. This was determined by employing the least squares linear fit technique to the envelopes of the complex data and comparing the resultant frequency correlations with those of Section 3.1.3. However, a constant complex mean was removed from the data of each photograph in determining the complex frequency correlations, for simplicity, and hence for consistency, the results with a constant mean removed from the envelopes of the complex data are used here.

Perhaps the most interesting observation to be made from comparing the envelope and complex frequency correlations is that the envelope correlations are not related to the magnitude of the complex frequency correlations as is theoretically expected if the multipath scattering process is complex Gaussian. The Gaussian scattering process implies a Rayleigh (or Rician if a steady component is present) envelope distribution, which is observed. Theoretically, $|\rho|^2 \approx \rho_{env}$ where $|\rho|$ is the magnitude of the complex frequency correlations and ρ_{env} is the envelope frequency correlations [Schwartz, Bennett and Stein, 1966]. The presence of a quasi-cyclic component in the envelope frequency correlations, as is evident here, is not considered in the theory. The presence of such a component, or other factor, in the data which, as observed here, causes the envelope frequency correlations to go negative, immediately precludes observing the theoretical relation because $|\rho|^2 \geq 0$. The lack of agreement also, of course, implies that our sample of the multipath process is not strictly Gaussian. The degree to which the sample process is not Gaussian is not known, nor is

it known why it is not Gaussian, but a very plausible explanation is that there are too few effective multipaths observed in the sample process. This would result if the major scattering, or multipaths, are from only a few large trees, which has been suggested from pulse measurements [Hicks and Robertson, 1969].

However, regardless of the relation between the envelope frequency correlations and the magnitude of the complex frequency correlations, there remains the question as to what criterion one uses here in establishing bandwidth limitations for the forest environment for avoiding frequency-selective fading, and in employing frequency diversity. If only the envelope frequency correlations are available, then one uses the 1/e point, as discussed in Section 3.1.3. However, when the complex frequency correlations are available then the 1/e point of the magnitude appears to be recommended in general. In some of the present cases, however, the latter would place virtually no restriction upon the allowable operational bandwidth, at least over the 4 MHz sweep examined, and also virtually rule out frequency diversity. This is not consistent with the fact that multipaths are present in the forest environment, which must naturally affect the allowable bandwidth, as demonstrated by the envelope frequency correlations. This suggests that a measure of the magnitude of the complex frequency correlations, namely the 1/e point, is not a suitable criterion for establishing bandwidth requirements here and there is some further basis to support this. This latter is based upon the fact that it is theoretically possible to obtain, from two equal strength multipaths (two interfering sine waves), a complex correlation function whose magnitude is constant, while the envelope correlation will have a cyclic component. The present correlations, while certainly more complicated, are similar to the results of this idealized example, and this similarity is also in keeping with the suggestion that only a few multipaths may be the major contributors.

Of equal, or perhaps greater, importance in defining the characteristics of a multipath channel is the multipath intensity profile. Figure 3.9a-f shows the intensity profiles computed from the above complex frequency correlations. The intensity profile gives the distribution of the relative intensity of the multipaths as a function of their delays relative, in the present case, to a steady component if one existed. The intensity profiles show that the multipaths of greatest intensity have an average delay $\tau \approx 0.25$ μsec.

Figure 3.10a-b shows the complex distance correlations. A linear phase trend has been removed from the phase of the distance correlations to simplify the plotting. Note the quasi-cyclic variations in the phase of the correlations for vertical polarization and in the radial runs for horizontal polarization, while the phase for the transverse run for horizontal polarization shows no such variations. This behavior is consistent with the explanation of the distance correlations of the envelope given in Section 3.1.3.

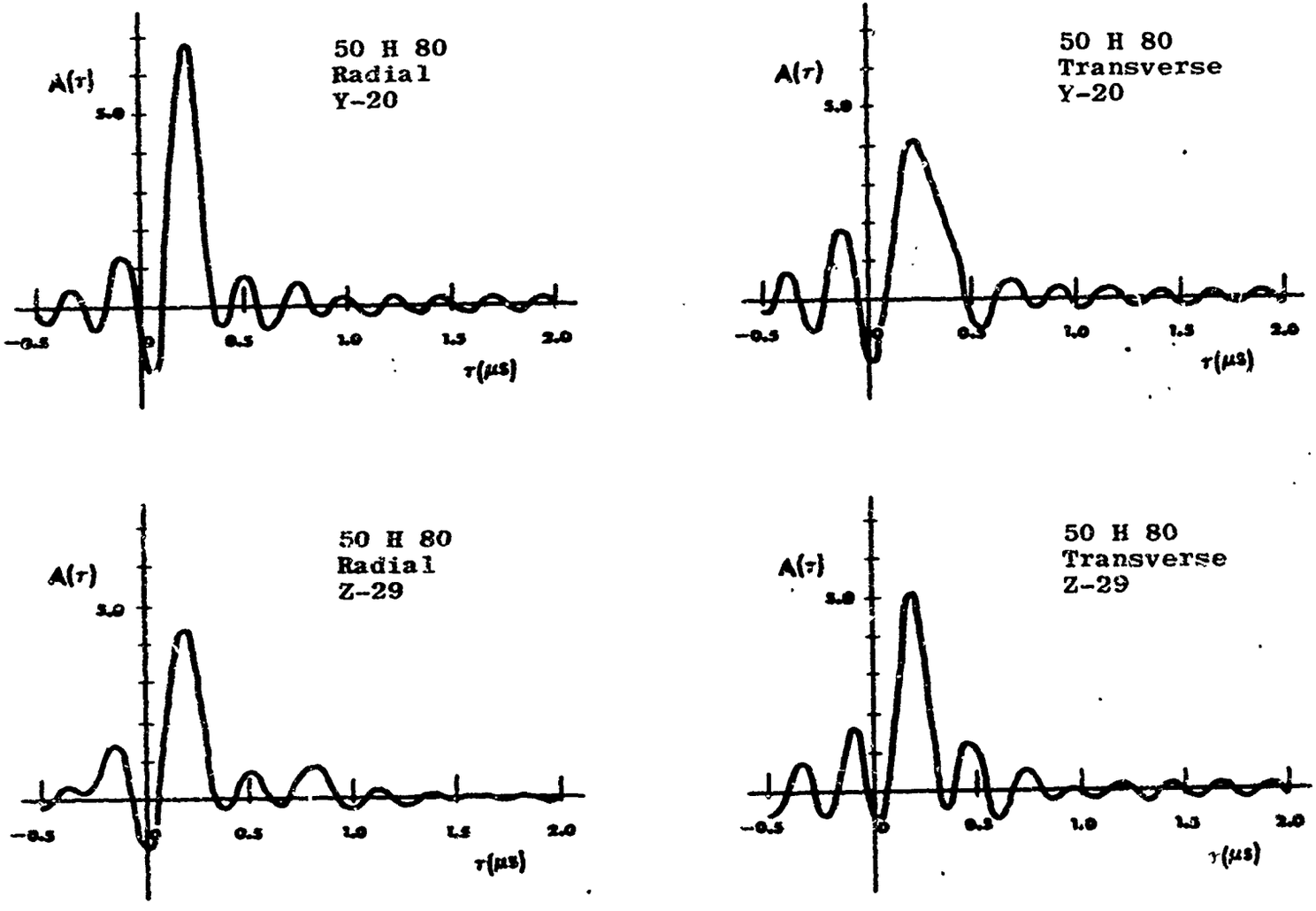

Figure 3.9a Intensity Profiles

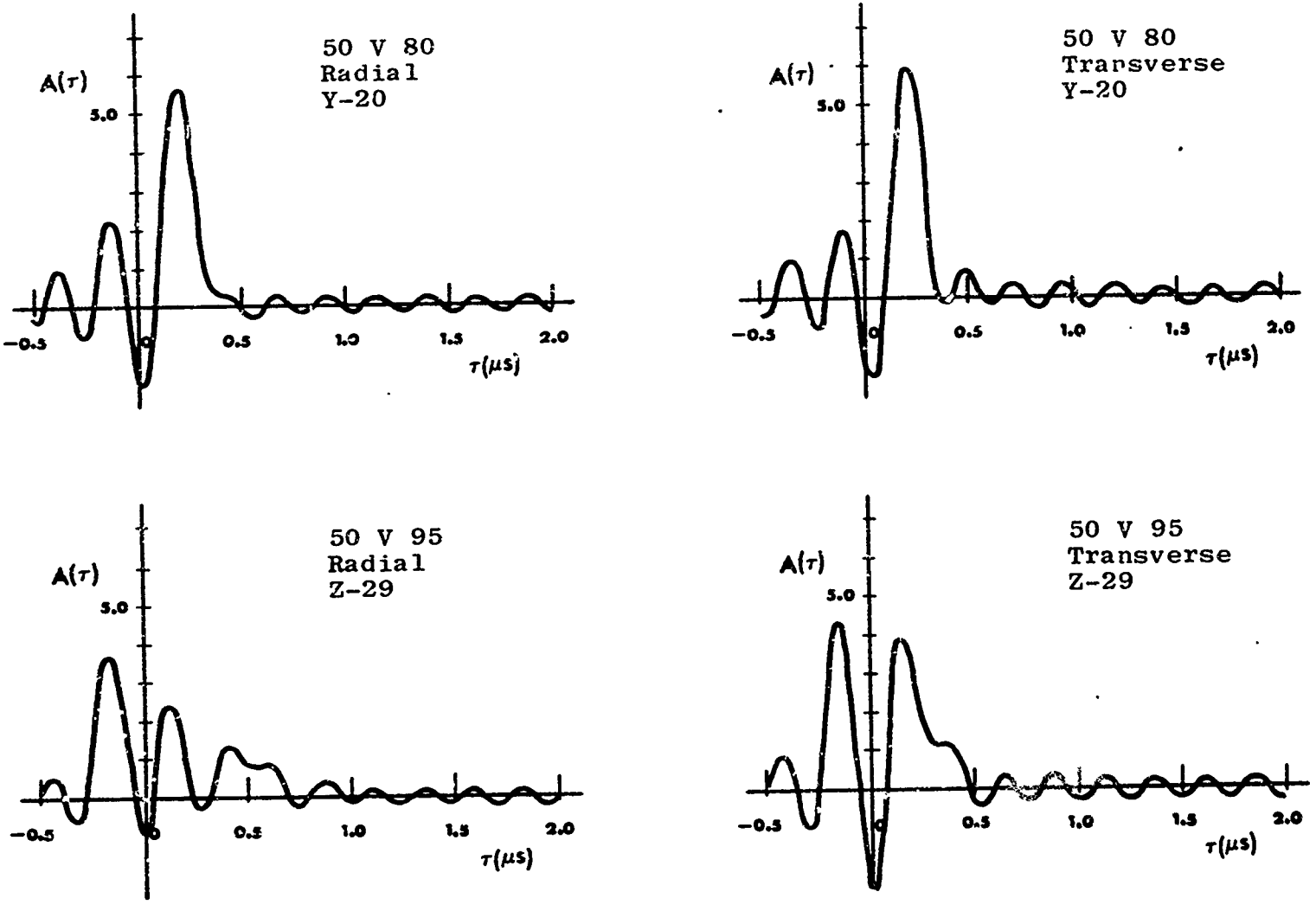

Figure 3.9b Intensity Profiles

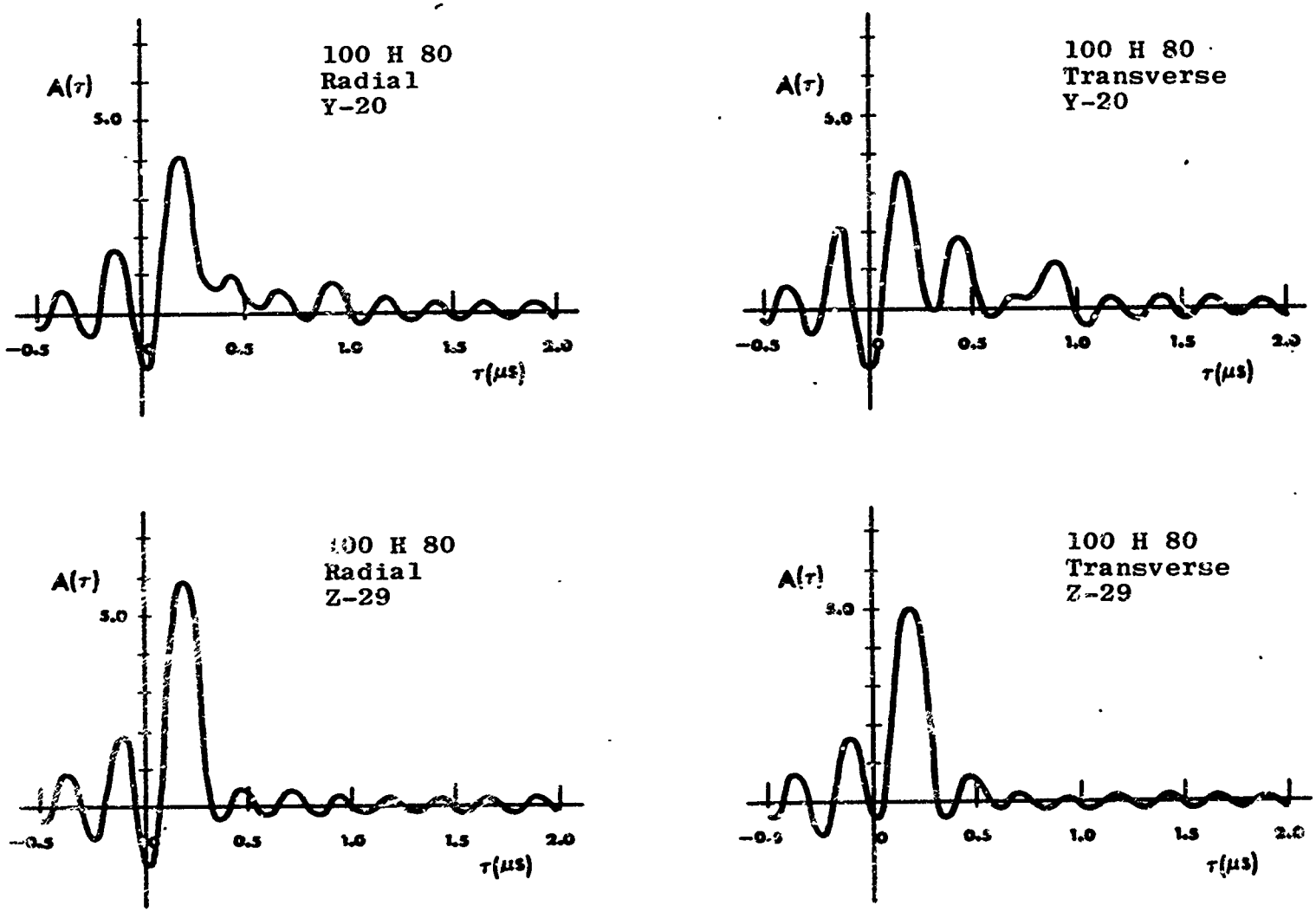

Figure 3.9c Intensity Profiles

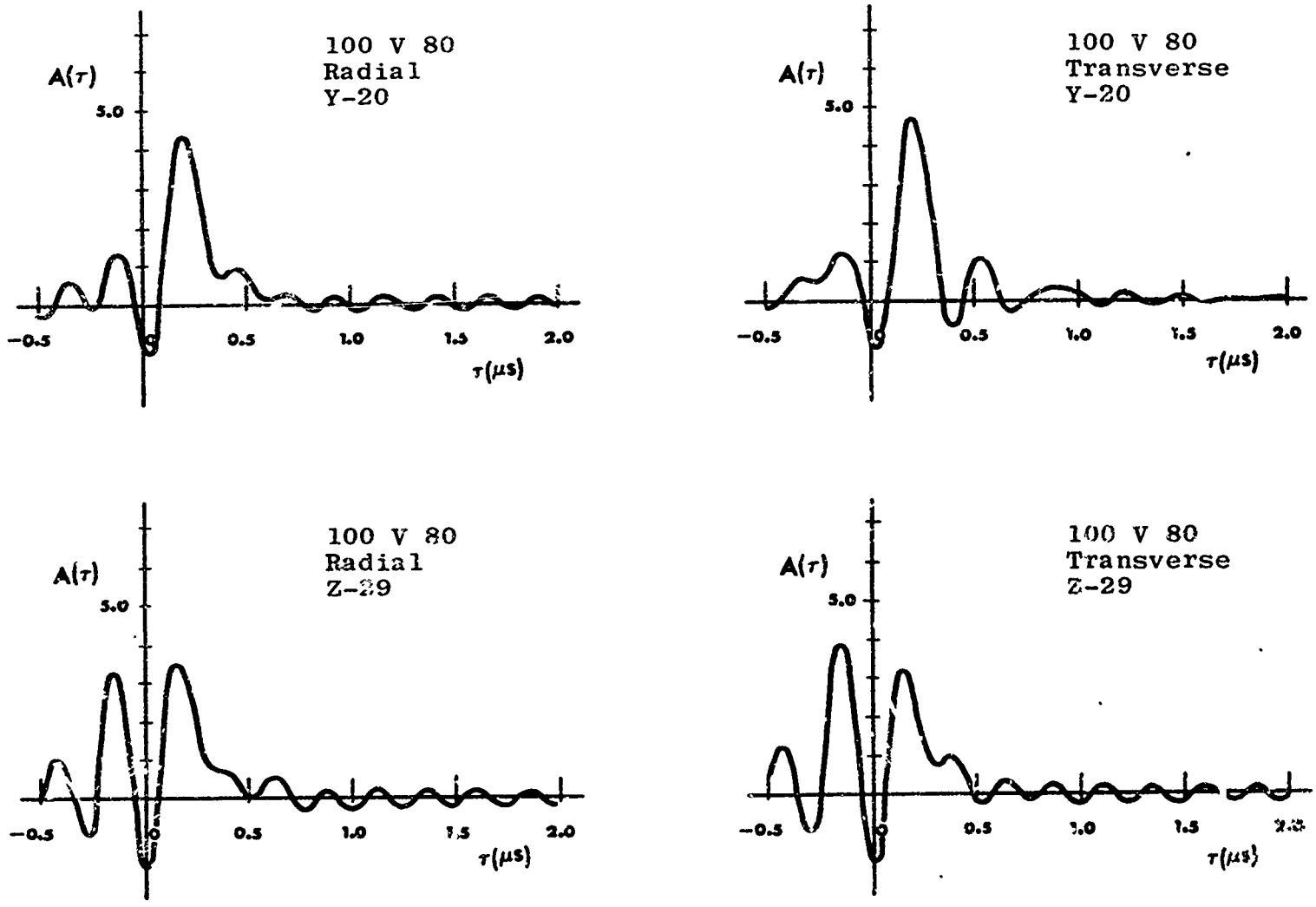

Figure 3.9d Intensity Profiles

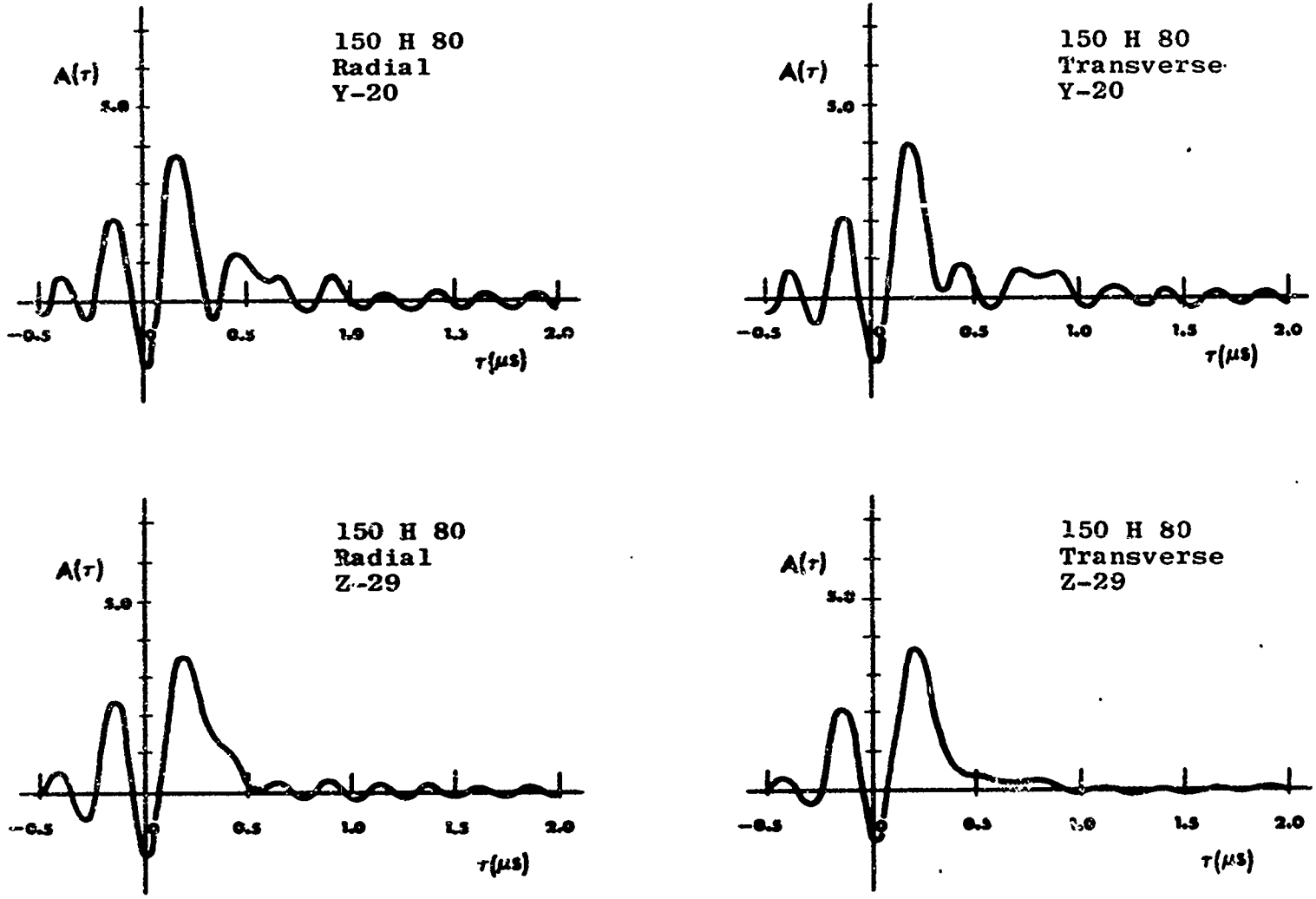

Figure 3.9e Intensity Profiles

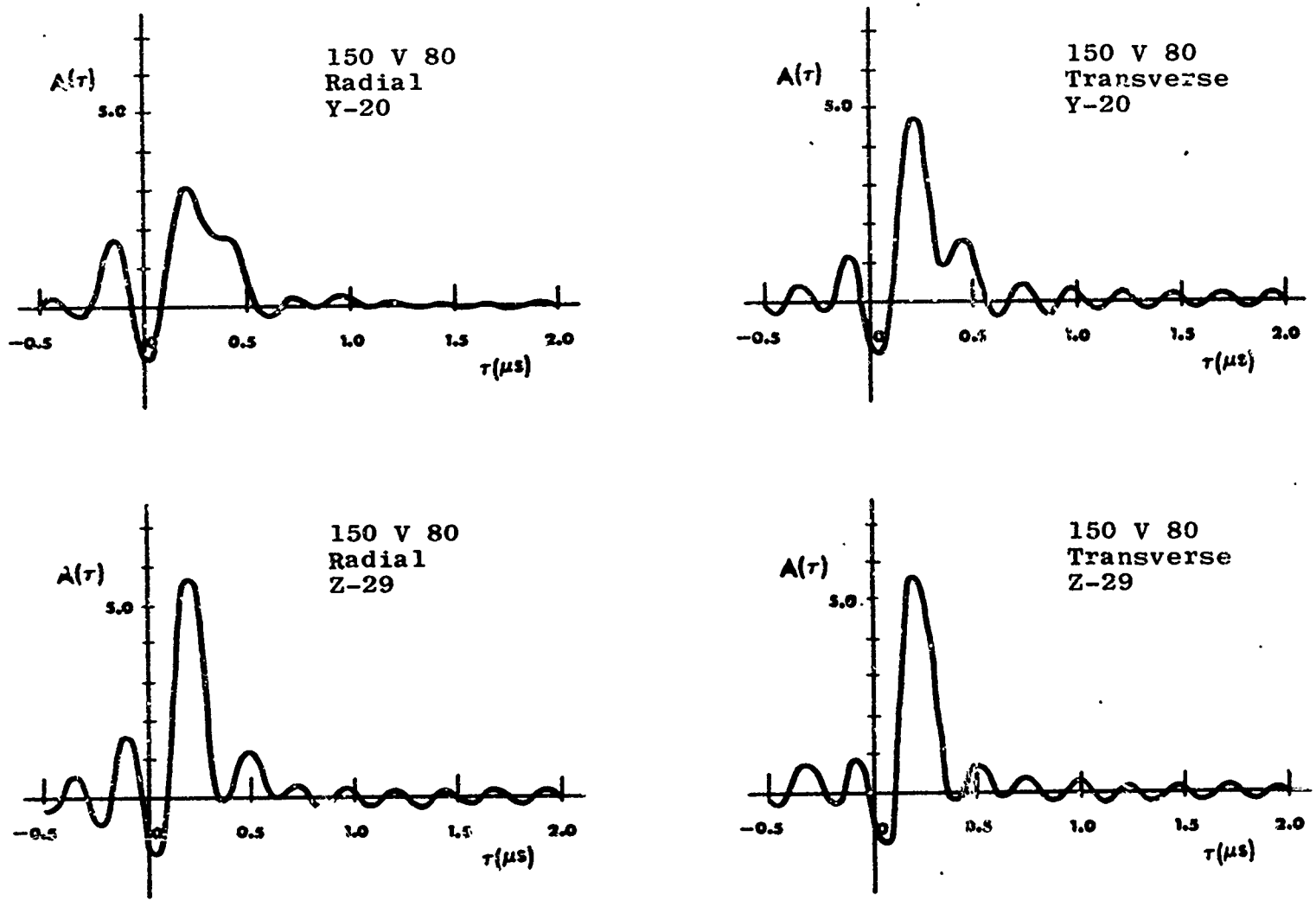

Figure 3.9f Intensity Profiles

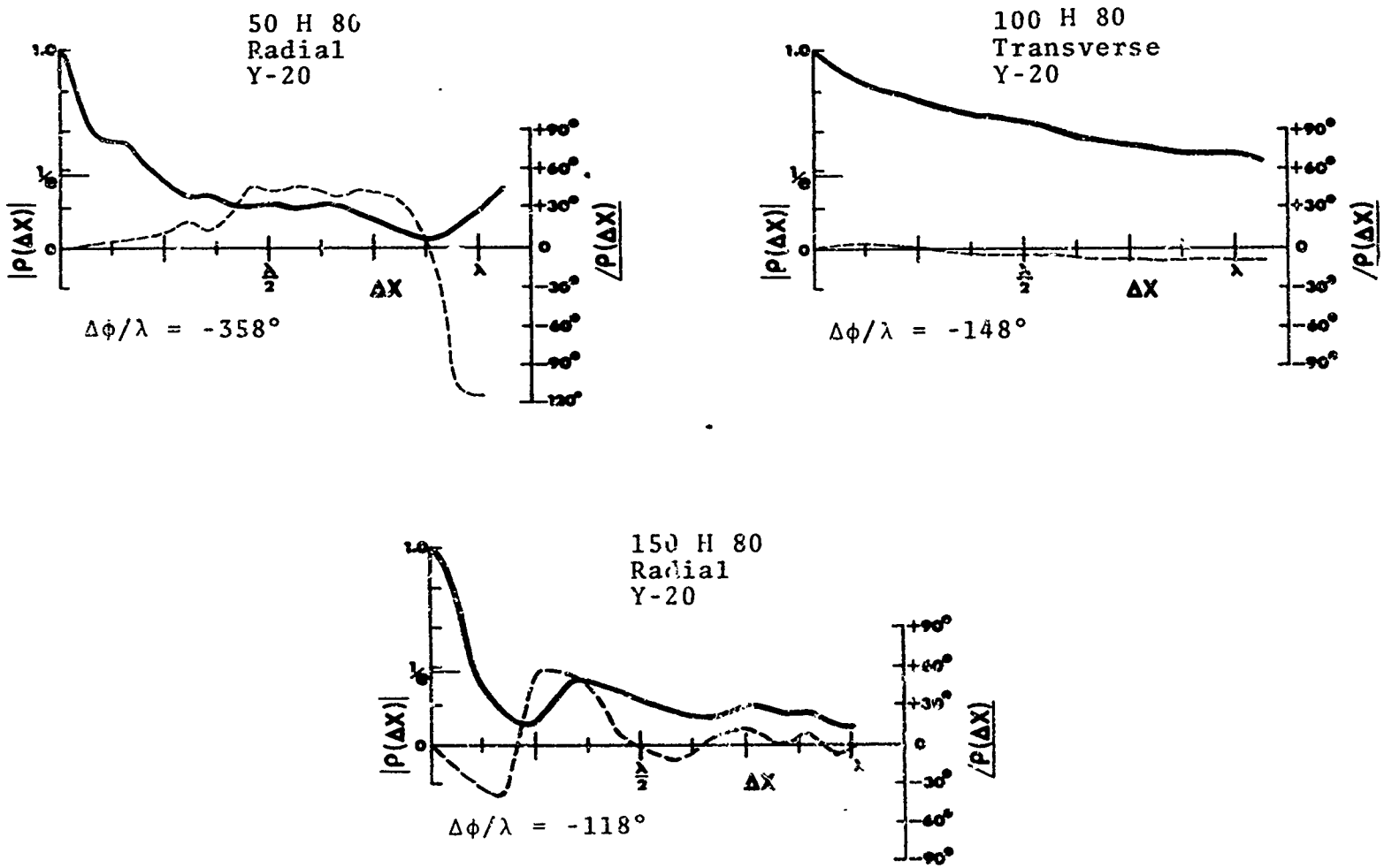

Figure 3.10a Complex Distance Correlation Functions

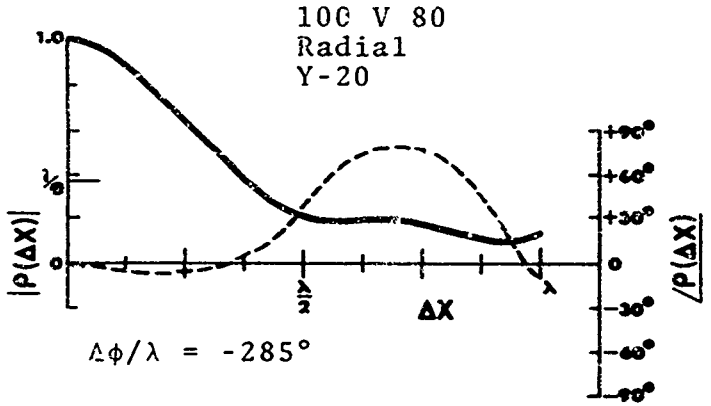

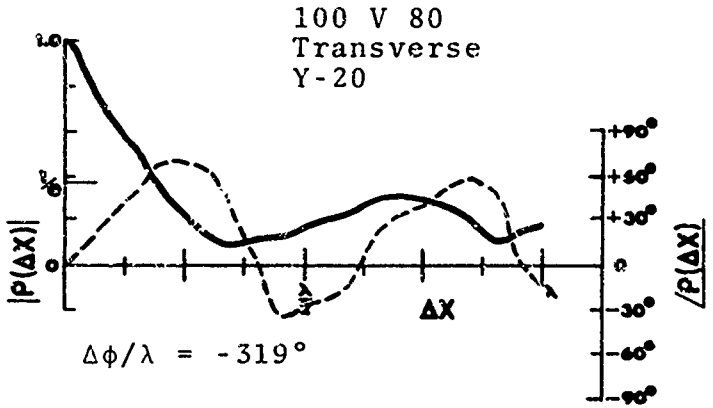

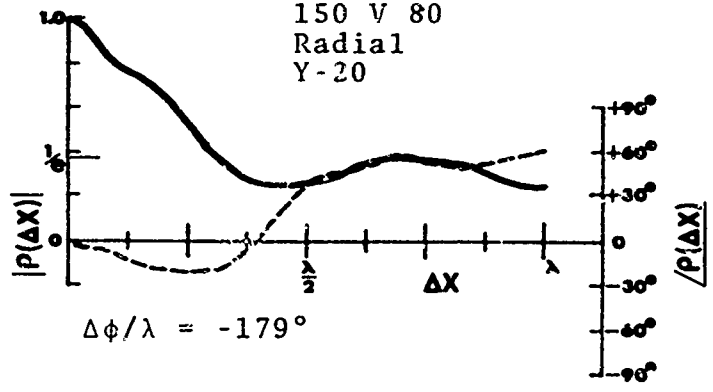

Figure 3.10b Complex Distance Correlation Functions

APPENDIX A

PROPAGATION BETWEEN HORIZONTALLY POLARIZED ANTENNAS IMMERSED IN A NONHOMOGENEOUS, LOSSY SLAB BOUNDED ABOVE BY AIR AND BELOW BY GROUND

The nonhomogeneous model under investigation is sketched in Figure A.1 which serves to identify the coordinates, dimensional and electrical parameters of the slab, and bounding regions.

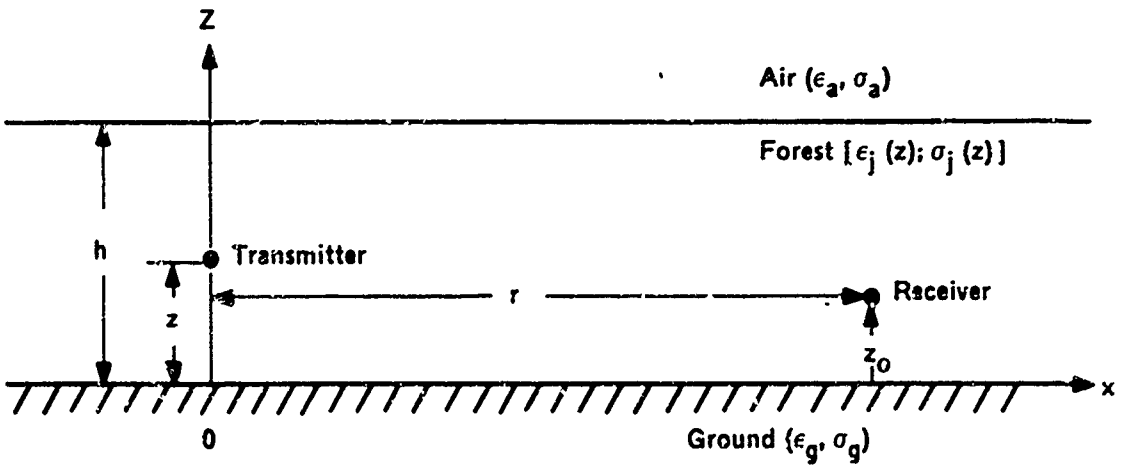

Figure A.1 Sketch of Nonhomogeneous Slab Model. Note that the nonhomogeneity is in the z direction only.

The theoretical relations describing propagation in such a bounded, nonhomogeneous slab have not, to the authors' knowledge, been previously obtained. Fortunately, however, a

great deal of work dealing with propagation in homogeneous and nonhomogeneous stratified media has been done [Brekhovskikh, 1960; Wait, 1962] and will provide the foundation for the present development. In particular, the work of Brekhovskikh [1960] in nonhomogeneous media will be followed where applicable, and when it becomes necessary to further these results, his work in homogeneous media will provide the concepts and be closely paralleled.

The rationalized MKS system of units will be employed and the time dependence of $e^{-i\omega t}$ will be understood throughout. The slab is assumed to be nonhomogeneous in the z-direction only, as described by the complex dielectric permeability

$$\varepsilon_f'(z) \equiv \left(\varepsilon_f + \frac{i\sigma}{f}\right)$$

Further, $\varepsilon_f'(z)$ is assumed to be continuous and slowly varying. For some purposes here it will be convenient to consider the nonhomogeneous slab as composed of a large number of thin, plane-parallel, homogeneous layers each of which has properties slightly different from its neighboring one. In the limit as the thickness of the layers approaches zero and their number approaches infinity, the nonhomogeneous slab with continuously varying parameters is, of course, obtained. The magnetic permeability, μ, is assumed to be that of a vacuum in all media.

Let us begin the derivation with the magnetic vector potential for a Hertzian dipole [Ramo and Whinnery, 1953, p. 497]

$$\bar{A} = \mu I \overline{dl} \frac{e^{ikR}}{4\pi R} \tag{A-1}$$

where I is the uniform rms current in the element of length dl, k is the wave number, and R is the distance from the current element to the point of observation. Further, through the relations

$$\bar{B} = \nabla \times \bar{A} \tag{A-2}$$

$$\bar{E} = - \nabla\phi - \frac{\partial \bar{A}}{\partial t} \tag{A-3}$$

and

$$\nabla \cdot \bar{A} \equiv - \mu\varepsilon_t \frac{\partial \psi}{\partial t} \tag{A-4}$$

the fields may be obtained if the vector potential $\bar{A}$ at the observation point is known [Brekhovskikh, 1960; p. 236]. In these equations $\bar{B}$ is the magnetic flux density, $\bar{E}$ the electric field, and ϕ is a scalar potential.

Attention is restricted here to the case of horizontal polarization with the $\bar{E}$-field perpendicular to the plane of incidence and with the terminals (dipoles) immersed in the slab. Thus, assuming only a y-component of $I\overline{dl}$ and using $\varepsilon' = \varepsilon'(z)$, one obtains $\nabla \cdot \bar{A} = 0$. From Eq. (A-3) one then gets $E_y = i\omega A_y$, $E_x = 0$, $E_z = 0$; and the $\bar{H}$-fields may be similarly determined from Eq. (A-2). For present purposes, we seek

$$E_y = i\omega\mu I dl \frac{e^{ikR}}{4\pi R} \tag{A-5}$$

and the problem is thus to determine the spherical wave $(e^{ikR})/R$ at the observation point, subject to the inhomogeneity and boundaries involved.

To accomplish this, it is convenient to first obtain the spherical wave dependency $(e^{ikR})/R$ for an unbounded nonhomogeneous medium in terms of plane waves, which are simpler to work with in view of the plane boundaries involved, and consider the effects of the boundaries later. Thus, restricting attention at first to an unbounded homogeneous medium with the source and receiver at height $z_o = z$, the cylindrical wave $(e^{ikr})/r$, where $r = \sqrt{x^2 + y^2}$ is the cylindrical radius, can be expressed as [Brekhovskikh, 1960; p. 239]

$$\frac{e^{ikr}}{r} = \frac{i}{2\pi} \int_{-\infty}^{\infty} \int \frac{\exp\left[i(k_x x + k_y y)\right] dk_x dk_y}{\sqrt{k_z(z)}} \quad . \qquad \text{(A-6)}$$

The exponent in the integrand of Eq. (A-6) represents plane waves propagating in the direction given by the wave vector components k_x, k_y. Note that the imaginary part of k must be positive to satisfy the requirement that the field vanish as $r \to \infty$. To extend the expansion of Eq. (A-6) to spherical waves in an unbounded region it is necessary to multiply Eq. (A-6) by a factor, say $f(k_z,z)$, which describes plane wave propagation in the z-direction and which will, of course, include the nonhomogeneity aspects. We shall employ the geometrical optics approximation for the plane wave field $f(z,k_z)$ for the case where the electric field is perpendicular to the plane of incidence and has unity amplitude at z_o. The result is [Brekhovskikh, 1960; p. 201]

$$f(z,k_z) = E_y(z) = \frac{Z(z)}{Z(z_o)} \exp\left[\pm i \int_{z_o}^{z} k(z)dz\right] \qquad (A\text{-}7)$$

where $Z(z)$ and $Z(z_o)$ are the normal wave impedances at z and z_o respectively and the $\pm$ sign in the exponent represents propagation in the $\pm$ z direction relative to z_o.

In deriving Eq. (A-7) the unbounded nonhomogeneous medium has been assumed to be composed of a large number of thin homogeneous layers with slightly different properties, as mentioned above, such that reflections from the slightly different layers are negligible. Employing the relations [Brekhovskikh, 1960; p. 46]

$$Z(z) = \frac{1}{\cos \delta(z)} \sqrt{\frac{\mu}{\varepsilon(z)}} \quad , \qquad (A\text{-}8)$$

$$Z(z_o) = \frac{1}{\cos \delta(z_o)} \sqrt{\frac{\mu}{\varepsilon(z_o)}} \quad , \qquad (A\text{-}9)$$

the general relation $k_z = k \cos \delta$, where δ is the angle of incidence, and [Brekhovskikh, 1960; p. 8]

$$\frac{k(z)}{k(z_o)} = \sqrt{\frac{\varepsilon(z)}{\varepsilon(z_o)}} \quad , \qquad (A\text{-}10)$$

in Eq.(A-7), and multiplying Eq.(A-6) by the result, one obtains the expansion

$$\frac{e^{ikR}}{R} = \frac{i}{2\pi}\int_{-\infty}^{\infty}\int \frac{\exp\left[i\left(k_x x + k_y y \pm \int_{z_o}^{z} k_z(z)\,dz\right)\right]dk_x dk_y}{\sqrt{k_z(z_o)\,k_z(z)}} \quad . \quad \text{(A-11)}$$

It is interesting to note that Eq.(A-11) reduces to the spherical wave in a homogeneous medium if $k_z(z) = k_z(z_o) =$ constant [Brekhovskikh, 1960; p. 239], as expected. The effects of the boundaries, air and ground in our case, are next accounted for.

The method of images will be used to account for the boundaries. The method is given by Brekhovskikh [1960, p. 341] for a homogeneous layer, or slab, bounded above and below by arbitrary boundaries (i.e., not perfectly conducting). The method is inexact when the boundaries are not perfectly conducting, but may be applied if the slab thickness is large relative to a wavelength or, if not large, there are a large number of reflections. A straightforward application of the method to the present nonhomogeneous case gives the total field

$$\frac{e^{ikR}}{R} = \frac{i}{2\pi}\int_{-\infty}^{\infty}\int \exp\left[i\left(k_x x + k_y y\right)\right]\left\{ e^{i\int_{z_o}^{z} k_z dz} + \left[\Gamma_a e^{i\left(\int_{z_o}^{h} k_z dz + \int_{z}^{h} k_z dz\right)}\right.\right.$$

$$+ \Gamma_g e^{i\left(\int_{o}^{z_o} k_z dz + \int_{o}^{z} k_z dz\right)} + \Gamma_a\Gamma_g e^{i\left(\int_{o}^{z} k_z dz + \int_{o}^{h} k_z dz + \int_{z}^{h} k_z dz\right)} \qquad \text{(A-12)}$$

$$\left.\left. + \Gamma_a\Gamma_g e^{i\left(\int_{z_o}^{z} k_z dz + 2\int_{o}^{h} k_z dz\right)}\right] \Big/ \left[1 - \Gamma_a\Gamma_g e^{2i\int_{o}^{h} k_z dz}\right] \right\} \frac{dk_x dk_y}{\sqrt{k_z(z_o)k_z(z)}}$$

where Γ_a and Γ_g are the moduli of the plane wave reflection coefficients at the air and ground boundaries respectively. Also, we are explicitly considering only the case $z > z_o$ at present, and will generalize to arbitrary z and z_o later.

It is convenient to make a change of variable at this point to

$$k_x = q \cos \psi$$

$$k_y = q \sin \psi$$

$$q = \sqrt{k_x^2 + k_y^2}$$

and

$$x = r \cos \xi$$

$$y = r \sin \xi$$

$$r = \sqrt{x^2 + y^2}$$

which, after performing the integration over ψ, gives

$$\frac{e^{ikR}}{R} = \int_{-\infty}^{\infty} \frac{H_o'(qr)\ F\{\}\ q\,dq}{\left(\sqrt{q^2 - k_j^2(z)}\ \sqrt{q^2 - k_j^2(z_o)}\right)^{\frac{1}{2}}} \qquad \text{(A-13)}$$

where $H_o'(qr)$ is the Hankle function of the first kind and zeroth order, F is the term in braces in the integrand of Eq.(A-12), and the general relation $k_z = \sqrt{k^2 - k_x^2 - k_y^2}$ is employed.

The reflection coefficients Va and Vg are defined as the ratios of the reflected to incident electric fields at

the air and ground boundaries. They may be obtained in the usual manner of matching the tangential fields at the boundaries, and the resulting modulus of the ratios of reflected to incident $\bar{E}$-fields are

$$\Gamma_a = \frac{\sqrt{q^2 - k_j^2(h)} - \sqrt{q^2 - k_a^2}}{\sqrt{q^2 - k_j^2(h)} + \sqrt{q^2 - k_a^2}} \qquad \text{(A-14)}$$

$$\Gamma_g = \frac{\sqrt{q^2 - k_j^2(o)} - \sqrt{q^2 - k_g^2}}{\sqrt{q^2 - k_j^2(o)} + \sqrt{q^2 - k_g^2}} \qquad \text{(A-15)}$$

where the values of $k_j(h)$ and $k_j(o)$ are the values of $k_j(z)$ evaluated at the forest-air boundary ($z = h$) and the forest-ground boundary ($z = o$) respectively.

Effecting a solution to Eq.(A-13) requires numerical integration, in general, but an approximate analytical solution may be obtained and is done here. First, $qr \gg 1$, $H_o'(qr)$ may be written as [Brekhovskikh, 1960; p. 250]

$$H_o'(qr) \simeq \sqrt{\frac{2}{\pi qr}}\, e^{i\left(qr - \frac{\pi}{4}\right)}\left(1 + \frac{1}{8iqr} + \ldots\right) \qquad \text{(A-16)}$$

Employing the first term of Eq.(A-16) in Eq.(A-13), and making the transformation $q = \omega\sqrt{\mu\varepsilon_o}\,\alpha$ and $r = (c/\omega)\rho = \rho/\omega\sqrt{\mu\varepsilon_o}$ gives

$$\frac{e^{ikR}}{R} \simeq \frac{\sqrt{2}\, e^{-i\frac{\pi}{4}}\, \omega\sqrt{\mu\varepsilon_o}}{\sqrt{\pi}\,\sqrt{\rho}} \int_{-\infty}^{\infty} \frac{\alpha^{\frac{1}{2}}\, e^{i\alpha\rho}\, F(\alpha)\, d\alpha}{\left(\sqrt{\alpha^2 - \eta_j^2(z_o)}\,\sqrt{\alpha^2 - \eta_j^2(z)}\right)^{\frac{1}{2}}} \qquad \text{(A-17)}$$

where the index of refraction $\eta^2(z) \equiv \varepsilon(z) = \varepsilon'(z)\varepsilon_o$ and $k(z) = \omega\sqrt{\mu\varepsilon(z)} = \omega\sqrt{\mu\varepsilon_o\varepsilon'(z)} = \omega\sqrt{\mu\varepsilon_o}\,\eta(z)$ has been employed.

Equation (A-17) may be solved as a contour integral in the complex α-plane. The integrand, due to $e^{i\alpha\rho}$, is zero on the infinite semi-circle in the upper half α-plane. Thus, the value of the integral is equal to the contributions of the residues at the poles in the upper half-plane plus the value of the integral along any branch cuts of the integrand in the upper half-plane.

The pole terms are exponentially damped with distance ρ by the $e^{-\mathrm{Im}(\alpha_p)\rho}$ term in the integrand [Brekhovskikh, 1960; p. 365] where α_p denotes the value of α at the pole, p, considered. Similar damping occurs for the contributions along all branches in the upper half α-plane whose branch points have a finite imaginary part. This is most easily seen by making the transformation

$$\alpha = n + is^2 \qquad \text{(A-18)}$$

in Eq.(A-17). This gives

$$\frac{e^{ikR}}{R} \simeq \frac{2i\sqrt{2}\, e^{-i\frac{\pi}{4}}\, e^{i\mathrm{Re}(n)\rho}\, e^{-\mathrm{Im}(n)\rho}\, \omega\sqrt{\mu\varepsilon_o}}{\sqrt{\pi}\,\sqrt{\rho}} \qquad \text{(A-19)}$$

$$\int_{s(\alpha_1)}^{s(\alpha_2)} (n + is^2)^{\frac{1}{2}}\, e^{-s^2\rho}\, G(s)\, s\, ds \quad .$$

The integration will be along branch cuts in the s-plane which correspond to the appropriate cuts in the α-plane, each of which emanates from a branch point $\alpha = n$. Hence, for all branch cuts except those with a branch point at $\mathrm{Im}(n) = 0$, the result is damped with distance ρ by the $e^{-\mathrm{Im}(n)\rho}$ term outside the integral of Eq.(A-19). Examination of the terms of the integrand shows that there is only one branch point in the upper half α-plane for which $\mathrm{Im}(n) = 0$, which is due to the double value $\pm\sqrt{\alpha^2 - 1}$ of Eq.(A-14). Note that $k_a = \omega\sqrt{\mu\varepsilon_o}$ and $q = \omega\sqrt{\mu\varepsilon_o}$ in Eq.(A-14). It is now assumed that ρ is sufficiently large to make all remaining pole and branch cut contributions negligible relative to the contribution along the branch cut emanating from the branch point $\alpha = 1$. Hence, we evaluate the integral only along the branch cut from the point $\alpha = 1$. The cut is made along the line $\mathrm{Re}(\alpha) = 1^{\infty} \geq \mathrm{Im}(\alpha) \geq 0$, in the α-plane. The limits of integration in the α-plane are thus from $\alpha = 1^{-} + i\infty$ to $\alpha = 1^{-}$ using the $-\sqrt{\alpha^2 - 1}$ value in the integrand, and from $\alpha = 1^{+}$ to $\alpha = 1^{+} + i\infty$ using the $+\sqrt{\alpha^2 - 1}$, where the $\bar{+}$ superscript on the real part of α indicate the integration path is slightly to the left (-) and right (+) of the cut at $\alpha = 1$. The proper sign to attach to $\pm\sqrt{\alpha^2 - 1}$ on each side of the cut was determined by writing

$$\sqrt{\alpha^2 - 1} = (\alpha - 1)^{\frac{1}{2}}(\alpha + 1)^{\frac{1}{2}} = \sqrt{r_1 r_2}\, e^{i\frac{(\theta_1 + \theta_2)}{2}},$$

where θ_1 and θ_2 are the angles of $(\alpha - 1)$ and $(\alpha + 1)$ in polar form and are defined for the branch cuts along $\theta_1 = \pi/2$ for the branch point cut $\alpha = 1$ and $\theta_2 = -\pi/2$ for the point $\alpha = -1$ [Morse and Feshbach, 1953; p. 402]. The corresponding paths of integration in the s-plane may be determined from Eq.(A-18) with $n = 1$. For the branch on the left of the cut in the upper half α-plane

$$\alpha = 1 + is^2$$

$$\sqrt{i}\, s = -\sqrt{\alpha - 1} \quad .$$

For $\alpha = 1 + i\xi$, where $0 \le \xi \le \infty$

$$\sqrt{i}\, s = -\sqrt{i\xi} = -\sqrt{i}\,\sqrt{\xi} \quad .$$

Hence, the integral in the s-plane along $s = -\infty$ to $s = 0$ corresponds to the integral from $\alpha = 1 + i\infty$ to $\alpha = 1$ in the α-plane. Similar reasoning gives the limits for the integral in the s-plane of $s = 0$ to $s = +\infty$, which corresponds to the limits $\alpha = 1$ to $\alpha = 1 + i\infty$ for the integral in the α-plane. Hence, Eq.(A-19) evaluated along the branch $s = -\infty$ to $s = +\infty$, is

$$\frac{e^{ikR}}{R} \simeq \frac{2i\sqrt{2}\, e^{-i\frac{\pi}{4}} e^{i\rho\omega\sqrt{\mu\epsilon}}}{\sqrt{\pi}\,\sqrt{\rho}} \left[\int_{-\infty}^{0} (1 + is^2)^{\frac{1}{2}}\, e^{-s^2\rho} G^{-}(s)\, s\, ds \right. \qquad \text{(A-20)}$$

$$\left. + \int_{0}^{\infty} (1 + is^2)^{\frac{1}{2}}\, e^{-s^2\rho}\, G^{+}(s)\, s\, ds \right]$$

where the superscripts $\mp$ on G refer to G evaluated with $-\sqrt{(1 + is^2)^2 - 1}$ and $+\sqrt{(1 + is^2)^2 - 1}$. Due to $e^{-s^2\rho}$ and the restrictions already imposed for large ρ, the integrals of Eq.(A-20) will have significant value only for small s. Thus, the integrals may be evaluated by expanding the integrands in a Taylor series about $s = 0$ and integrating term-by-term. Expanding $(1 + is^2)^{\frac{1}{2}}$ and G(s) in a Taylor series is a bit

tedious but straightforward, and is not reproduced here. Taking the first two terms of the resulting product of the expansions as approximations to the integrals; and recognizing that $G^-(0) = G^+(0)$, and

$$\left.\frac{\partial G^-}{\partial s}\right|_{s=0} = \left.\frac{\partial G^+}{\partial s}\right|_{s=0}$$

and that odd powers of s will then cancel in the integration, gives

$$\frac{e^{ikR}}{R} \simeq \frac{2i\sqrt{2}\, e^{-i\frac{\pi}{4}}\, e^{i\rho\omega\sqrt{\mu\varepsilon}}}{\sqrt{\pi}\,\rho}\, G'(0) \int_{-\infty}^{\infty} e^{-s^2\rho}\, s^2 ds \,. \quad \text{(A-21)}$$

The value of the integral in Eq.(A-21) is tabulated in several standard references, and we finally have

$$\frac{e^{ikR}}{R} \simeq \frac{i\sqrt{2}\, e^{-i\frac{\pi}{4}}\, e^{i\rho\omega\sqrt{\mu\varepsilon_o}}}{\rho^2}\, G'(0) \quad \text{(A-22)}$$

where

$$G'(0) = \frac{-2i\sqrt{2i}}{\left[\eta_j^2(h) - 1\right]^{\frac{1}{2}}\left[\eta_j^2(z) - 1\right]^{\frac{1}{4}}\left[\eta_j^2(z_o) - 1\right]^{\frac{1}{4}}} \left\{ e^{i\left(\int_{z_o}^{h} f(a)da + \int_{z}^{h} f(a)da\right)} \right.$$

$$+ \Gamma_g(0)\left[e^{i\left(\int_{o}^{z_o} f(a)da + \int_{o}^{h} f(a)da + \int_{z}^{h} f(a)da\right)} + e^{i\left(\int_{z_o}^{z} f(a)da + 2\int_{o}^{h} f(a)da\right)} \right]$$

$$\left. + \Gamma_g^2(0)\left[e^{i\left(\int_{o}^{z_o} f(a)da + \int_{o}^{z} f(a)da + 2\int_{o}^{h} f(a)da\right)} \right] \right\} \Bigg/ \left[1 - \Gamma_g(0) e^{2i\int_{o}^{h} f(a)da}\right]$$

and $f(a) = i\omega\sqrt{\mu\varepsilon_o}\left(\eta^2(a) - 1\right)^{\frac{1}{2}}$ where the dummy of integration "a" is employed to avoid confusion, and

$$\Gamma_g(0) = \frac{\sqrt{1 - \eta_j^2(0)} - \sqrt{1 - \eta_g^2}}{\sqrt{1 - \eta_j^2(0)} - \sqrt{1 - \eta_g^2}} \quad .$$

With some factoring and rearrangement of the terms in the braces of $G'(0)$, we may write Eq.(A-22)

$$\frac{e^{ikR}}{R} \simeq \frac{4e^{i\rho}\omega\sqrt{\mu c_o}}{\rho^2} F(z)\ F(z_o) \qquad \text{(A-23)}$$

where

$$F(z) = \frac{e^{i\int_z^h f(a)da}\left[1 + \Gamma_g(0)e^{2i\int_0^z f(a)da}\right]}{\left[\eta j^2(h) - 1\right]^{\frac{1}{4}}\left[\eta_j{}^2(z) - 1\right]^{\frac{1}{4}}\left[1 - \Gamma_g(0)\,e^{2i\int_0^h f(a)da}\right]} .$$

and $F(z_o) = F(z)$ with z replaced by z_o. The latter statement is simply a statement of reciprocity and shows that Eq.(A-23) holds for $z < z_o$ as well as for $z > 0$, which has been the explicit case treated as mentioned earlier.

Using Eq.(A-5), and recognizing that the field of a short dipole is 1/2 that of the Hertzian dipole [Jordon, 1958; p. 312], and using Eq.(A-23) where $\rho = r\omega\sqrt{\mu\varepsilon_o}$, gives the field for short dipoles as

$$E_{y\ rms} = \frac{9 \times 10^{10}\sqrt{P}}{\sqrt{2}\ \pi f r^2} |F(z)||F(z_o)| \ \mu v/m \qquad (A\text{-}24)$$

where P is the transmitted power in kw, f is frequency in megahertz, and the relation $P = 80\pi^2(Idl/\lambda)^2$ for the short dipoles were used. The expressions for the transmitted and received powers are sometimes modified by a factor of $1/Re[\eta(z)]$ as an approximation to account for the dipoles radiating in a dissipative media, but the factor is small in the present case and is neglected here.

APPENDIX B

LINEAR TRENDS IN PHASE OF THE COMPLEX DATA

It was mentioned in Section 3.2.2.1 that linear trends in the phase of the complex data were removed before computation of the normalized complex frequency-distance cross-covariance coefficients. The causes of these trends and their removal are discussed in this section.

Figure B.1 is a plan view of the geometry of the measurement region pertinent to the phase measurement.

As discussed in Section 3.2.1, the recorded data are a set of photographs of the signal envelope and relative phase as a function of swept frequency and distance. The recorded phase is the difference between the phase of the test antenna and the phase on a reference antenna. The reference antenna was positioned to obtain an undisturbed replica of the transmitted signal and held stationary throughout each run. The test antenna was moved in a horizontal line, in discrete steps, in either a radial or transverse direction for each run. The initial position of the test antenna for each run is designated as the origin of a rectangular coordinate system with the x-axis being along the radial direction.

The envelope and relative phase of the received signal as a function of swept frequency and distance, for a constant transmitted signal (flat spectrum), is equal to the channel transfer function $H(f,x)$ to within an arbitrary magnitude and time delay, or phase [Schwartz, Bennett and Stein, 1966]. The magnitude is of no consequence in the final correlation coefficients of the complex signal (and, hence, channel transfer function) since these are normalized quantities. The

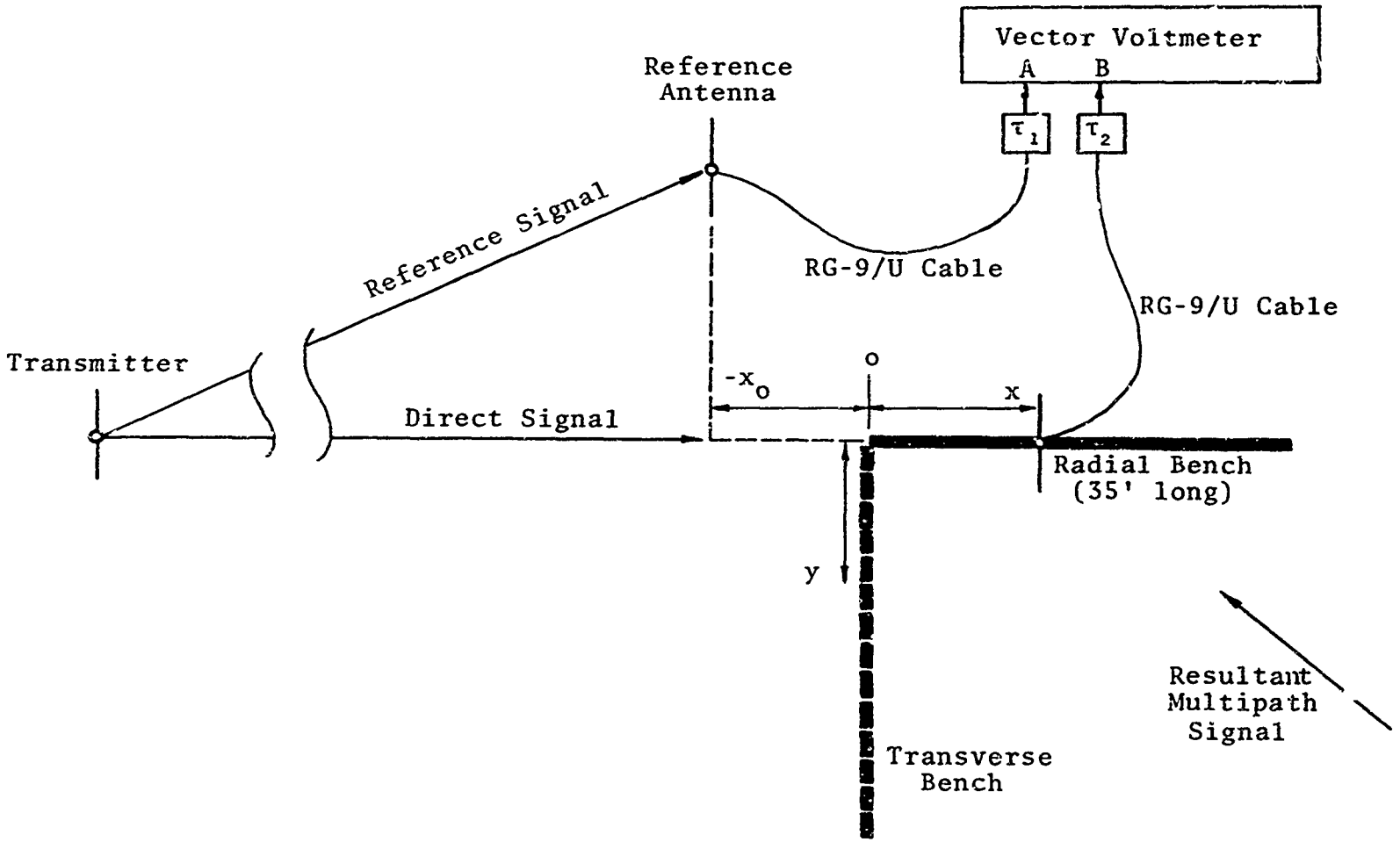

Figure B.1 Plan View Sketch of Phase Measurement System

time delay results in a linear trend in the phase of the complex correlations (and in the data as well) and if the delay is constant it might be ignored in some cases during analysis and simply removed from the final complex signal correlations to arrive at the correlations for the channel transfer function.

In the present case, however, this delay changes for each photograph throughout a radial run because the test antenna position, and hence propagation delay, is changed between each photograph. The effect of this change in delay is to introduce nonstationarity and must, therefore, be removed from the data of each run. Also, because the channel is generally Rician [Robertson, et al., 1970], it is necessary to remove a steady component from the signal before performing the correlations [Stein and Jones, 1967]. This, in turn, requires application of the phase information in a manner which, unlike the correlations, requires the removal of the effects of the fixed delay as well. These effects and their removal from the data are discussed in detail below.

Let the transmitted signal be $T(t) = K \cos 2\pi ft$ where K is a constant and the frequency, f, is $(f_c - 2\,\text{MHz}) \leq f \leq (f_c + 2\,\text{MHz})$, where f_c is the center frequency of 50, 100 or 150 MHz. The signal received on the reference antenna is a replica of the transmitted signal with the exception of arbitrary magnitude and delay factors of k_r and τ_r. There are generally additional magnitude, k_1, and delay, τ_1, factors introduced in the reference signal due to cable losses, cable length, amplification, etc., prior to comparison of the reference phase and test phase. As a result, the reference signal available at the phase comparitor may be written as

$$R(t) = k_1 k_r K \cos 2\pi f(t + \tau_r + \tau_1) \quad . \qquad \text{(B-1)}$$

This reference signal, R(t), remained constant throughout each run.

The signal at the test antenna, which generally consisted of a direct wave plus a number of scattered or reflected signals (multipaths) may be expressed as [Stein and Jones, 1967]

$$S(t) = C(f,x) \cos [2\pi f (t + \tau_s) + \phi(f,x)]$$

where $C(f,x)$ is the frequency and distance dependent envelope of the complex signal, τ_s is the propagation delay time of the most direct wave, and $\phi(f,x)$ is the instantaneous phase of the various multipaths. Accounting for amplitude, k_2, and delay, τ_2, factors of the cables and equipment in the test signal line, the test signal may be written

$$S'(t) = k_2 C(f,x) \cos [2\pi f (t + \tau_s + \tau_2) + \phi(f,x)] \qquad (B-2)$$

Note that the required complex channel transfer function is $H(f,x) = C(f,x)e^{i\phi(f,x)}$. The envelope of the test signal $k_2C(f,x)$ is, thus, to within an arbitrary constant as mentioned above, the magnitude of the complex transfer function. This envelope (or equivalently the magnitude of the complex transfer function) was displayed on one trace of a dual beam oscilloscope and photographically recorded along with the relative phase which was displayed on the other trace. The relative phase of the test signal is not so easily related to the phase of the complex transfer function.

The relative phase of the test signal, $\Delta\phi$, is the difference between the phases in the test and reference channels and may be written

$$\Delta\phi = \text{phase of } S'(t) - \text{phase of } R'(t)$$

$$= 2\pi f(t + \tau_s + \tau_2) + \phi(f,x) - 2\pi f(t + \tau_r + \tau_1)$$

$$= \phi(f,x) + 2\pi f(\tau_s + \tau_2 - \tau_r - \tau_1) \quad . \qquad \text{(B-3)}$$

Hence, the measured relative phase, $\Delta\phi$, differs from the desired phase $\phi(f,x)$ by $2\pi f(\tau_s + \tau_2 - \tau_r - \tau_1)$ which changes linearly with frequency, and is clearly due to the time delay differences between the test and reference channels.

With reference to Figure B.1, the time delay, τ_s, of the most direct signal to the test antenna may be written as $\tau_s = \tau_r + \tau' + \frac{x}{c}$ where τ' is the propagation time delay due to the physical separation of the reference and test antennas for the test antenna positioned at the origin x = o, x is the radial distance of the test antenna from the origin, and c is the speed of light. Using this expression for τ_s, we may write

$$2\pi f(\tau + \tau_2 - \tau_r - \tau_1) = 2\pi f(\tau' + \frac{x}{c} + \tau_2 - \tau_1)$$

$$= 2\pi f \frac{x}{c} + 2\pi f(\tau' + \tau_2 - \tau_1) \quad . \qquad \text{(B-4)}$$

The first term in the right-hand side of Eq.(B-4) represents a linear change in phase with frequency, the slope of which changes with antenna position, x. This changing phase slope is a nonstationary effect in the data and must be removed from the phase data of each run.. At position x = o this phase slope is zero, and since f and x are known for all photographs, this phase slope is easily removed. This was done, which essentially refers the phases of all photographs to the relative phase between the reference antenna and the test antenna at x = o.

The delay given by the final term in the right-hand side of Eq.(B-4) represents the fixed delay between the reference and test channels. This constant delay introduces a linear change in phase with frequency, which has a constant slope, for all swept frequency photographs of a run. If the complex channel transfer function were a zero mean random process, then this constant phase slope would also be present in the phase of the complex frequency correlation function of the signal, as mentioned above, and need not be removed from the data prior to correlation analysis. If the complex channel transfer function is not zero mean, as is the general case here, then the mean, or steady component, as also mentioned above, should be removed from the data prior to correlation analysis [Stein and Jones, 1967]. The steady component is the mean of the complex signal for a Rician channel. However, the time delay between the reference and test antenna causes the phase of the steady component to change linearly with frequency across the sweep, as mentioned. If this phase changes sufficiently (e.g., by $\simeq 2\pi$) during a frequency sweep, then the complex mean of the total process, ignoring this phase trend, could result in an apparent zero mean process while, in fact, the steady component along with the lesser components have simply revolved about the origin due to the time delay. Hence, before computing the steady component the effect of this delay must be removed or accounted for. The effect of this delay, or the phase slope, may be determined, for example, by computing the least squares linear fit of the phase response on the swept-frequency photograph at the origin, $x=o$, which is then easily removed from each photograph. Essentially, this was the procedure employed but, rather than computing the phase slope from the photograph of the origin, the phase slope from the photograph exhibiting the strongest Rician character (large signal amplitude with small fluctuations, and a linear phase)

was used, and then transformed to the origin through the first term in the right-hand side of Eq.(B-4).

Note that the removal of these phase trends from the data refers the phase of all data points in each run to the (zero) phase of the steady (most direct) wave at the test antenna. Thus, the phase of the steady component has been removed from all photographs by this procedure, but the magnitude has not. This latter is accomplished by removing the complex mean from the data of each swept-frequency photograph after the phase trends have been removed.

REFERENCES

1. Measurement and Analysis of Random Data, by Julius S. Bendat and Allan G. Piersol, New York, John Wiley & Sons, Inc., 1966, 390 pp.

2. Waves in Layered Media, by L. M. Brekhovskikh, New York, Academic Press, 1960, 561 pp.

3. Tropical Propagation Research Final Report Volume II, by John J. Hicks, A. Page Murphy, E. L. Patrick and L. G. Sturgill, Jansky & Bailey Engrg. Dept., Atlantic Research Corp., Alexandria, Va., 1969.

4. Tropical Propagation Research Semiarnual Report No. 11, by J. J. Hicks and R. G. Robertson, Jansky & Bailey Engrg. Dept., Atlantic Research Corp., Alexandria, Va., 1969.

5. Tropical Propagation Research Final Report Volume I, Jansky & Bailey Engrg. Dept., Atlantic Research Corp., Alexandria, Va., 1966.

6. Spectral Analysis and Its Applications, by Gwilym M. Jenkins and Donald G. Watts, San Francisco, Holden-Day, 1968, 525 pp.

7. Electromagnetic Waves and Radiating Systems, by E.C. Jordon Prentice-Hall, Inc., Englewood Cliffs, N.J., 1950, 710 pp.

8. Statistical Theory of Communication, by Y. W. Lee, New York, John Wiley & Sons, Inc., 1960, 509 pp.

9. Methods of Theoretical Physics (Part I), by Philip M. Morse and Herman Feshbach, New York, McGraw-Hill, 1953, 997 pp.

10. Transmission Loss in Radio Propagation - II, by K.A. Norton, National Bureau of Standards Tech. Note No. 12, 1959.

11. Fields and Waves in Modern Radio, by Simon Ramo and John R. Whinnery, New York, John Wiley & Sons, Inc., 1953, 576 pp.

12. Tropical Propagation Research Semiannual Report No. 12, by Richard G. Robertson, Jansky & Bailey Engrg. Dept., Atlantic Research Corp., Alexandria, Va., 1969.

13. Tropical Propagation Research Final Report Volume III, by Richard G. Robertson, John J. Hicks, Charles B. Sykes, and Per A. Anti, Jansky & Bailey Engrg. Dept., Atlantic Research Corp., Alexandria, Va.

14. A Conducting - Slab Model For Electromagnetic Propagation Within a Jungle Medium, by D. L. Sachs and P. J. Wyatt, General Research Corp., Tech. Memorandum, May 1966 (AD 679 171). Also, Radio Science, pp 125-134, February 1968.

15. A Conducting - Slab Model For Electromagnetic Propagation Within a Jungle Medium, II, by D. L. Sachs, General Research Corp., Internal Memorandum 471, September 1966.

16. Communications Systems and Techniques, by Mischa Schwartz, William R. Bennett, and Seymour Stein, New York, McGraw-Hill, 1966, 618 pp.

17. Modern Communication Principles, by Seymour Stein and J. Jay Jones, New York, McGraw-Hill, 1967, 382 pp.

18. On Radio - Wave Propagation in Forest Environments, by Theodor Tamir, IEE Transactions on Antennas and Propagation, Vol. AP-15, No. 6, November 1967.

19. Electromagnetic Waves in Stratified Media, by J. R. Wait, New York, Pergamon Press, 1962, 372 pp.

20. Tropical Propagation Research, Jansky & Bailey Engineering Department of Atlantic Research Corporation, Semiannual Report No. 1, Contract No. DA 36-039 SC-90889, AD 609-284.

Semiannual Report No. 2	AD 609-285
Semiannual Report No. 3	AD 609-286
Semiannual Report No. 4	AD 451-045
Semiannual Report No. 5	AD 460-634
Semiannual Report No. 6	AD 474-377
Semiannual Report No. 7	AD 486-499
Final Report Volume I	AD 660-318
Semiannual Report No. 8	AD 662-267
Semiannual Report No. 9	AD 673-142
Semiannual Report No. 10	AD 676-870
Semiannual Report No. 11	AD 697-158
Final Report Volume II	AD 706-232
Semiannual Report No. 12	AD 708-902
Final Report Volume III	AD 714-300